

University of Windsor

Scholarship at UWindor

Electronic Theses and Dissertations

Theses, Dissertations, and Major Papers

1-1-2019

Brake Squeal reduction through improved rotor damping

Raju Karthik
University of Windsor

Follow this and additional works at: <https://scholar.uwindsor.ca/etd>

Recommended Citation

Karthik, Raju, "Brake Squeal reduction through improved rotor damping" (2019). *Electronic Theses and Dissertations*. 8169.

<https://scholar.uwindsor.ca/etd/8169>

This online database contains the full-text of PhD dissertations and Masters' theses of University of Windsor students from 1954 forward. These documents are made available for personal study and research purposes only, in accordance with the Canadian Copyright Act and the Creative Commons license—CC BY-NC-ND (Attribution, Non-Commercial, No Derivative Works). Under this license, works must always be attributed to the copyright holder (original author), cannot be used for any commercial purposes, and may not be altered. Any other use would require the permission of the copyright holder. Students may inquire about withdrawing their dissertation and/or thesis from this database. For additional inquiries, please contact the repository administrator via email (scholarship@uwindsor.ca) or by telephone at 519-253-3000ext. 3208.

Brake Squeal Reduction through improved Rotor Damping

By

Raju Karthik

A Thesis

Submitted to the Faculty of Graduate Studies through the Department of
Mechanical, Automotive and Materials Engineering

In Partial Fulfillment of the Requirements for the Degree of Masters of Applied Science

at the

University of Windsor

Windsor, Ontario, Canada

2019

© 2019 Raju Karthik

Brake Squeal Reduction through improved Rotor Damping

by

Raju Karthik

APPROVED BY:

C. Novak

Department of Mechanical, Automotive and Materials Engineering

R. J. Bowers

Department of Mechanical, Automotive and Materials Engineering

J. H. Sokolowski, Co-Advisor

Department of Mechanical, Automotive and Materials Engineering

A. Sobiesiak, Co-Advisor

Department of Mechanical, Automotive and Materials Engineering

December 4, 2019

DECLARATION OF ORIGINALITY

I hereby certify that I am the sole author of this thesis and that no part of this thesis has been published or submitted for publication.

I certify that, to the best of my knowledge, my thesis does not infringe upon anyone's copyright nor violate any proprietary rights and that any ideas, techniques, quotations, or any other material from the work of other people included in my thesis, published or otherwise, are fully acknowledged in accordance with the standard referencing practices. Furthermore, to the extent that I have included copyrighted material that surpasses the bounds of fair dealing within the meaning of the Canada Copyright Act, I certify that I have obtained a written permission from the copyright owner(s) to include such material(s) in my thesis and have included copies of such copyright clearances to my appendix.

I declare that this is a true copy of my thesis, including any final revisions, as approved by my thesis committee and the Graduate Studies office, and that this thesis has not been submitted for a higher degree to any other University or Institution.

ABSTRACT

Brake Squeal Noise is a significant concern in the automotive industry and incurs enormous costs during brake system development and in brake system warranty. Several methods are utilized to minimize brake squeal, including frequency manipulation of individual brake system components through design and material modifications, active damping elements like pad shims and insulators, which typically add mass and cost to the brake system, as well as retesting costs. Brake rotors are made of grey cast iron due to their low cost, good machinability, wear and damping properties. Strength requirements limit the material damping obtainable on a consistent basis. Other methods to improve rotor damping include the use of steel inserts in the rotor plates and EDM machining of the brake rotors. Parts made with either process have been observed to reach very high levels of damping (Q factor of ~ 200) and entirely eliminate noise occurrences in the brake system.

This research involves the characterization of the material and the additional processes required to achieve highly damped rotors, with a Q factor in the range of 100 to 300, which can provide significant brake noise reduction. It was discovered that electrical or magnetic processing of the rotors can create damping improvements in the range of 10 to 50 %, which are beneficial to reducing noise occurrences. EDM processing was primarily used for the study and Q factor improvements in the range of 30 to 50 % observed. Rotors with High C.E., Large Type A graphite with flake size 2 to 4, showed the largest benefits from the processing. Process DOE showed no effects of current on the damping improvements. A low processing time of 5 seconds on Non FNC rotors generated over 30 % damping improvements consistently. Noise occurrence reductions of 80 to 100 % were seen with the processed rotors. No detrimental effects were noted on other rotor performance characteristics including thermal cracking, brake torque variation, wear, and corrosion. Effects of time, temperature and wear on the damping improvements have been researched, and no significant losses were seen in typical operating conditions.

DEDICATION

To my loved ones.

To my colleagues and friends at Rassini International Brakes Group and Rassini Frenos.

ACKNOWLEDGEMENTS

I sincerely thank my supervisor, Dr. Jerry Sokolowski, for his tireless support and efforts in this research. I am thankful and proud to have worked with him over the years.

I appreciate the help from my co-supervisor, Dr. Andrzej Sobiesiak; whose feedback and mentoring were essential for this project.

I want to thank my PhD committee members, Dr. Bowers and Dr. Novak, for their support and friendly feedback.

My thanks to Dr. Peter Guba for helping me to create micrographs.

Many thanks to Dr. Marcin Kasprzak for the help in building the IESV power generator and his feedback and help in running experiments on IESV and magnetic fields.

Thanks to Chris Kain at Apollo EDM for help with EDM processing equipment and electrodes.

Thanks to Jason Mitchick for his work and support during the initial stages of the project.

I especially thank Rassini International Inc. for sponsoring the research. Special thanks to Mauricio González for his constant support and his enthusiasm throughout the project.

I am forever thankful:

To my parents;

To my wife Aarthi, and daughters Veena and Varsha, for all their love and support,

To all my family and friends that have always been there for me.

To all my colleagues at Rassini International Inc. Brakes Group.

TABLE OF CONTENTS

DECLARATION OF ORIGINALITY	iii
ABSTRACT	iv
DEDICATION	v
ACKNOWLEDGEMENTS	vi
LIST OF TABLES.....	x
LIST OF FIGURES	xi
LIST OF ABBREVIATIONS/SYMBOLS	xvii
CHAPTER 1 INTRODUCTION.....	1
CHAPTER 2 LITERATURE REVIEW.....	3
2.1. Introduction to Brake Rotors	3
2.2. Rotor Materials.....	6
2.3. Brake Noise	14
2.4. Brake Squeal: Mechanisms and possible causes	16
2.5. Typical brake NVH solutions.....	17
2.6. Rotor Material Damping.....	22
2.7. Rotor Damping Measurement	26
2.8. Other methods used to improve rotor damping	30
2.9. Summary of the Literature Review	34
2.10. Further Study	35
CHAPTER 3 EXPLORATORY RESEARCH.....	36
3.1. EDM Experiments.....	36

3.1.1. EDM Test Results.....	38
3.2. Magnetic Field Experiments.....	39
3.3. Process Benchmarking	41
3.4. Development of the IESV Power Generator	43
3.5. Large sample batch study	49
3.6. Noise Validation.....	53
3.7. Summary of Exploratory Research	55
3.7.1. Processing.....	55
3.7.2. Material.....	56
3.7.3. Noise Validation.....	56
3.8. Project Justification	57
3.9. Project Objectives and Goals.....	57
CHAPTER 4 MATERIAL CHARACTERIZATION FOR DAMPING IMPROVEMENTS.....	59
4.1. Material Selection.....	59
4.2. Non Destructive Testing.....	67
4.2.1. Effects of processing on Q Factor	68
4.2.2. Effects on Elastic Modulus.....	71
4.2.3. Brinell Hardness measurements	76
4.2.4. Magnetic Field measurements.....	79
4.3. Effects of C.E.	84
4.4. Microstructure Characterization.....	86
4.5. Summary of material characterization.....	91
CHAPTER 5 MATERIAL AND PROCESS CONFIRMATION STUDY.....	92
5.1. Material Selection and prototypes.....	92

5.2. Process DOE.....	.96
5.3. Discussion and Conclusions	102
CHAPTER 6 NOISE VALIDATION	104
6.1. Noise tests and test results	104
6.2. Noise testing and results on MC1 Rotors	105
6.3. Observations and Conclusions	108
CHAPTER 7 ROTOR PERFORMANCE VALIDATION.....	109
7.1. Rotor Performance Tests.....	109
7.2. Thermal Cracking Tests.....	110
7.3. Vibration Tests.....	111
7.4. Wear Tests.....	112
7.5. Corrosion Tests.....	114
7.6. Brake Output Testing.....	115
7.7. Effects of Machining on Rotor Damping Improvements.....	117
7.8. Effects of Time and Temperature.....	118
7.9. Validation Summary.....	122
CHAPTER 8 CONCLUSIONS AND FUTURE WORK	123
8.1 Conclusions	123
8.2 Future Work.....	125
REFERENCES.....	127
APPENDIX.....	136
VITA AUCTORIS	140

LIST OF TABLES

Table 2.1. Graphite Flake Size per ASTM A247	10
Table 2.2. Typical Rotor Material Compositions and Requirements based on application	12
Table 3.1. IESV Process DOE Parameter Matrix.....	46
Table 3.2. Second DOE Matrix with Current, Time and Frequency.....	48
Table 4.1. Rotor ID picked for the study and the C.E., E.C. and the inoculants used.....	59
Table 4.2. Chemistry for batch of S01, D11, F11 and F13 rotors	63
Table 4.3. Rotor mechanical properties (hardness and tensile strength) and Q factor.....	64
Table 4.3. Nondestructive Testing on Rotors before, during and after processing	67
Table 5.1. Chemical Analysis for the MC1 rotor batch.....	93
Table 5.2. Factors and levels used for the Process parameter study	97
Table 5.3. Q factor and % change at all bending and tangential modes.....	102
Table 6.1. Noise occurrences at various frequencies and dB levels on Baseline Rotors	106
Table 6.2. Noise occurrences at various frequencies and dB levels on Processed Rotors	108
Table 7.1. Effects of Time and Temperature on Q factor on processed rotors.....	119
Table 7.2. Test procedures and temperatures before and after testing baseline rotors.....	120
Table 7.3. Test procedures and temperatures before and after testing processed rotors	121
Table 7.4. Pre and post output test FRF and Q factor measurements on MC1 rotors.....	121

LIST OF FIGURES

Figure 2.1. Brake Rotor and Caliper Assembly illustration.....	4
Figure 2.2. Brake Rotor illustration of different important interface and design areas....	6
Figure 2.3. Rotor Micrograph showing Graphite, Pearlite and Free ferrite.....	8
Figure 2.4. Graphite Flake Types per ASTM A247.....	9
Figure 2.5. Graphite Distribution used to rate the Type VII Flake Graphite per ASTM A247. Figures reduced from magnifications shown.....	9
Figure 2.6. Micrographs showing the graphite flake size per ASTM A 247.....	10
Figure 2.7. Example of gating and riser designs to ensure hardness uniformity using Magmasoft.....	11
Figure 2.8. Characterization of brake noise based on frequency ranges.....	14
Figure 2.9. Noise Characterization based on Frequency Range.....	15
Figure 2.10. Out of plane bending modes and In plane tangential modes of rotor.....	19
Figure 2.11. Pad Insulators and Shims illustration.....	21
Figure 2.12. Double sticky layer and multilayer constrained shims.....	21
Figure 2.13. Illustration of Damping and Vibration Attenuation.....	22
Figure 2.14. Damping vs Stress – Coarse and Fine Flake Graphite and Nodular Iron...24	
Figure 2.15. Graphite flake shape factor vs damping.....	25
Figure 2.16. Frequency Response Plot showing the modal frequency peaks.....	27
Figure 2.17. Q factor calculation.....	28
Figure 2.18. Damping measurement set up.....	29
Figure 2.19. Master Rotor Q factor variation with time and temperature.....	30
Figure 2.20. Inserts cast into the brake plates for improved damping.....	31
Figure 2.21. EDM Machining process illustration.....	33

Figure 3.1. Power source and Ingersoll EDM machine.....	37
Figure 3.2. Machined areas during processing.....	37
Figure 3.3. Damping improvements after processing.....	38
Figure 3.4. Maxwell's law and Magnetic Coil.....	39
Figure 3.5. Boxplot of pre and post process Q Factor.....	40
Figure 3.6. Power Generator and controls for the EDM machine.....	41
Figure 3.7. EDM machine setup and the sacrificial steel machined on rotor plate.....	42
Figure 3.8. EDM setup and the Rogowski Coil wrapped around the rotor.....	42
Figure 3.9. EDM signal measured by the Rogowski probe and the oscilloscope.....	43
Figure 3.10. IESV equipment set up and current and frequency.....	44
Figure 3.11. IESV connections.....	44
Figure 3.12. Q factor pre and post processing with IESV.....	45
Figure 3.13. Comparison of % Q improvements from EDM and IESV processing	45
Figure 3.14. DOE results showing the effects of time, current and frequency on Q factor improvements.....	47
Figure 3.15. Main effects plot for % Q factor improvement after IESV processing.....	48
Figure 3.16. Fitted line plot of the % Q factor change after processing vs Pre process Q factor.....	50
Figure 3.17. Pre process vs post process Q factor results.....	50
Figure 3.18. Contour Plot of % Q factor vs Brinell hardness, tensile strength (MPa).....	51
Figure 3.19. Micrographs (100X) showing the graphite flake distribution in 3 samples of varying Q factor improvements from processing.....	52
Figure 3.20 Noise Test results of a baseline rotor	53
Figure 3.21. Noise test results of EDM processed rotor.....	54

Figure 3.22. Noise Testing on baseline and EDM processed rotors.....	55
Figure 4.1. Relation between the baseline Q factor vs C.E of the 5 grades of rotors .61	
Figure 4.2. Contour Plot of Baseline Q factor vs Carbon Equivalent and Eutectic Carbon.....	62
Figure 4.3. Scatterplot of Baseline Q factor vs Hardness and Tensile Strength.....	65
Figure 4.4. Contour Plot of Baseline Q factor vs Hardness and C.E.....	65
Figure 4.5. Microstructure of S01, D11, F11 and F13 inoculated and uninoculated rotors on a Olympus GX 71 Optical Microscope.....	66
Figure 4.6. Boxplot of % change in Q factor for the study parts.....	68
Figure 4.7. Fitted line plot of pre vs post test Q factor.....	68
Figure 4.8. Fitted Line Plot of % change in Q factor vs pre test Q factor.....	69
Figure 4.9. Q factor pre and post processing at all bending and tangential modes....	70
Figure 4.10. % Q factor change at each mode on S01 rotor.....	71
Figure 4.11. Through the thickness and radial directions for Modulus measurements .71	
Figure 4.12. ETEK Ultrasound Equipment.....	72
Figure 4.13. Typical Ultrasonic pulse and its parameters.....	72
Figure 4.14. Example of locations for non destructive test measurements – S01....	74
Figure 4.15. Boxplot of the velocity measurement in axial and radial directions.....	74
Figure 4.16. Average Modulus changes in the through the thickness direction on the rotors.....	75
Figure 4.17. Rotors showing the different locations for Hardness measurements.....	76
Figure 4.18. Hardness on Outer Diameter OB and IB plate on all rotors.....	77
Figure 4.19. Hardness change at OD on OB plate for S01 Rotors.....	78
Figure 4.20. Pre and post processing hardness on rotors OB Outer.....	78
Figure 4.21. Pre vs Post processing hardness on OB and IB outer – all rotors.....	79
Figure 4.22. Hall sensor.	80

Figure 4.23. Hall sensor Voltage measurements on D11 rotors before, during and after EDM processing.....	81
Figure 4.24. Hall sensor magnetic field measurements – F11- multiple rotors.....	82
Figure 4.25. Hall sensor field voltage measurements on all part numbers before, during and after processing.....	83
Figure 4.26. % Q Factor Change vs C.E.	84
Figure 4.27. Contour Plot of the % Q factor change vs C.E. and E.C.....	85
Figure 4.27. Contour Plot of the % Q factor change vs C.E and Hardness.....	85
Figure 4.28. 100 X LOM Micrographs of S01 rotors on OB and IB plate.....	86
Figure 4.29. 1000 X Polished and Etched LOM Micrographs S01.....	86
Figure 4.30. 100 X LOM Micrographs of D11 rotors on OB and IB plate.....	87
Figure 4.31. 1000 X Polished and Etched LOM Micrographs D11.....	87
Figure 4.32. 100 X LOM Micrographs of F11 rotors on OB and IB plate.....	88
Figure 4.33. 1000 X Polished and Etched LOM Micrographs F11.....	89
Figure 4.34. 100 X LOM micrographs of F13 rotors on OB and IB plate.....	90
Figure 4.35. 500 X Polished and Etched LOM Micrographs F1314.....	90
Figure 4.36. 100 X LOM Micrographs of Uninoculated F1314 rotors on OB and IB plate.....	90
Figure 4.37. 500 X Polished and Etched LOM Micrographs F1314 uninoculated.....	90
Figure 5.1. Microstructure 100 X LOM micrograph and 1000X As polished and Etched LOM of the MC1 rotors (IB Plate)	92
Figure 5.2. Microstructure 100 X LOM micrograph and 1000X As polished and Etched LOM of the MC1 rotors (OB Plate)	93
Figure 5.3. Boxplot and Histogram of MC1 rotors Q factor Pre processing.....	94
Figure 5.4. FNC White Layer seen in the micrographs of the brake rotor plates.....	95

Figure 5.5. Boxplot of Q Factor on FNC rotors.....	96
Figure 5.6. Histogram of post process Q factor on all MC1 rotors.....	97
Figure 5.7. Histogram of pre and post process Q factor on MC1 rotors.....	98
Figure 5.8. Boxplot of pre and post process Q Factor on MC1 rotors.....	98
Figure 5.9. Boxplot of % Q Factor change due to the electrical processing.....	99
Figure 5.10. Mean Effects Plot showing the effects of different factor and levels on post process Q Factor.....	100
Figure 5.11. Mean Effects Screener Plot showing the effects of different factors and levels on % Q factor change	101
Figure 5.12. Interaction plots for % Q factor change.....	101
Figure 5.13. Histogram of pre and post process Q Factor showing a damping improvement.....	103
Figure 6.1. Noise Testing on Baseline and Processed rotors of S01.....	105
Figure 6.2. Noise test results on a baseline rotor	106
Figure 6.3. Noise Test per customer Noise Test Specification on processed rotors...	107
Figure 7.1. Test parts from Thermal Cracking test on processed rotors.....	111
Figure 7.2. BTV data for baseline and processed rotors for the test.....	112
Figure 7.3. Wear Tests on No FNC Baseline and Processed Rotors.....	113
Figure 7.4. Results of wear test on baseline and processed rotors with FNC.....	113
Figure 7.5. Corrosion Test Chamber to run salt spray testing.....	114
Figure 7.6. Post ASTM B117 Corrosion test pictures on processed part # 1	115
Figure 7.7. Post ASTM B117 Corrosion test pictures on processed part # 2	115
Figure 7.8. Post ASTM B117 Corrosion test pictures on processed part # 3	115

Figure 7.9. Brake Output testing results for baseline and processed rotors with no FNC.....	116
Figure 7.10. Brake Output testing results for baseline and processed rotors with FNC.....	117
Figure 7.11. Change in Q factor with machining and wear.....	118
Figure 7.12. Waterfall Plot of Q factor changes with time and temperature.....	120

LIST OF ABBREVIATIONS / SYMBOLS

ASTM	American Society for Testing and Materials
BHN	Brinell Hardness
BTV	Brake Torque Variation
C.E.	Carbon Equivalent
CNC	Computer Numerical Control
dB	Decibels
DIN	Deutsches Institut für Normung
DOE	Design of Experiments
E	Young's Modulus
E.C.	Eutectic Carbon
EDM	Electrical Discharge Machining
FNC	Ferritic Nitro Carburizing
FRF	Frequency Response Function
G	Shear Modulus
HB	Hardness Brinell
IB	Inboard
ID	Inner Diameter
IESV	Integrated Electromagnetics Stirring and Vibration
ISO	International Standards Organization
LOM	Light Optical Microscopy
MC	Material Confirmation
MMC	Metal Matrix Composite
ND	Nodal
NVH	Noise, Vibration and Harshness
OB	Outboard
OD	Outer Diameter
Q factor	Quality Factor
SAE	Society of Automotive Engineers
T	Tangential
T.S	Tensile Strength
wt%	Weight %

CHAPTER 1

INTRODUCTION

This thesis documents the research efforts to produce a brake rotor with high damping, which can significantly reduce brake squeal noise occurrences.

Chapter Two reviews the literature in the research area. Brake systems and brake rotors are introduced, and the causes of brake noise and typical solutions are discussed. Damping measurements and their associated challenges are noted, and the methods of measurement used for the project are defined. Brake rotor materials are discussed and the effects of the material on damping are reviewed. Various other methods to further improve brake rotor damping including EDM, coulomb damping with inserts, stress relief, etc., are studied, and their limitations are identified. A summary of the review is provided, which leads into the Project Justification and the Project Objectives.

Chapter Three details the initial exploratory research and experimental work done with different electrical and magnetic processes to obtain additional damping improvements in rotors. Benchmarking of various processes and the opportunities for simpler processing methods are discussed. Damping improvements on a large sample size of parts are studied. Material effects are briefly discussed. The chapter ends with a summary of the damping improvements associated with electrical and magnetic processing of brake rotors, and the major findings / discoveries.

Chapter Four describes the experimental work. It includes the characterisation of the material structure and composition required to provide the maximum damping

improvements from electrical processing. Several materials, covering a range of damping and mechanical properties, were studied. Non-destructive tests to evaluate parts before, during, and after processing are shown, the results are discussed. Material microstructure, chemistry and the mechanical properties are all correlated with the base damping of the parts, as well as the damping improvements post processing. The best material structures for maximizing improvements from processing are defined.

In chapter Five, experiments are conducted using the characterised material structure on parts of a different geometry. A confirmation study was completed, to ensure that consistently high damping improvements are achieved. A DOE on some of the most critical process parameters is conducted with these parts and the results analyzed. Material structure and the optimum processing parameters are summarized.

Chapter Six discusses the Noise Validations on various baseline and processed parts. The purpose of this validation was to ensure that the damping improvements translate into a reduction of Noise occurrences.

In Chapter Seven, the other critical rotor performance characteristics are validated. Testing results from baseline and processed parts are compared and analyzed. The effects of time, temperature and wear on the damping improvements are reported and discussed.

Chapter Eight provides the conclusions from the study. It highlights the major findings and discusses the opportunities for future study.

CHAPTER 2

LITERATURE REVIEW

The literature review covers multiple areas associated with this research on the improvement of damping for brake squeal noise reduction. It begins with an introduction to brake rotors and a brief discussion of typical brake rotor materials and properties. Brake Noise and the typical solutions to address noise, damping, measurements of rotor damping and various methods to improve the damping in brake rotors are discussed. This chapter ends with a summary of the literature review showing areas where further improvements could be achieved.

2.1. Introduction to Brake Rotors

Brake rotors are part of the braking system which consists of the brake pedal, hydraulic actuation system with boosters etc., hydraulic lines including brake pipes and hoses and the Foundation Brake System consisting of knuckles, hubs and bearings, rotors, calipers and brake linings [2, 3]. Brake rotors, as shown in Figure 2.1, serve the primary function of stopping a moving vehicle, converting the kinetic energy of the vehicle to heat. This is accomplished by the generation of a braking torque produced due to the frictional forces between the rotor and the pads/linings as shown in Figure 2.1 [2]. The rotors are attached to the wheel using lug nuts as shown in Figure 2.1. When the brakes are applied, the caliper clamps the linings/pads onto the rotor braking surface. Due to the friction between the brake linings and the rotor, a frictional force is generated opposing the direction of motion, which provides the braking torque necessary to stop the vehicle.

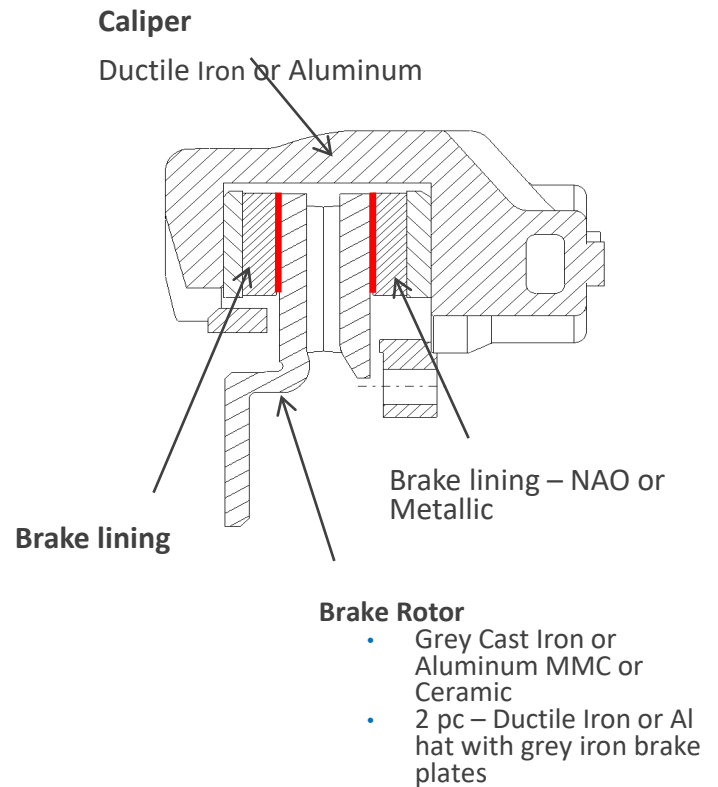


Figure 2.1. Brake Rotor and Caliper Assembly Illustration

Both the rotors and the pads wear with use and the wear rate is dependent on various factors like speeds, braking loads, temperatures, environmental conditions, rotor and pad materials etc. [2, 5, 6, 7, 9]. A stable friction coefficient is essential for safe operation of the vehicle as well as to avoid typical brake warranty issues like Noise, Vibration and also to maintain the brake effectiveness and pedal feel which are essential braking performance attributes and also federal requirements [5, 9]. Brake rotors are a safety critical component and hence the thermal and structural integrity of the rotors are very important [2, 4]. Brake sizing plays an important role to ensure the system has the ability to generate the torque needed to

stop the vehicle, without overheating of components, as well as to ensure that the performance of the individual components does not degrade significantly after usage.

The heat generated due to the frictional force between the brake linings and the rotor depends of the weight of the vehicle and the speed. This heat is then conducted into the rotor and the brake pads. Based on historical engineering work performed at Rassini, thermal models and calculations are most accurate when approximately 80 to 85% of the kinetic energy is transferred to the brake rotor, and the remaining 15% is absorbed by the brake pads and other unaccounted losses [1, 2]. Depending on the nature of the braking schedules, surface temperatures of the rotors could reach over 800 °C [2, 4, 10]. Hence thermal integrity of the rotor and its ability to withstand the thermal shock (generated by the heating and accelerated cooling), as well as thermal fatigue, is extremely critical [10]. Since the brake rotors also have to withstand very high torque generated from extremely high deceleration conditions, structural strength of the different areas of the rotor, including the hat, stress groove, the brake plates and the fins, as shown in the illustrations in Figure 2.2, are very essential to the safe function of the rotor.

The three most critical functions of the rotor in the braking system broadly could be listed as:

- 1) Manage mechanical stresses and maintain structural integrity during the transfer of braking torque from the friction interface to the wheel.
- 2) Absorb the kinetic energy of the moving vehicle by conducting heat from the friction interface.

- 3) Dissipate the heat through conduction and convection, thus retaining a constant capacity to absorb additional braking energy.

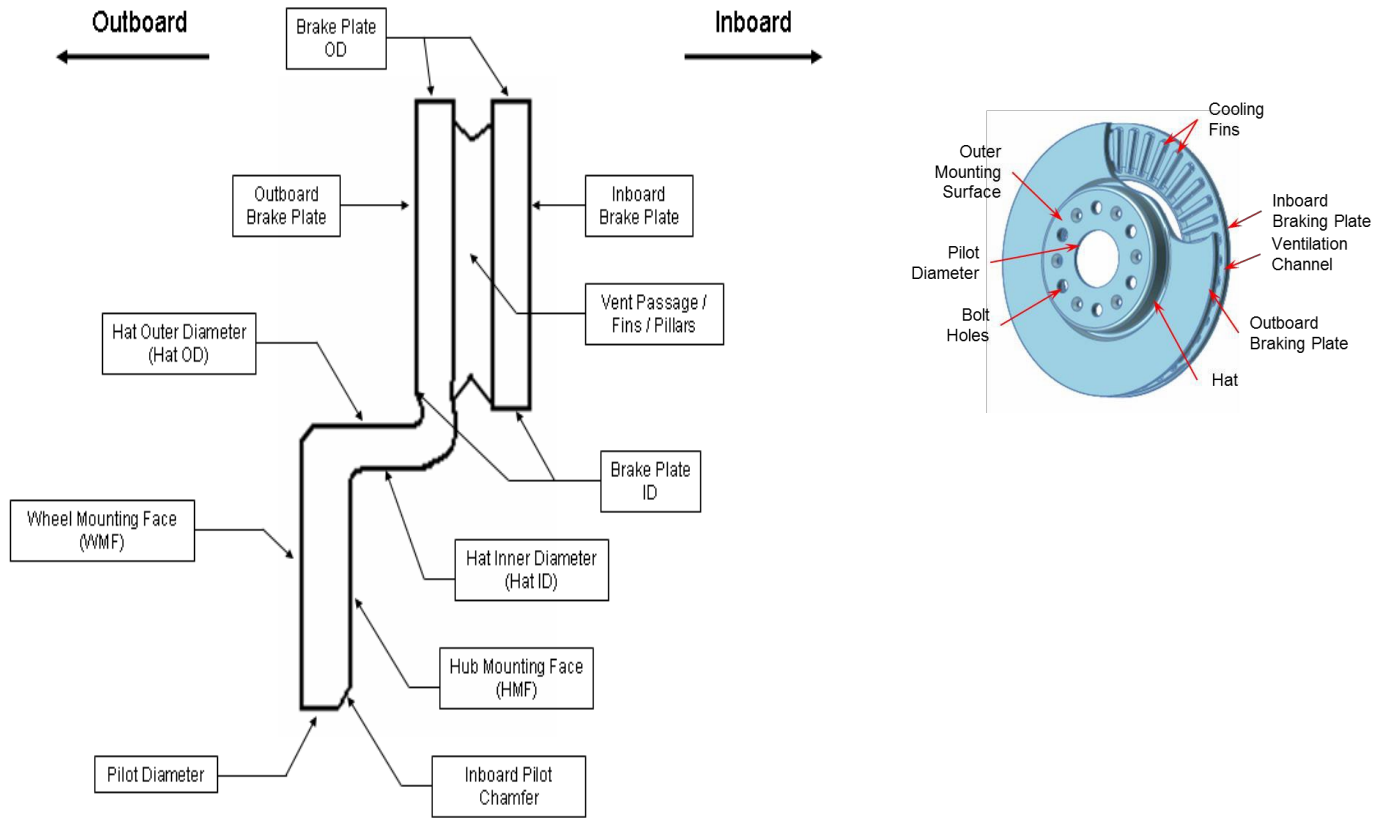


Figure 2.2. Brake Rotor Illustration of different important interface and design areas

2.2. Rotor Materials

Brake Rotors are typically made of Grey Cast Iron with flake graphite, which has been found to be the optimal material for mass production, based on its cost and performance. Grey Iron has very good thermal properties, (mainly thermal conductivity which is very essential for braking performance), great damping properties and excellent friction and wear properties [2, 4, 5, 11, 13]. Despite many efforts to use Aluminum MMC and other

materials for brake rotors, in the quest for light weight components, grey cast iron continues to be the mainstream material for the foreseeable future. Steels and cast irons are classified based on the Carbon and Silicon contents as shown in the Fe-C phase diagram (Appendix 1). Cast irons are further divided based on their phase morphology [54].

Grey cast iron rotors are typically cast in a foundry and then machined to fit the interface dimensions. The rotor materials in common use, fall into the broad categories of the regular grade SAE G3000 Iron (similar to ASTM A48 Class 30B, German DIN GG25, Japanese FC 200), High Carbon materials (same as ASTM A48 Class 25B, Germany DIN GG15, Japanese FC150) and High strength materials (ASTM A48 Class 40B, Germany DIN GG25) [14], which are all characterized by their mechanical properties (Hardness, Tensile Strength). The chemistry and the alloys used, are within a specific range, in order to obtain the correct microstructure and mechanical properties. The microstructure primarily consists of graphite flakes dispersed in a Pearlite metal matrix as shown in Figure 2.3. Pearlite is a hard matrix structure formed by stacked layers of ferrite and cementite and can be coarse, medium or fine and is mostly controlled by the solidification rate and the alloys used. Free ferrite which is the ferrite not part of the pearlite matrix shows up as white spots in the microstructure as seen in Figure 2.3.

Graphite can be many different types (nodular, flake, vermicular etc.) as shown in the Figure 2.4 [17]. Flake type iron is used for brake rotors and the graphite distributions used to rate the Type VII graphite are shown in Figure 2.5. The mechanical properties and the microstructure of the gray cast iron used for brake rotors are regulated by the ASTM, DIN/ISO and SAE standards [16, 17, 18]. The standards show that the graphite is classified according to its type, distribution, and size. Seven graphite types in ASTM A247 are

shown in Figure 2.4 and different distributions of graphite per ASTM A247 [17] are shown in Figure 2.5.

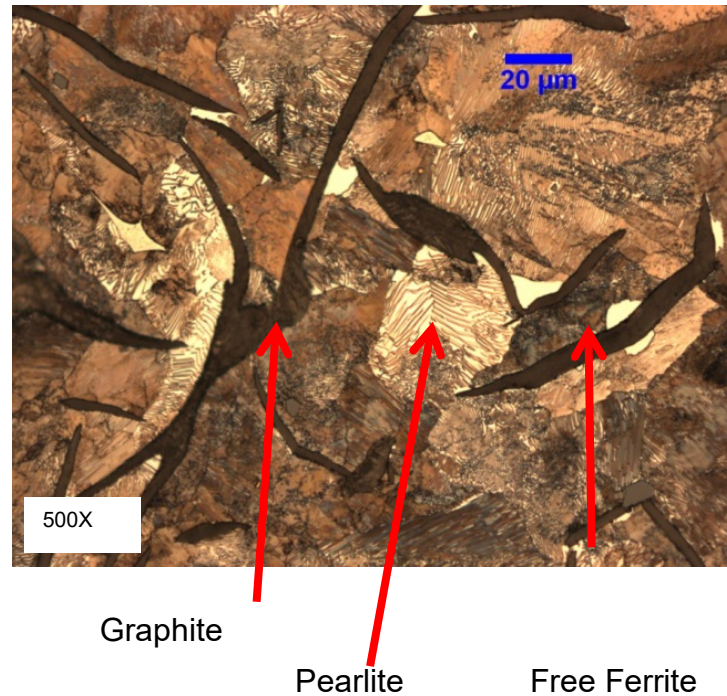


Figure 2.3. Rotor Micrograph showing Graphite, Pearlite and Free Ferrite

Brake rotors are usually made with predominantly Type A Flake graphite for the optimum properties needed for brake performance. Type D & E flakes are typically avoided since they produce a hard brittle structure which could lead to thermal cracking issues during braking and also accelerated wear [5, 6, 9]. In some cases, small amounts of Type B and Type C flakes are allowed. Pearlite Matrix can be coarse or fine depending on the lamellar spacing between the cementite and ferrite plates. Low strength metals typically have finer pearlite and vice versa.

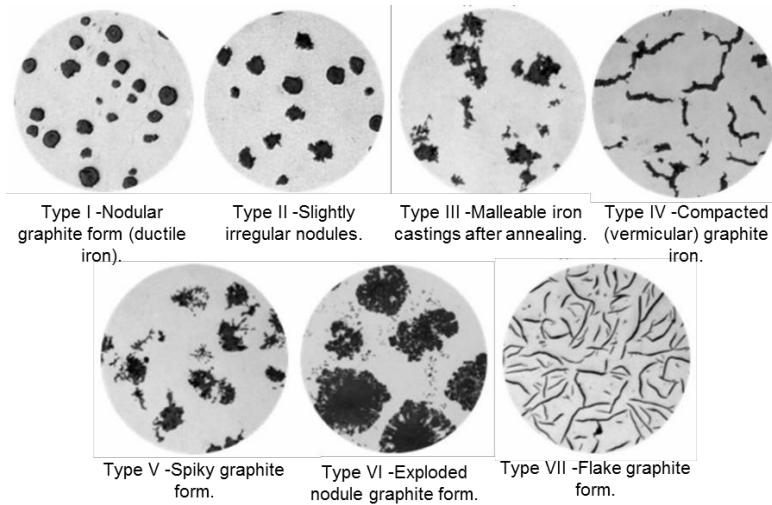


Figure 2.4. Graphite Flake Types per ASTM A247 [17]

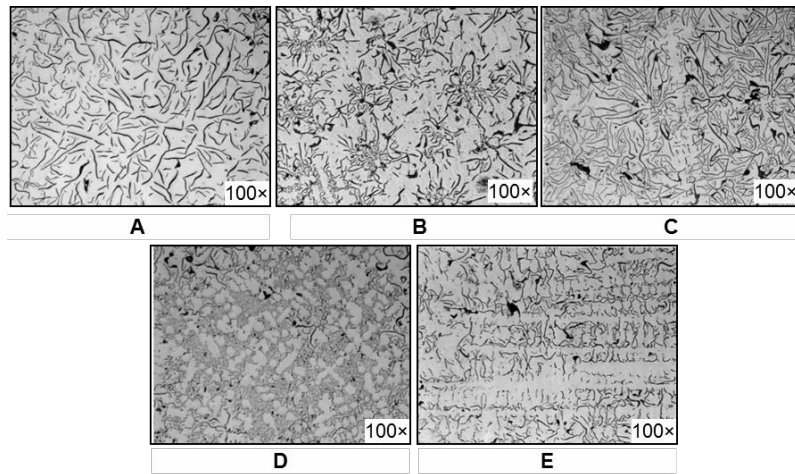


Figure 2.5. Graphite Distributions Used to Rate Type VII Flake Graphite in Gray Iron per ASTM A247. Figures reduced from magnification shown. [17]

Flake size and length also plays a prominent role, and can typically range from 2 to 7 in rotors, depending on the material grade. Larger flake size will result in reduced strength and higher damping and higher thermal conductivity while typically smaller and finer flakes will result in increased strength but lower damping. Classification of graphite flake sizes per

ASTM A247 are shown in Figure 2.6 [17]. The graphite flake size and type are mainly controlled by the Carbon and Silicon content, Inoculation, Solidification and Cooling rates. To ensure proper microstructure uniformity around the entire circumference of the rotors, care must be take in the casting process and gating and riser design as the example shown in Figure 2.7. Typical test specifications in the brake industry include some control of the microstructure uniformity based on hardness measurements.

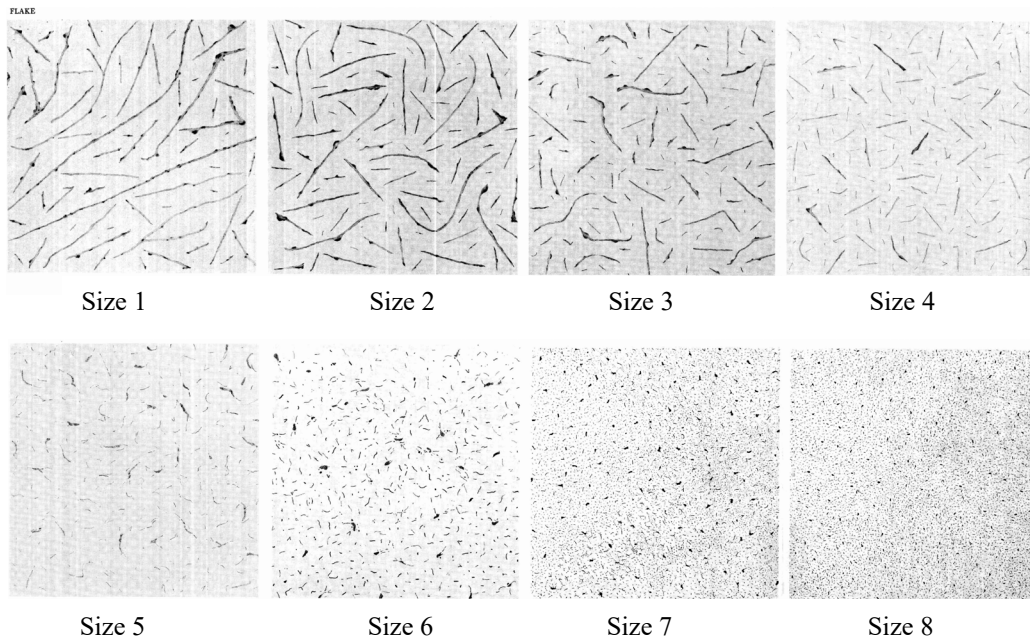


Figure 2.6. Micrographs showing graphite flake size per ASTM A247

Size Class	1	2	3	4	5	6	7	8
Dimension (µm)	>1280	640 to <1280	320 to <640	160 to <320	80 to <160	40 to <80	20 to <40	<20

Table 2.1. Graphite Flake Size per ASTM A 247

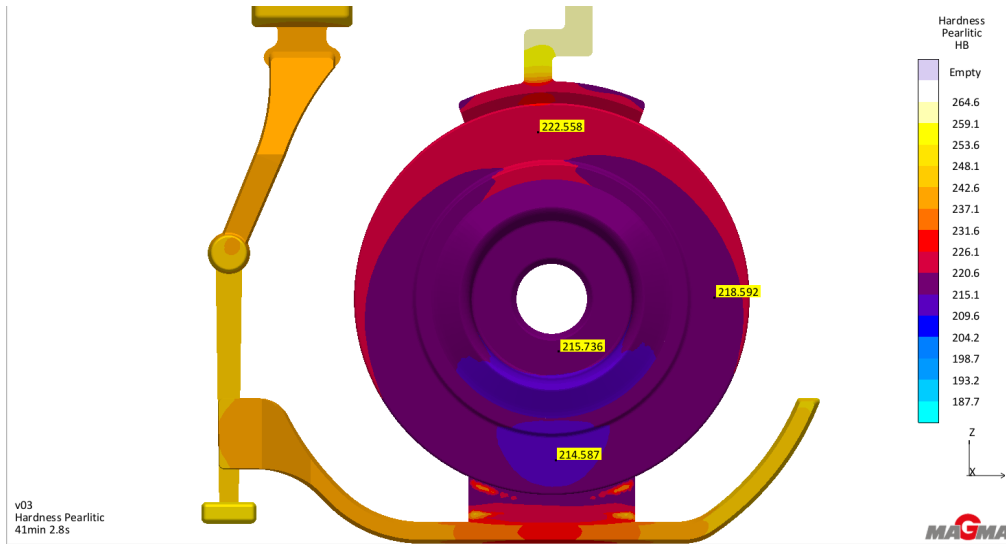


Figure 2.7. Example of Gating and Riser designs to ensure hardness uniformity - using MagmaSoft

Typical composition of a brake rotor for regular and high carbon grades is shown in Table 2.2, where some of the above mentioned characteristics can be observed. The mechanical properties are typically mandatory while the chemistry and the alloy contents can be adjusted within the ranges specified. Based on the strength and damping requirements, different metals are selected based on application. Typically the tensile strength and hardness decrease by ~ 15 to 20% when graphite volume increases from 30 to 50% [36]. So, higher carbon metals typically have lower strength.

The required properties are achieved by adjusting the alloy contents as well as controlling the solidification rate, cooling time and inoculation. The alloy elements which increase graphitization are Si, Cr, Te, N, Co and Al. Ce, Mo and Te are added to refine the graphite size [55 - 59]. N makes the graphite shape shorter and thicker, and develops rounded ends [60, 61]. The quantity of graphite flakes increases with the addition of Ni and Ce in the

inoculant [55, 62]. Cu Mn, Mg, Sn, Cr, Mo, N, Ce promote the formation of pearlite, while Ni refines the pearlite [55 - 57].

The inoculation process is the addition of particles in the melt to promote the nucleation of eutectic grains, and to generate the desired form of A-Type graphite with a minimum amount of undercooling [34]. The chill, which is the tendency of the melt to form iron carbide (white iron), is reduced if the undercooling is minimized [43].

	Low Carbon	Medium Carbon	High Carbon
Benefits and Requirements	High strength and wear Resistance	Good Resistance to distortion and cracking, Moderate damping and Moderate Strength	Improved thermal conductivity and cracking performance, Better damping, Lower Strength
Application	Passenger car market	Passenger vehicles and CUV / SUV markets - Used for Most Automotive applications	Performance Vehicles
Min. Tensile Strength, N/mm ²	250	205	135
Hardness, BHN	197 - 241	187 - 227	145 – 200
Chemical Composition, wt. %			
Carbon	3.0 -3.4	3.3 -3.5	3.6 -3.9
Silicon	1.9 -2.2	1.9 - 2.2	1.8 -2.1
Manganese	0.5-0.8	0.5 -0.8	0.5 -0.8
Sulfur	0.10 Max	0.10 Max	0.10 Max
Phosphorus	0.10 Max	0.10 Max	0.10 Max
Graphite	Predominant Flake A	Predominant Flake A	Predominant Flake A
Size	4 to 6	3 to 6	3 to 5
Matrix		Pearlitic	Pearlitic
Ferrite	5% max	5% max	5% max

Table 2.2. Typical Rotor Material Compositions and Requirements based on application

There are four inoculants groups

1. Standard - mainly Si, Al and Ca
2. Intermediate - Ba, Ti and/or Mn
3. High potency - rare earth, Ce or Sr
4. Stabilizer - contain elements which help to stabilize pearlite; Cr is the most common

Ba, Ca and Sr as inoculants with FeSi were studied by Riposan et al. [63] and they found that the graphitising efficiency ranking was Ba<Ca<Sr. Control of S and Al was found to be important to control the conditions for chill. Use of FeSi and SiC inoculants help to create higher liquidus and eutectic temperature, more A Type graphite as well as a higher eutectic count [68].

The evaluation of the state of the alloy is usually made using the carbon equivalent (C.E.) value. The common C.E. formulae proposed by various authors are identified and shown in Appendix 2. The C.E. and the eutectic carbon establishes the hyper or hypo eutectic state of the alloy. Most common formulae in the industry only use Carbon and Silicon for the calculations and are not very accurate in the prediction of the liquidus or the eutectic point. ASM handbook adds the phosphorous element to the equation. Bazhenov [64] and Shobolov [65] include multiple other alloys to the equation to more accurately predict the eutectic.

The formula by Bazhenov [64] has been used in this research study to calculate the carbon equivalent as well as the eutectic carbon.

2.3. Brake Noise

Brake noise is the most significant warranty concern in the automotive brake industry with some references putting a cost of over a billion dollars spent every year in noise development and warranty costs. Though brake noise is not a safety concern, the effects on customer satisfaction make it one of the most studied components in the brake system development, contributing for over 50 % of the brake development costs [8, 20, 21, 22, 24].

Brake noise have been categorized into many different categories in the industry depending on the frequency ranges. Couple of examples are shown below. Bagwan et al. [29] have categorised them as shown in Figure 2.8. Another very similar categorization as noted by Dunlap [23] is shown in Figure 2.9. Some other authors have categorised them with other names, but in general the noises are divided into three ranges – Low Frequency Noise, Low Frequency Squeal and High Frequency Squeal as mentioned by Dunlap et al. [23]. The low frequency noises like groan, moan, judder etc. are noises in the frequency range of 1 to 1000 Hz. Some of these noise frequencies may be low enough that the vibration is experienced as roughness on the vehicle rather than an audible noise.

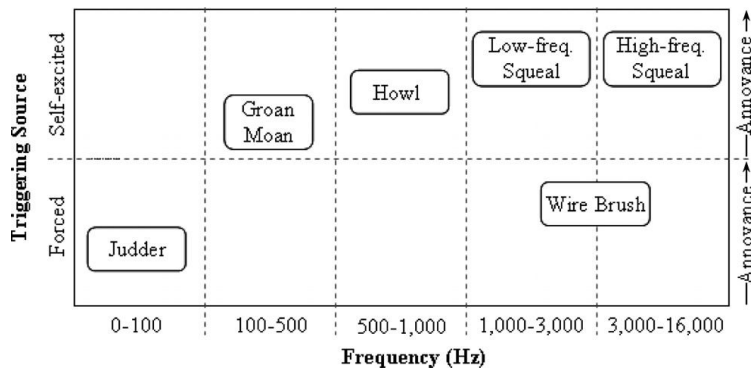


Figure 2.8 – Characterization of brake noise based on frequency ranges. [26]

Noise frequencies in the range of 1000 Hz to 20000 Hz are all categorised as brake squeal. Low frequency brake squeal noises cover the ranges 1000 to 5000 Hz and everything above that to the audible frequency range of 20000 Hz is termed as high frequency brake squeal.

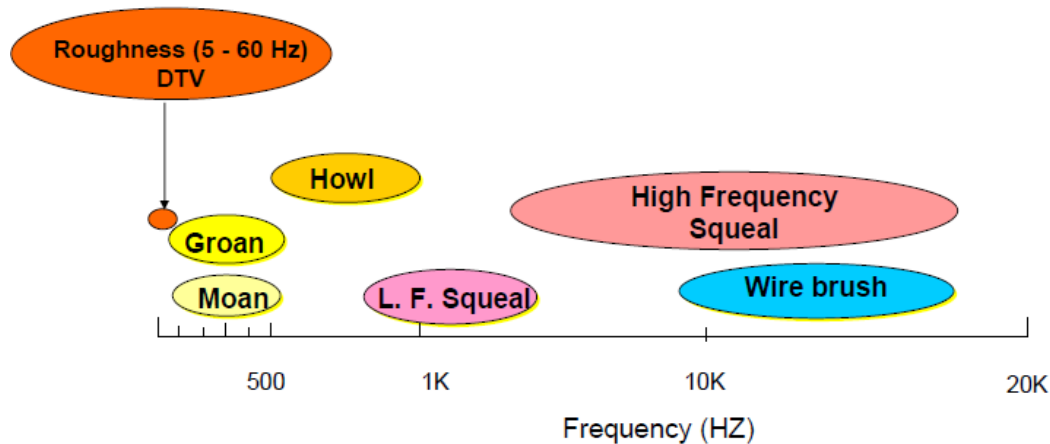


Figure 2.9 – Noise characterization based on frequency range. [23]

Though the brake squeal noise issues have existed since the dawn of automobiles, considerable research and development is still invested in it, due to its unpredictability and system dependence of the squeal on variables, including design of individual corner components, interactions between them and usage history, as well as a significant effect of environmental conditions and other factors. The interactions of various variables make it very difficult to predict the onset of squeal noise.

Once the system design and development is complete and a squeal noise concern arises, the options to have it fixed are limited, incurring lot of costs and tooling changes and timing loss. As mentioned by Triches et al. [19], the noise fixes are iterative and need to be tested on a dynamometer or a vehicle which is time consuming and expensive. Hence a better understanding and prediction of the brake squeal helps prevent future concerns.

2.4. Brake Squeal: Mechanisms and possible causes

Lot of literature exists on the understanding of the squeal and Nouby et al. have done an extensive review of the brake squeal mechanisms and the typical causes [29, 33]. Brake squeal is typically caused due to frictional instability between the rotor and the brake pads. Many different squeal mechanisms have been proposed by various authors over time including the stick slip, sprag-slip, modal coupling, splitting the doublet modes, hammering etc. [20, 21, 29, 33]. Most theories attribute the brake system vibration and consequent noise, to variable friction forces at the pad-rotor interface. These variable friction forces introduce energy into the system. During the squeal event, the system is not able to dissipate part of this energy, and the result is the high level in the amplitude of vibration.

As mentioned by Nouby et al. [33], the difference between the low and high frequency brake squeal, is the mode shapes involved in the modal coupling mechanism. For the low frequency squeal, the modal coupling occurs between the out-of-plane modes of the rotor and bending modes of the brake pad. For the high frequency squeal, the modal coupling occurs between the in-plane modes of the rotor. The brake rotor is typically much stiffer in the in-plane direction than in the out-of-plane direction [33]. Other authors [19, 20, 24, 26, 29] mention that the low frequency squeal is typically a feature that occurs due to frictional excitation coupled with modal locking of the brake corner. Modal decoupling from the calipers and rotors are accomplished by changing metals. High frequency squeal typically coincides with the tangential in plane frequencies of the disc and changes to the brake rotor dynamic stiffness at the specific problem frequency can reduce squeal propensity.

As discussed by Sebastian et al., low frequency squeal, generally considered to be between 1 kHz and 5 kHz (where the first tangential in-plane rotor mode normally occurs), is

influenced by the dynamic behavior of brake caliper, its mounting, the steering knuckle and other suspension components. On the other hand, high frequency squeal (greater than 5 kHz) is usually dominated by the dynamic properties of the brake rotor and brake pads. The primary nature of brake squeal is transient, fugitive and often cannot be repeated under apparently similar conditions. Small changes in speed, brake line pressure, temperature, contact conditions, material properties, geometry or environmental conditions can produce significantly different results.

2.5. Typical brake NVH solutions

As discussed earlier, it can be seen that the material properties and the geometry and temperature play a significant role in the frictional instability produced between the contact surfaces. The typical causes and the components involved in the generation of brake squeal were also briefly discussed in Sections 2.3 and 2.4.

The parameters that seem to affect squeal are braking pressure, rotor and pad materials and geometry, speed, friction coefficient and damping [29].

Increases in pressure were shown to lead to an increase in the unstable frequencies, due to an increase in the friction between rotor and pads. In general, higher friction has higher squeal propensity. This is the reason NVH issues are more prominent in high performance cars in which higher friction low metallic linings are typically used. Shorter lining, groove textured surfaces etc. can reduce or suppress squeal. Most squeals also occur at lower speeds where most of the stick slip, sprag slip phenomena can occur. Damping is utilized extensively to reduce the amplitude of the vibrations. The ideal ways to address the issue would be to design the components in order to avoid the propensities to brake squeal.

Nouby et al. [25] showed that the most significant improvement in brake squeal performance could be achieved by using a combination of rotor material (Al-MMC), cast iron caliper and friction material with elastic properties of 2.6 GPa. It was also seen that the pad friction material contributed 56% of the total system instability (squeal generation). The rotor material contributed 22% of the system instability. Caliper and bracket materials contributed 11% each.

Bagwan et al. [29] mentions that the structural modification in brake disc is the most important parameter to reduce brake squeal. Asymmetry introduced to the geometry was shown to resolve high frequency squeal at higher modes. However, the effects of asymmetry on any other performance characteristics is not investigated.

Belhocine et al. [30] related the Young's modulus of all the components and studied their effects on brake squeal. It was observed that increasing the modulus of the rotor, friction material and anchor brakes all help reduce the number of unstable frequencies and provide better squeal performance.

Malosh [28] also used the relations between C.E. and Young's Modulus to determine the material necessary to resolve the squeal.

Some of the methods to resolve brake squeal, as suggested by Lu et al. [26] are

- Reduce excitation using Brake pad chamfer design
- Increased damping using insulators and shims etc. on brake pad backing plates.
- Shifting component natural frequencies through rotor, pad backing plate, caliper and anchor bracket modification

The methods typically used across the industry, include designing the brake rotors and calipers and pads to ensure modal coupling between these components are avoided. In plane and out of plane modal frequencies are analyzed at the onset of the design studies to ensure

1. There is no modal coupling between the components and
2. There is no coupling between the bending out of plane and the in plane tangential modes of the rotors as shown in the example in Figure 2.10.

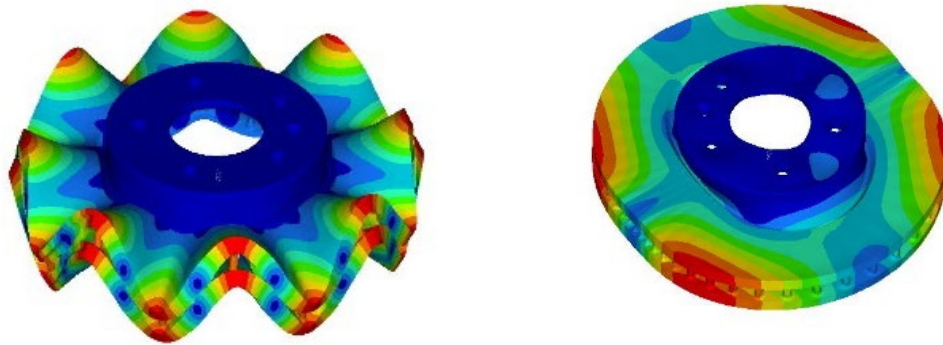


Figure 2.10. Out of plane bending modes and In plane tangential modes of rotor

The frequencies are typically measured using a hammer and a microphone or accelerometers to generate the Frequency Response Function (FRF) plot. Malosh [28] shows a linear relationship between C.E. and elastic modulus and the natural frequency of the rotors. Shift in resonant frequencies based on C.E., was used to resolve noise issues. This was based on changes to the grey iron rotor as well as pad frequencies to eliminate resonance [1, 28].

Material and geometry changes have both been shown to have a significant effect on the modal frequencies of the components. However, geometry changes to the rotors and pads can sometimes be very difficult depending on the timing for the development and associated costs for tooling changes as well as retesting costs.

Damping plays a critical role in reducing the amplitudes of the vibrations and thus reducing brake squeal. Damping is typically achieved through the following means as discussed by Glisovic et al. [32].

- Rotor damping – Typically driven by rotor microstructure and the amount of Carbon and Silicon in the metal. Higher rotor damping helps reduce noise. However, higher the damping, lower the strength and hardness of the rotor [36].
- Friction modification - increase pad damping and compressibility (isolate excitation and increase damping effectiveness), modify the friction level characteristics (to reduce excitation and mode coupling propensity). However, suppliers are typically hesitant to make these changes since they affect friction, wear and other properties also significantly.
- Pad geometry modification (use of chamfers and slots to reduce excitation and mode coupling)
- Under layer modifications (for increased damping, increased compressibility)
- Insulator design (add damping and isolation).

Insulators are a sandwich of steel and other viscoelastic material layers typically with a total thickness of ~ 1 mm and are attached to the pad backing plate as shown in Figure 2.11. They are very efficient damping mechanisms, and are widely used in the braking industry. They provide material damping as well as Coulomb damping.

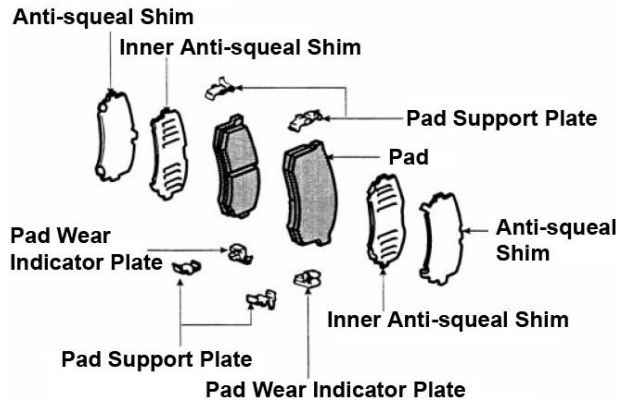


Figure 2.11. Pad Insulators and Shim Illustration [32]

Different insulators typically used are single layer, constrained layer (single and multi layer), double sticky insulators and clip on insulators as shown in Figure 2.12 below.

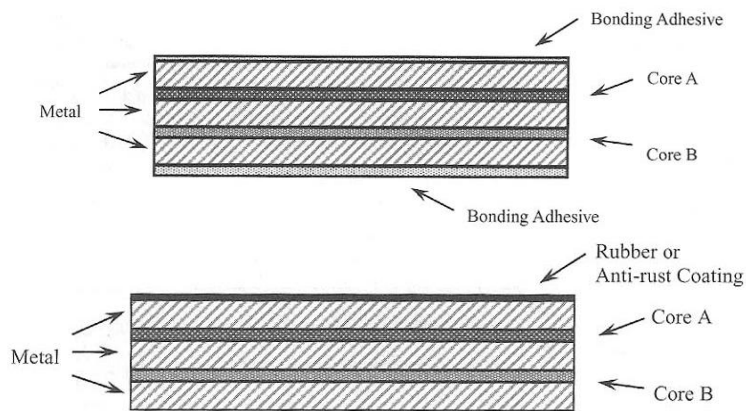


Figure 2.12. Double sticky layer and multi layer constrained shims. [32]

Pad geometry and its effects are also discussed by Dunlap et al. [23] and has been shown to be a significant factor in resolving brake squeal.

2.6. Rotor Material Damping

Damping is an intrinsic property of the material created by internal friction due to the microstructure of the part. It is a measure of the attenuation of the vibration and measures the speed of the decay of its amplitude. As shown in Figure 2.13, the top section shows the amplitude of the vibration decreasing over almost 8 seconds on the time scale. The part with the better damping shown in the lower section shows the same vibration amplitude decreasing to zero in only 3 seconds. This faster decay helps reduce the chances of the noise radiation.

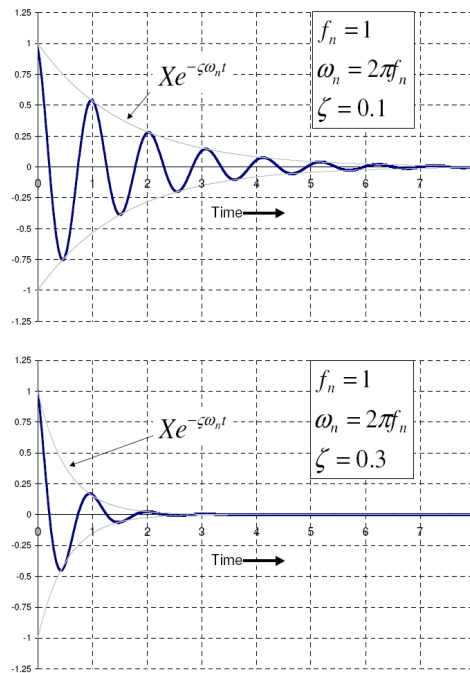


Figure 2.13. Illustration of Damping and Vibration Attenuation

Internal friction and damping in grey cast iron occurs due to the movement of dislocations, domain boundaries and grain boundary movement and precipitated graphite and secondary

particles [35]. Park et al. [36] concluded that the damping of a rotor occurs primarily by the viscous or plastic flow at the interphase boundaries between the pearlite matrix and graphite particles and that the damping capacities are proportional to the total perimeter of graphite per unit area. Typically, the pearlite based grey cast iron has better damping than ferrite or martensitic based grey iron and the damping capacities of the cast iron increases with higher carbon content. Golovin [27] says that the level of the damping capacity of lamellar cast iron depends on the relationship between the elastic and strength characteristics of graphite and the matrix phase. In cast irons with a rigid matrix structure (pearlite, martensite), the energy dissipation is determined by the volume fraction and morphology of the initial graphite phase. In cast irons with a softer metallic phase (ferrite), the contact interaction of graphite inclusions with the matrix and the properties of the matrix introduce additional sources of high damping. It has been observed that with increasing stresses, two stages of the an-elastic absorption of energy of the applied oscillations are seen: a stage of oscillations of pinned dislocations and a stage of micro plasticity caused by the breakaway of dislocations from impurity atmospheres and dislocation motion with the overcoming obstacles existing in the slip planes.

One theory of the damping mechanism in cast iron is that the energy dissipation occurred in the graphite inclusions, so that the damping should be roughly proportional to the amount of graphite in the matrix. However, Adams [37] and Zhao et al. [38] show that the damping of cast iron is only loosely dependent on the carbon equivalent or the amount of graphite, but is better related to the nature of the graphite, i.e. the size and shape of the graphite inclusions. The authors tested 3 different formulations of iron - a hypereutectic coarse flake graphite grey iron (K-123), a hypoeutectic fine flake graphite grey iron (K-148), and a

nodular graphite iron (K-N). The differences in damping of all these metals can be clearly seen in the Figure 2.14, which shows that the coarse flake hyper eutectic irons have the highest damping.

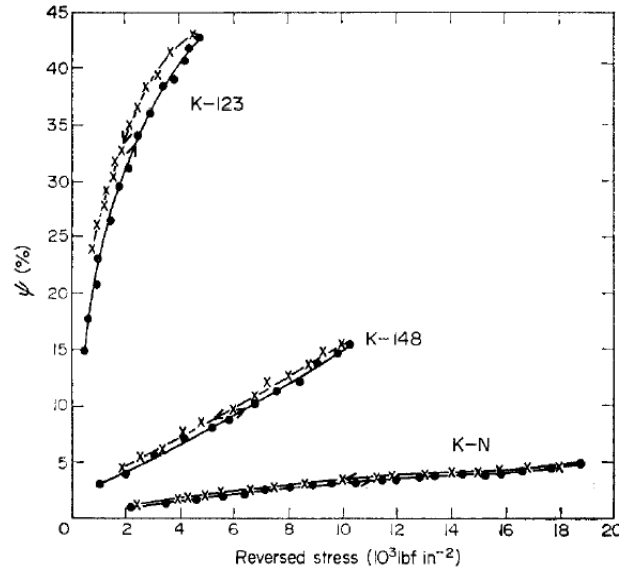


Figure 2.14. Damping vs Stress – Coarse and Fine Flake Graphite and Nodular Iron. [37]

Results from Zhao et al. [38] show that the damping capacity of grey cast iron has good correlation with the graphite shape factor K_o , which is the length of the periphery of the graphite divided by the square root of the area and the kind of matrix. The damping increases with the shape factor value, which means longer and thinner graphite flakes will promote higher damping capacity as show in Figure 2.15.

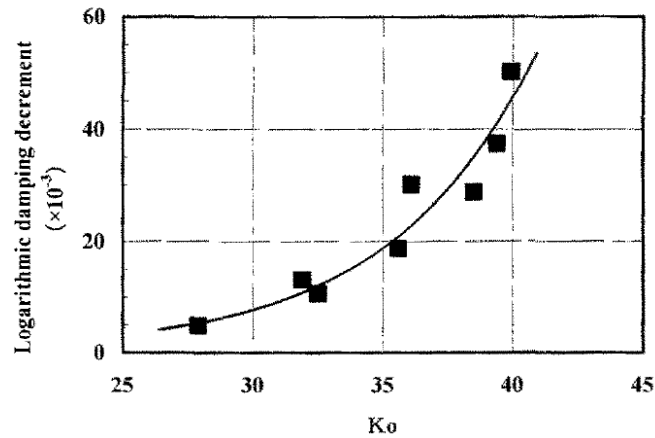


Figure 2.15. Graphite flake shape factor vs damping. [38]

Miller [13] defines that the damping capacity is a function of graphite, size, shape and quantity as well as the lamellar spacing of the pearlite matrix. The frequency dependent damping is due to elastoplastic and magnetoelastic mechanisms. A strong magnetic contribution to the total damping was noted at low frequencies. Magneto-mechanical damping effects are driven by losses due to macro and micro eddy currents in the ferromagnetic materials such as rotors, as well as hysteresis losses due to domain wall movements. Higher Silicon was shown to help dislocation motion leading to better damping. Low Chromium and higher Phosphorous was also found to improve the rotor damping due to formation of phosphides with chromium and manganese, thus resulting in a larger carbide lamellae spacing. In ferritic irons, damping is predominantly magneto mechanical and increases with growth in the size of grains and domains. Nonmagnetic damping contributions grow in pearlitic matrices with graphite etc. [40].

2.7. Rotor damping measurement

Material damping is an intrinsic property of the metal and can be measured in many different ways [34]. Various methods have been used to evaluate and measure damping and different factors have been used to express the levels of damping. Per Graesser and Wong [34], the most widely used measures of damping capacity include the Inverse Quality Factor Q^{-1} , tangent of the phase lag, $\tan \Phi$, ratio of loss modulus to storage modulus, E''/E' , loss factor, specific damping capacity, log decrement and damping ratio.

One of the easier and well utilized methods to measure bulky components like brake rotors is the Quality Factor (also known as Q factor). Q factor measurements are based on FRF data - frequency and amplitude plots (as shown in Figure 2.16), which are a standard quality control tool in the brake industry. If peak data is available and the damping factor is low, the Q factor can be a valuable tool to predict the damping capacity of the rotor. It is determined by the half power bandwidth of the response amplitude versus frequency (FRF) plot. Uhlig [44] had developed a method to measure the Q factor on brake rotors and a similar process was used for this study. This method is reliable in benchmarking the damping of a brake rotor.

The method is based on the 3db drop in the amplitude of the frequency response function (FRF) [1] for the 2ND mode. The modal Q factor is measured by applying an impact force to the part and measuring the frequency response using a microphone. Since power and energy are proportional to the square of the amplitude of the oscillation, the bandwidth on an amplitude-frequency graph should be measured to $1/\sqrt{2}$ of the peak or approximately -3 dB as shown in Figure 2.17. The width of the peak determines the damping of the part. In the Figure 2.17 below, f_3 is the natural frequency and f_1 and f_2 are

the frequencies at 3dB drop in the amplitude of the frequency response function (FRF) which is show in Figure 2.17.

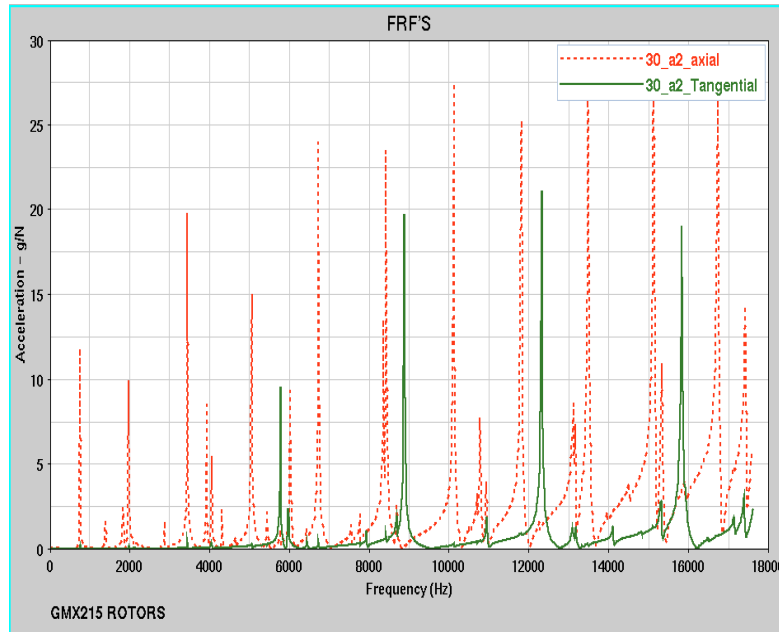


Figure 2.16. Frequency Response Function plot showing the modal frequency peaks

For this study the Q factor improvement was based on the measurement method discussed above and was limited to the 2 ND modal peak only. It was found in initial studies at Rassini that the damping at 2 ND mode translated to similar damping at all the other modal frequencies as well. Hence, to save time, only the 2 ND mode based Q was used.

The biggest disadvantage of this method is that it is not sensitive to stress changes. Also, the Damping measurements are very influenced by setup, temperature and geometry. Hence care must be taken to ensure repeatable and accurate measurements.

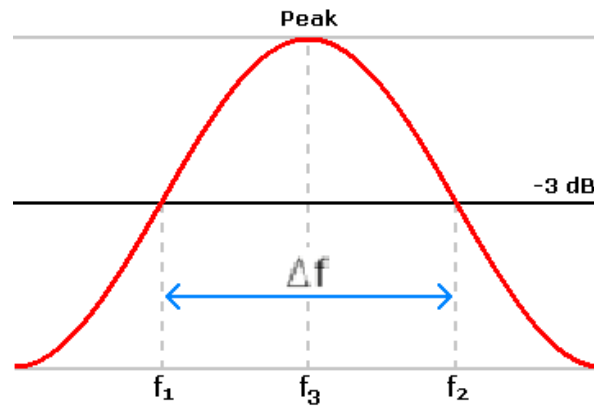


Figure 2.17. Q factor calculation

$$Q = \frac{f_3}{(f_1 - f_2)}$$

Experiments done at Rassini showed a lot of variation in results depending on the location of the hammer impact, the setup of the microphone, the temperature of the parts etc. So, care was taken to ensure all the variables were controlled during the project.

The set up for the measurements is based on an input from a hammer impact, the frequency response is recorded using a microphone set up exactly 180 degrees apart, as shown in the Figure 2.18. The spacing of the microphone and the hammer from the rotors is predetermined and is the same for all the measurements. Rassini procedures were implemented to have the impact at the antinode locations of the rotor to ensure the least variation. Multiple measurements are taken at the same location and an average of 3 measurements is used. [1]

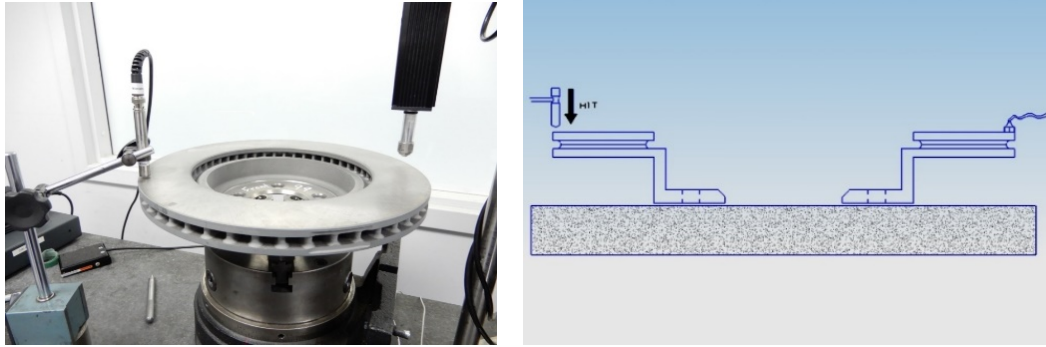


Figure 2.18. Damping measurement set up

The FRF plot thus obtained from the impact is used for the Q factor measurement, at the 2 ND mode using the 3 dB drop method, as discussed earlier.

A master rotor was used prior to every measurement to ensure the setup, temperature and other variations are minimal. The Master rotor Q measurements and the typical variation in Q is shown below in Figure 2.19. Temperature of the parts during measurements were maintained in the range of 70 to 73 F. Less than 3 % variation was seen on the master part Q factor, with time and multiple measurements.

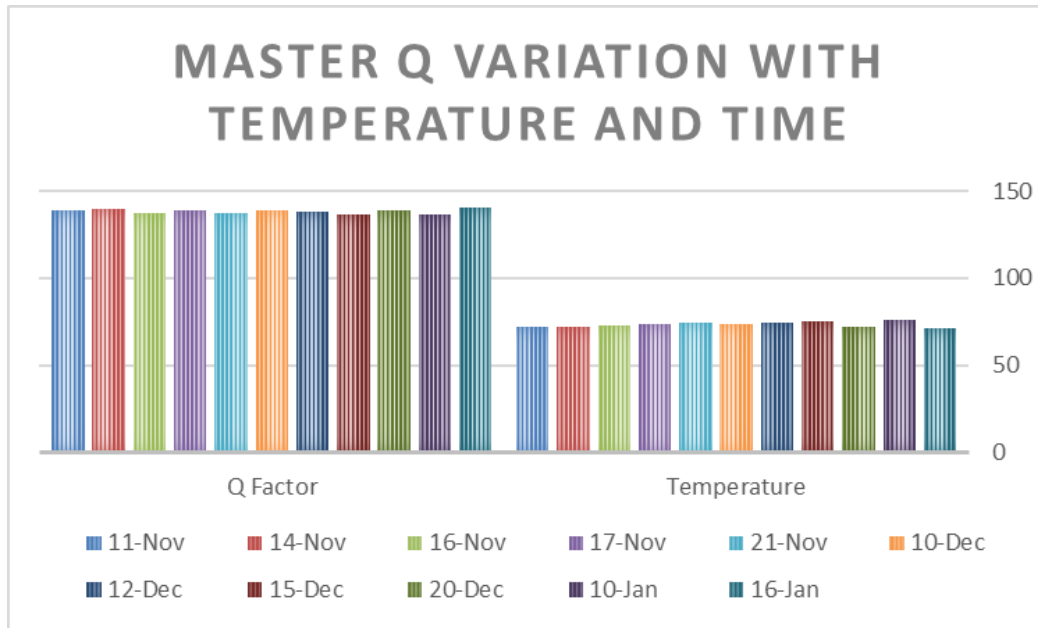


Figure 2.19. Master Rotor Q Factor Variation with time and temperature

2.8. Other methods used to improve rotor damping

Stress relieving processes have been used on brake rotors to improve damping performance. This can be achieved by multiple means including heat treatment, vibration, or magnetic treatment. Damping improvements of 10 to 15 % are seen. The thermal process typically involves heating the rotors to over 600 °C for a soak period of time (1 to 3 hrs.) before cooling them down back to room temperature. Typically, about 85 % of the residual stress in the parts are removed from this process [52]. Pulsed magnetic treatment has been used by [66, 67] to reduce the residual stress of parts by up to 24 %. All of the above processes relieve the residual stresses in the part produced from the casting process, thus allowing for freer movement of dislocations, slip planes, domain walls etc. This helps to improve the internal damping characteristics of the part. However, it has been noted that there is a drop in strength and hardness of ~ 15 to 20 % due to the heat treatment processes.

Much research has happened in the past years to incorporate active damping, using Coulomb damping techniques, in brake rotors. Inserts have been used in the rotors plates to promote damping. Very low Q factor and high damping are achieved through these techniques. Hanna et al. [45, 47] and Dessouki et al. [46] addresses the coulomb damping by casting steel inserts and rings in the grey iron brake plates as shown in Figure 2.20. The rings are positioned in the molds and the rotor plates are poured around it. The production feasibility remains an issue, since the rotor plates are cast around the steel plates as part of the casting process, which results in deformation of the steel inserts, porosity issues on the part and other casting defects. Other inserts like SiC have also been researched but most of these techniques induce a lot of stress points in the casting process due to the brake plates solidifying around the insert plates.

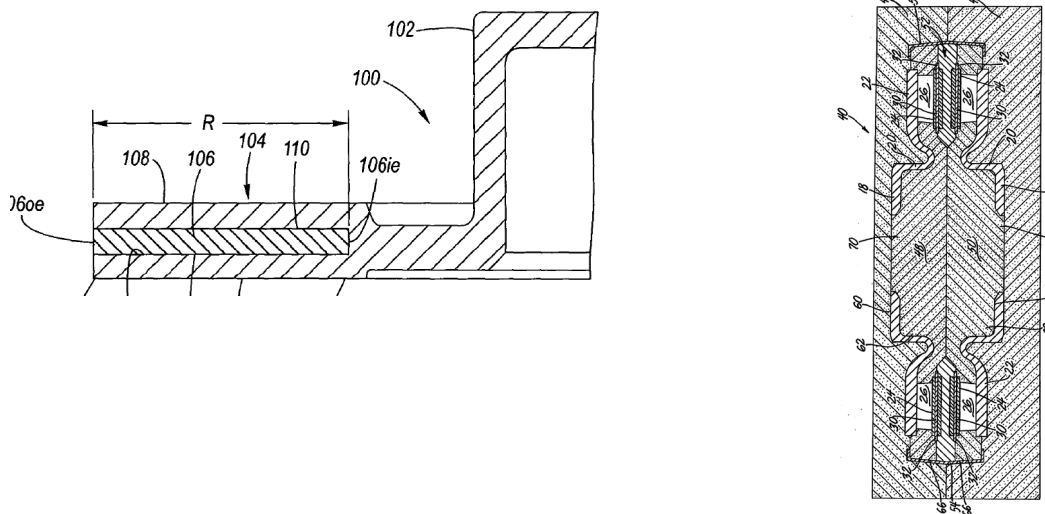


Figure 2.20. Inserts cast into the brake plates for improved damping [46]

Patent # US20180298964A1 from Ford addresses the deformation issue by having the rings in a sheath at different diameters thus providing inserts support at certain diameters instead

of using a full large ring covering the entire rotor radially. This helps in reducing the deformation associated with the insert plates.

The costs for achieving these kinds of rotors are exorbitant and involve a lot of additional materials requiring tight tolerances (steel plates, rings, ceramics etc.) and manufacturing costs (scrap rate due to casting defects). However, the important observation is that very highly damped rotors, that can completely eliminate noise, can be achieved. Authors mention complete elimination of noise occurrences with the use of these rotors.

EDM machining of the rotors has been researched and very high damping improvements have been observed [49]. Daudi et al. [49 - 50] discuss the machining of the brake rotor plates and other surfaces using the electrical discharge machining process and improved damping seen on these rotors. Authors [49 - 51] have also provided information on the high damped rotors, with the Q factor in the 200 range thus generated, help in the reduction of noise occurrences in vehicle testing. Dickerson [50] also discusses other grinding operations after EDM processing to generate a surface finish feasible for rotor performance. Typically ~ 300 microns of metal was removed from each brake friction plates, which is in the range normally used for the final finish turning operation of the rotors. Q factor improvements ranging from 40 to 70 % have been recorded, and a high reduction of noise occurrences is observed.

The two principle types of EDM processes in use are the die sinking and the wire EDM process. The removal of material in electrical discharge machining is based upon the erosion effect of electric sparks occurring between two electrodes. The rotor acts as the work piece or the cathode, and a conducting electrode, like graphite or copper, is the anode. The Voltage Difference between the electrode and work piece produces electron flow from

the electrode to the work piece. Electrons bombard the work piece vaporizing small areas of the surface thus machining the part.

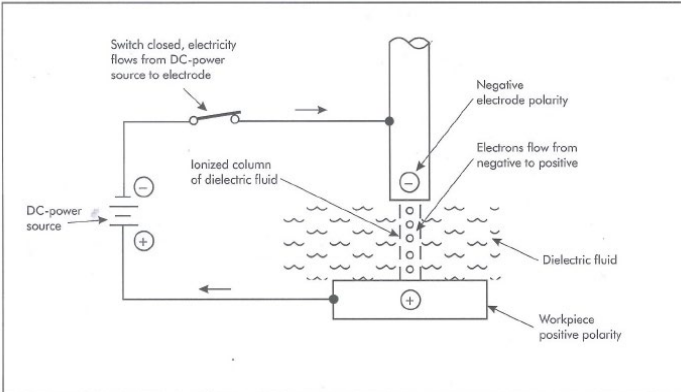


Figure 3-12. Spark-electron flow with negative electrode polarity.

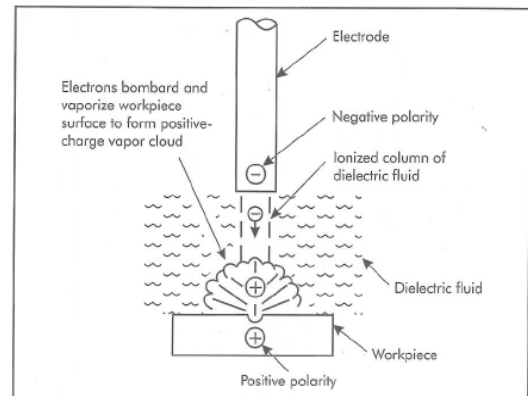


Figure 3-14. Electron bombardment produces vapor cloud.

Figure 2.21. EDM Machining process illustration

No understanding of the EDM processes and its variables / process parameters or its effects on the rotor damping are provided by any of the authors. Very little literature is available on why there are any damping improvements due to the EDM processing. Daudi [51] observes that the graphite length may be changed due to the EDM process. EDG machining was shown to generate thicker longer denser flakes as compared to a conventional machined rotor. Authors concluded that the rapid heating to over 3000 °C and the rapid quenching causes this phenomena [51].

Dynamometer test data on EDM machined parts show noise improvements. However, no understanding of the effects of this machining process on other rotor performance characteristics, is provided by the authors. The EDG machining process is very time consuming and cumbersome compared to the typical CNC turning processes used for high volume rotor production.

2.9. Summary of the Literature Review

Brake noise is a significant warranty concern in the automotive industry with many millions spent on development, testing and warranty costs every year. Noise reduction enhances customer satisfaction, saves a lot of money in warranty returns, and reduces brake development costs.

Typical methods for brake squeal reduction include active damping elements, frequency modifications based on geometry and material that can be expensive, as well as have an effect on other performance characteristics. All these modifications could also result in a lot of iterative retesting costs.

High Carbon materials with thin and long flake graphite type A have been shown to provide the best damping possible with the grey cast iron metals. Rotors with a very high damping with a Q factor < 300 , can help eliminate noise in brake systems. However, it is very difficult to achieve these levels on a consistent basis using material alone, due to strength and manufacturing restraints.

Additional processing techniques have been shown to further improve damping and reduce noise. Many methods, as listed below have been utilized:

Use of Steel or SiC inserts in brake plates, which is very effective in terms of damping improvements, but is expensive and a lot of manufacturing feasibility and performance issues exist.

EDM processing to machine the rotors, used by Hayes is time consuming, cumbersome and adds a lot of manufacturing costs. It also may have other performance issues, which have not been analyzed or reported.

Stress Relief operations (thermal, magnetic or vibratory) can be effective and reduce residual stress as well as improve damping. However the processes are time consuming and expensive. They also reduce the hardness and strength of the rotors.

2.10. Further study

Based on the above summary from literature review, it was evident that very high damped rotors can significantly reduce noise occurrences. Some of the additional processing seem to benefit these aspects significantly, and hence the initial research was geared toward understanding how to utilise one of these methods to create a highly damped brake rotor. EDM processing could work to improve damping and possibly may have fewer manufacturing feasibility issues compared to the coulomb insert damping process. If the process to attain these damping improvements from EDM was simpler, better understood and less time consuming, it could be a feasible solution. So, the initial exploratory research was geared toward better understanding of the EDM process and its effect on damping improvements.

CHAPTER 3

EXPLORATORY RESEARCH

Based on the conclusions from the literature review, initial exploratory research was carried out to fingerprint the variables in the EDM process and to analyze the effects of the processing, in a little more detail. The process as proposed by Daudi [49 – 51] is very cumbersome for higher volume production and not very feasible, due to the amount of machining and the extra processes needed for meeting the surface finish requirements. One of the biggest issue with the whole process is that the brake plates were being machined, which is time consuming. Also, the effects of the very high local temperatures seen during the EDM machining on the functional friction surfaces may have other performance effects and these effects are not very clear in all of the research. The initial plan of study was to determine if the damping benefits are obtained only if the rotor friction surfaces are machined or can also be obtained if any of the other non functional areas of the rotors are machined.

3.1. EDM Experiments

Tests were set up with a vented front rotor (278 mm OD x 25 mm rotor thickness) and processing was done on Ingersoll EDM equipment from Apollo EDM, as shown in the Figures 3.1 and 3.2 below. 16 rotors, all of the same rotor type and geometry as well as from the same casting foundry batch, were used for the study. Graphite electrodes were used for the test. Test was set up to only machine 3 raised extrusions on the back of the stress groove areas of the rotor, thus avoiding any contact with the friction surfaces. Figure 3.2 shows the areas of the rotor that were machined for this test. As seen, the areas of EDM

machining are not on the friction surfaces but in a location that should not affect the fit and function of the rotor.



Figure 3.1. Power source and Ingersoll EDM machine

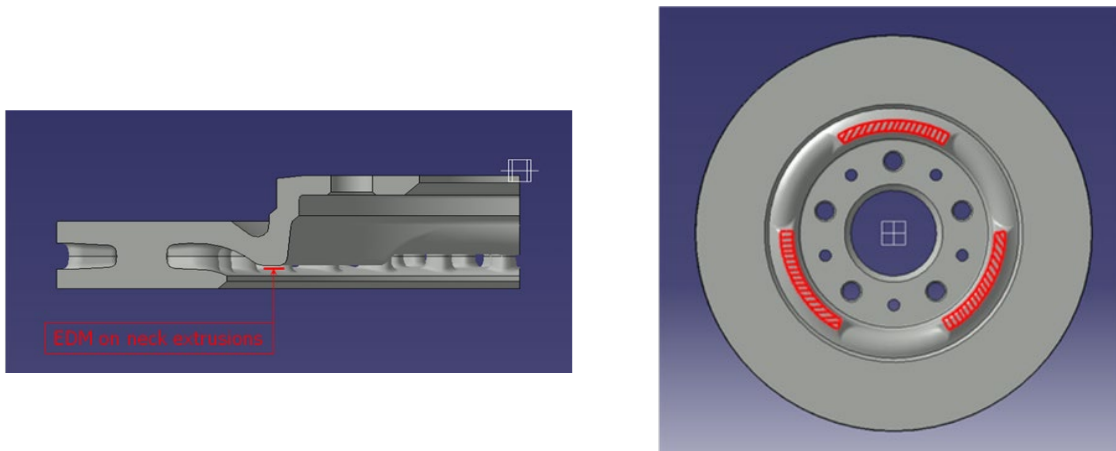


Figure 3.2. Machined areas during processing

Process was performed for 2 minutes and the current used was 20 amps. Material removed was less than 0.05 mm. These parameters were based on some initial tests which showed no significant differences in damping effects between 2 or 10 minutes of processing time, as

well as no effects of changing the polarity. Q factor was measured on the rotors before and after processing, to understand the changes in damping.

3.1.1. EDM Test Results

Pre Q factor on all these rotors were in the range of 570 to 650, as shown in the Figure 3.3. All processed rotors showed significant damping improvements, with some rotors showing as much as a 50 % reduction in Q factor. Post process Q factor is seen to be in the range of 300 to 440 with a mean Q factor of ~ 370, showing an improvement of the order of 30 to 50 %.

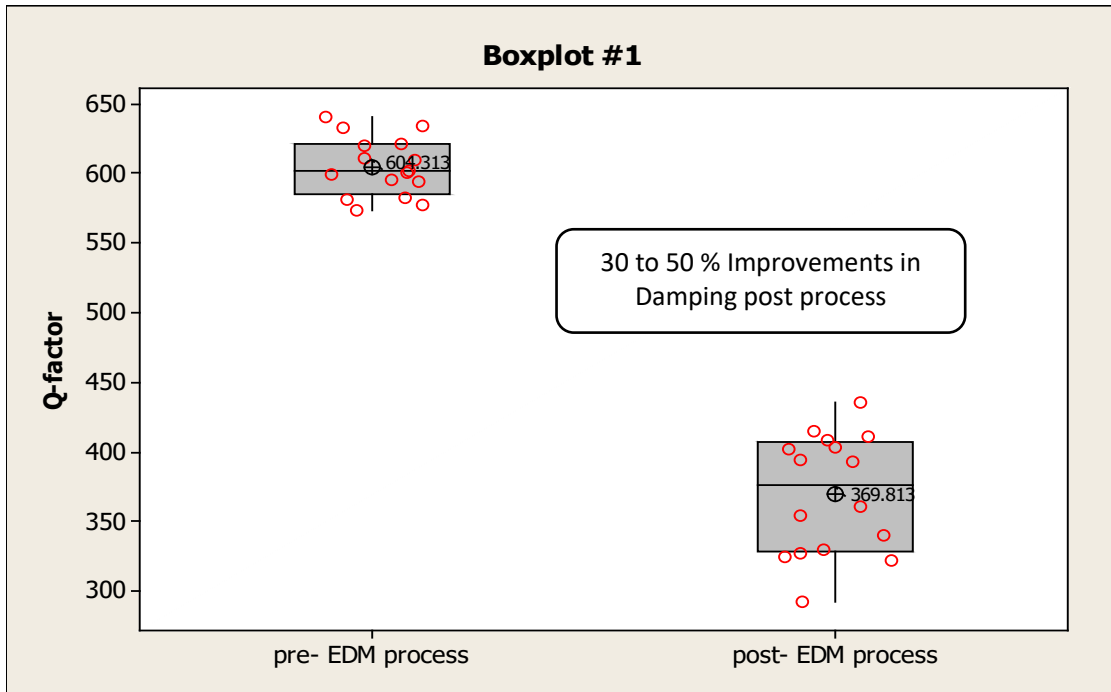


Figure 3.3. Damping improvements after processing

This is a very significant discovery since the processing time is minimal, large damping improvements are seen and the functional areas are not affected. Based on the literature

review, the information pointed toward microstructural changes to the graphite flakes in the brake plates due to the localised melting temperatures from the EDM process [5] as the primary reason for the damping changes. However, in this test case, the brake plates are untouched and still a large damping improvement is observed.

3.2. Magnetic Field Experiments

Due to the electric nature of this process and the rotor being in an electric circuit, the change was thought to be electromagnetic in nature. Some of the literature showed that pulsed magnetic treatment was effective for stress relief which typically should help internal damping. To determine if this theory held any value, rotors from the same batch were magnetised in a magnetic coil, typically used for Magnetic Particle Inspection tests. These tests were carried out at XRI Testing. Q factor was measured pre and post process. The magnetic coil works on the principle of Maxwell law of current passing through the coils thus producing a magnetic field as shown in the Figure 3.4 below.

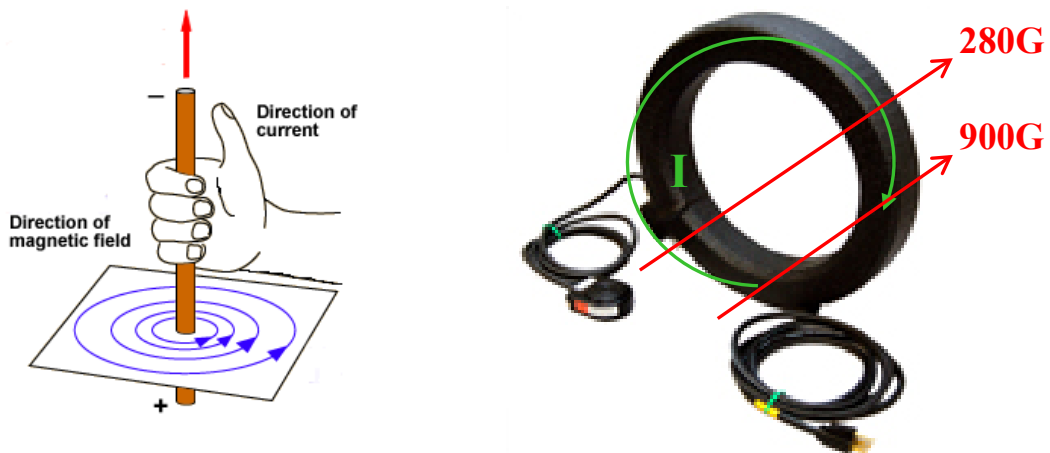


Figure 3.4. Maxwell's law and Magnetic Coil

A gauss meter was used to check the magnetic field on the rotor as well as in the magnetic coil, during the processing. The current used was ~ 3000 amps and the processing time was

approximately 5 seconds. At 3000 amps, the magnetic field was ~ 900 Gauss closer to the coil and ~ 280 Gauss at the center of the coil. Once the parts were magnetized in the coil, they were run through a demagnetizer and demagnetized. Magnetic fields of less than 0.5 Gauss was seen on the rotors after the demagnetization is completed. After both these processes are completed, the parts were re-measured for Q factor. As shown in the Figure 3.5 below, a 20 to 30 % improvement in the Q factor was seen. These tests indicated that the damping improvements were due to the rotor being in an electric or a magnetic field.

Different currents of 10 amps, 1000 amps, 3000 amps and 10000 amps were used to see if there is an effect of the amperage on the damping improvements. There was no significant difference observed, as all rotors showed approximately 20 to 30 % improvements in Q factor.

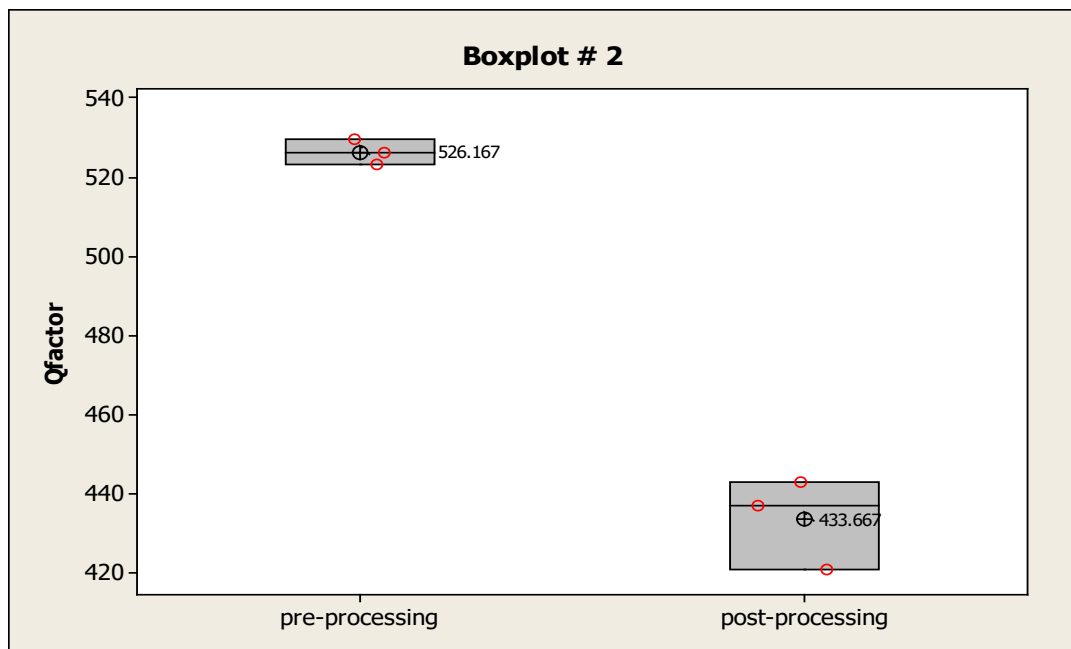


Figure 3.5. Boxplot of pre and post process Q factor

3.3. Process Benchmarking

The electrical and magnetic processes were benchmarked to characterize the electrical signals. The EDM process was benchmarked using a Rogowski coil, gauss meter and an oscilloscope. Rogowski coils were wrapped around the areas where the signals need to be measured. The Rogowski probes are a toroid of wire that can measure the current through the cable around which they are wrapped or encircled. The output of the coil gives a voltage that is proportional to the current.

As seen from the Figures 3.6, the EDM process uses a power generator that provides the required voltage to the electrodes. For this project, typical values used are a current of 20 amps and voltage is controlled in the 70 – 80 V range. The power generator is connected to the EDM machine as shown in Figure 3.7. It was also discovered during the trials that the EDM machining could be performed on any conducting sacrificial metal placed on the brake plates, as shown in Figure 3.7 and Figure 3.8. This method achieved similar damping improvements as the other processes. The Rogowski coil is wrapped around the rotor in the locations shown in Figure 3.9.



Figure 3.6. Power Generator and controls for the EDM machine

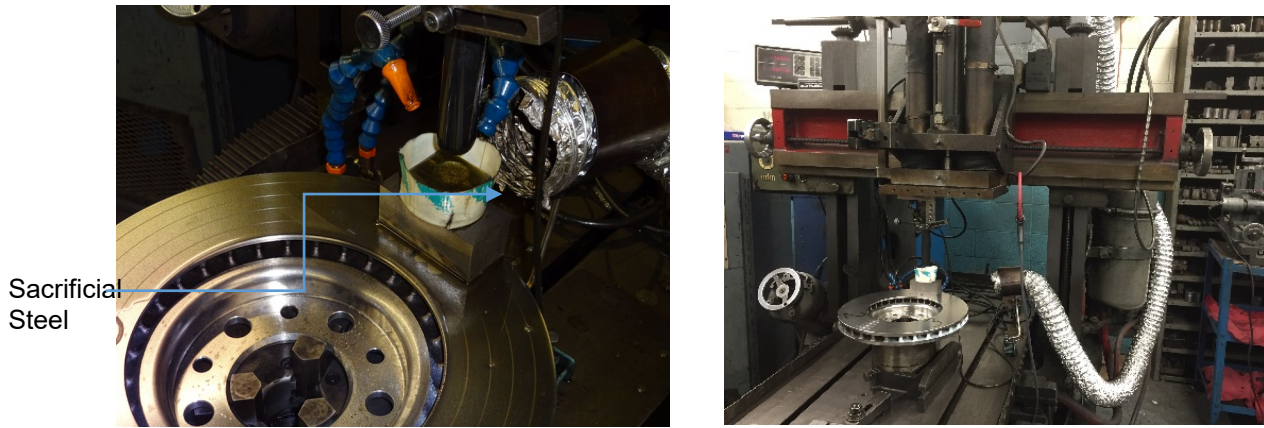


Figure 3.7. EDM Machine setup and the sacrificial steel machined on rotor plate

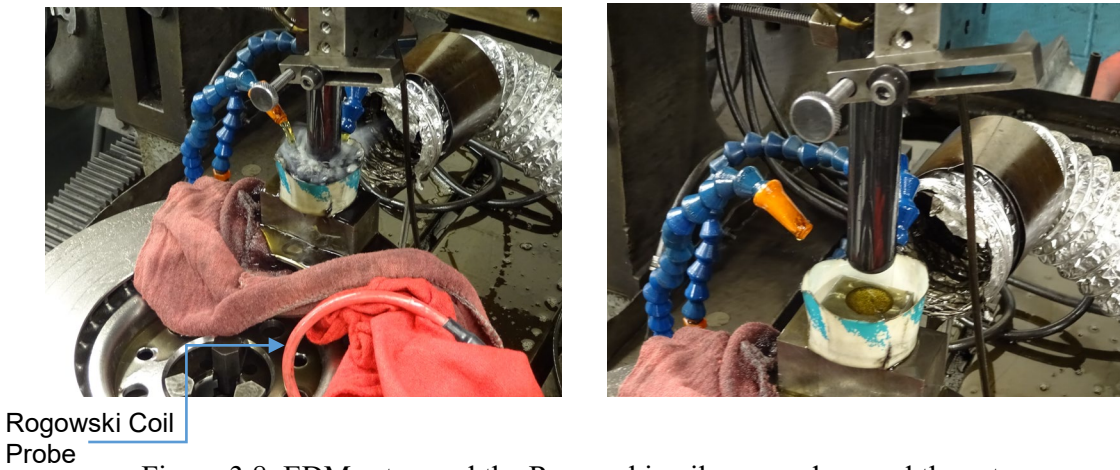


Figure 3.8. EDM setup and the Rogowski coil wrapped around the rotor

As the machine is running, the signals are monitored on the oscilloscope. The signals as seen on the oscilloscope are shown in Figure 3.9 shown below. Current is ~ 20 amps and the frequency of the signal is ~ 6 KHz.

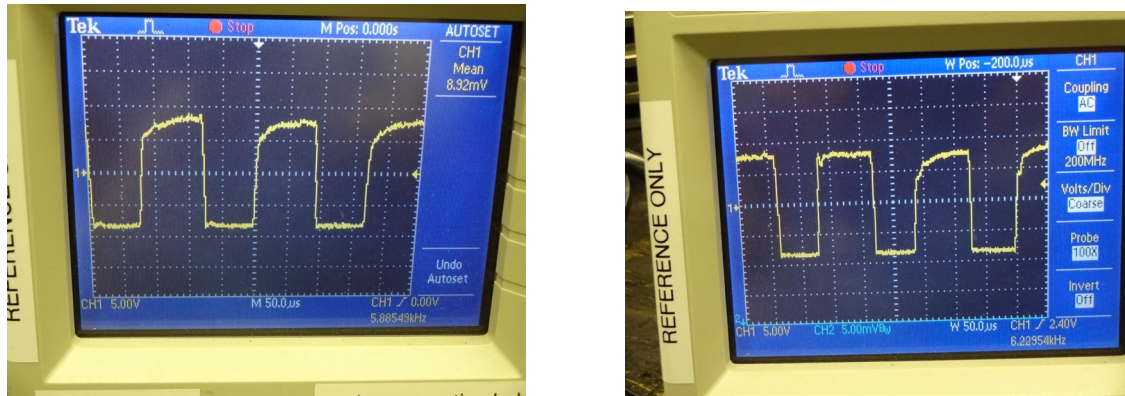


Figure 3.9. EDM signal measured by the Rogowski probe and the oscilloscope

The power source used for the EDM is bulky, has a lot of complexity and controls that may be not very applicable to the machining needed for this project. Polarity changes and gap control and voltages are not very important. Current, time of processing, frequency etc. may need to be monitored more to understand any variations.

3.4. Development of the IESV power generator

Based on the results from the EDM machine, a much more compact IESV – PDCS50 power signal machine was built by Dr. Marcin to simulate the EDM signals, as well as provide a range of currents and frequencies, for further optimization. The equipment is patented under US Patent # 7,255,828 and Canada Patent # 2,455,072. It could produce currents up to 50 amperes and has a signal frequency range of ~ 50 KHz. The parts can be continuously monitored using the Rogowski coil and oscilloscopes. The connections were set up similar to the EDM. The rotor is in circuit and the current flows through the part as shown in Figure 3.10 and Figure 3.11.

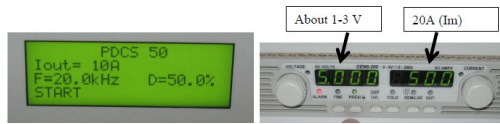
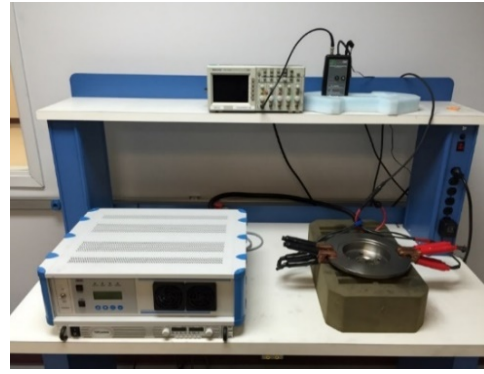
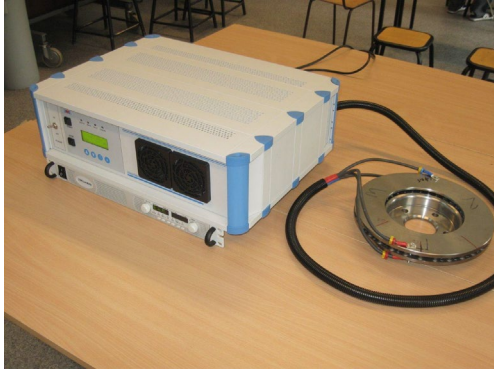


Figure 3.10. IESV equipment set up and the current and frequency

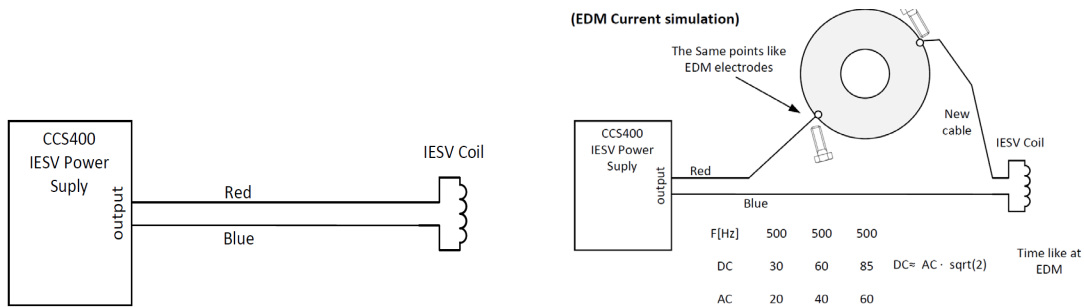


Figure 3.11. IESV connections

The IESV equipment was built in Poland by Dr. Marcin and shipped to the University of Windsor for further experiments. Rotors were processed using the IESV PDCS and Q factor was measured before and after processing. Result show a damping improvement of 15 to 25 % as shown in Figure 3.12. A similar part was processed by both EDM and IESV, and the results compared to ensure similar benefits were seen from both process. Results are comparable, as shown in Figure 3.13. The parts show between 10 to 25 % improvements from IESV and ~ 15 % with EDM process.

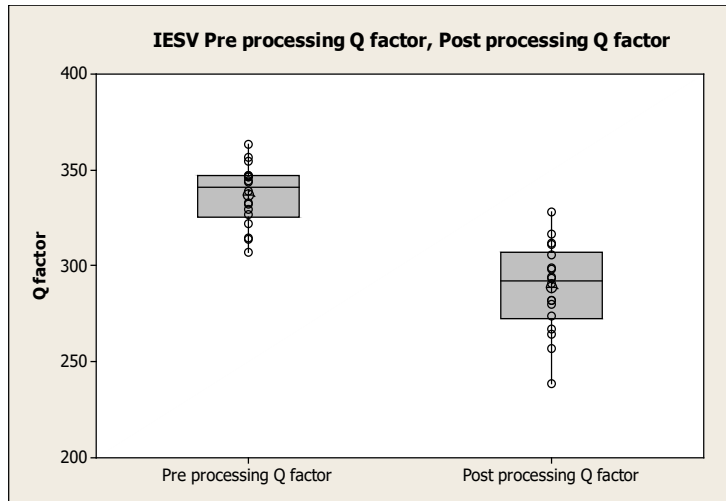


Figure 3.12. Q factor pre and post processing with an IESV

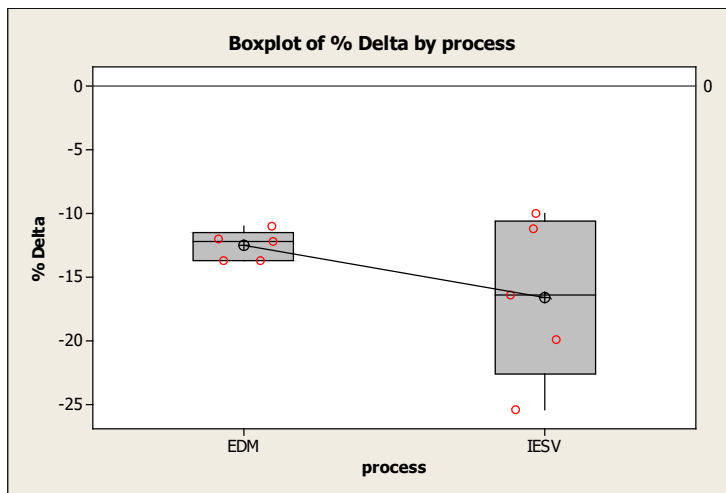


Figure 3.13. Comparison of % Q improvements from EDM and IESV processing

A simple DOE was set up to determine the main process factors affecting the damping improvements from the IESV processing. The DOE matrix was set up with 3 main variables of current, frequency and time as shown in the Table 3.1 below.

Configuration	Frequency (kHz)	Current (Amps)	Time (s)
(1)	5kHz	5A	10s
a	40kHz	5A	10s
b	5kHz	25A	10s
c	5kHz	5A	120s
ab	40kHz	25A	10s
ac	40kHz	5A	120s
bc	5kHz	25A	120s
abc	40kHz	25A	120s

Table 3.1. Process DOE parameters matrix

Q factor was measured before and after processing. The results, as shown in Figure 3.14, show no statistical effects of any of the 3 variables studied.

A second DOE was set up with a different rotor and similar variables at more levels. Q factor was measured pre and post processing. Results show ~ 10 to 20 % improvements in Q factor. As seen from the main effects plots in Figure 3.15, time and current may have a statistical effect but there is no effect of frequency.

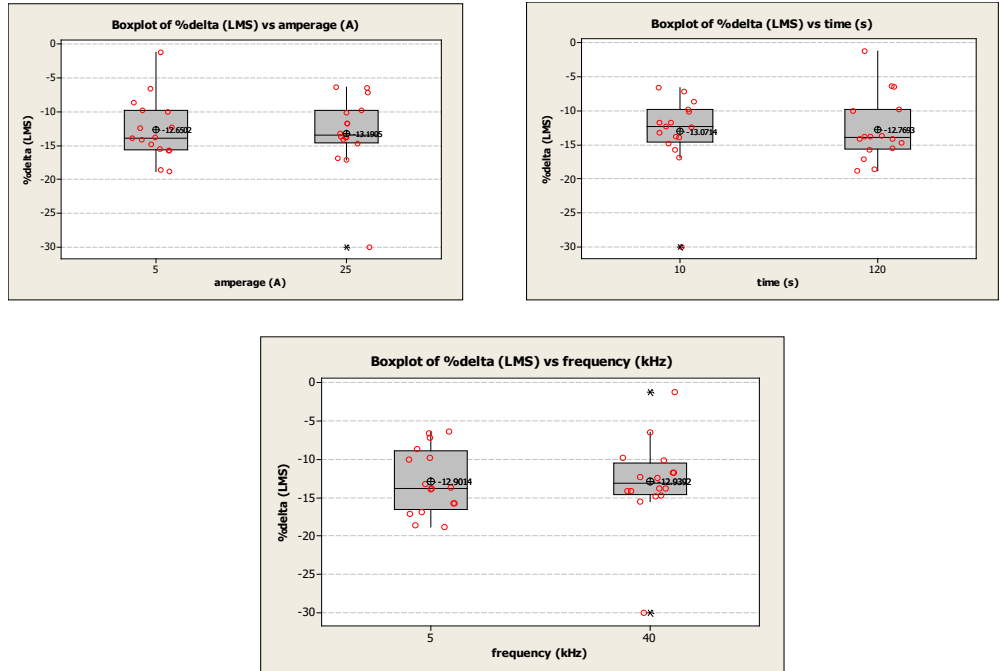


Figure 3.14. DOE results showing the effects of time, current and frequency on Q factor improvements

Part ID	Frequency (KHz)	Time (seconds)	Current (amps)
15	50	10	50
14	50	10	20
1	5	10	5
7	20	10	5
12	20	120	50
2	5	10	20
18	50	120	50
16	50	120	5

8	20	10	20
9	20	10	50
17	50	120	20
11	20	120	20
4	5	120	5
6	5	120	50
10	20	120	5
13	50	10	5
5	5	120	20
3	5	10	50

Table 3.2. Second DOE Matrix with current, time and frequency

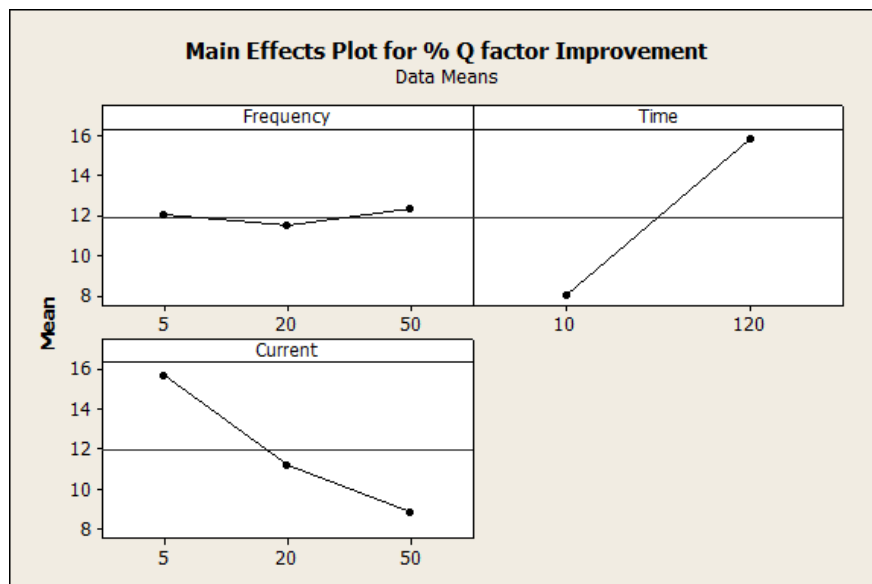


Figure 3.15. Main Effects plot for % Q factor improvement after IESV processing

The two DOE show slightly different results in terms of the statistical effects of the variables. However both show improvements from the processing. The effects of the rotor geometry and material are not well understood and may have an effect.

3.5. Large Sample Batch Study

Based on the results seen from these initial experiments, the study was expanded to a larger scale to understand if there was any variability to the consistency of the damping improvements from the processing. 63 vented front rotors with a rotor OD of 300 mm and Thickness of 26 mm were used for the study. All the parts were premeasured for FRF and Q factor and then processed by EDM. The EDM process done was 2 minutes and 20 amps current plates on the Ingersoll machine. Graphite electrodes were used and the three plates (placed approximately 120 degrees apart on the inboard plates as shown in Figure 3.6) were machined. This ensured no changes to the geometry of the rotors.

The results were absolutely not consistent. Some parts showed 0 % improvement and some showed over 50 % improvements in Q factor as seen in Figure 3.16. This was a very odd result since all the tests to this point on the parts, showed very consistent improvements in damping. A quick analysis as seen in the figure 3.16 shows that the rotor pre process Q factor seems to be ranging from ~ 400 to almost 1200. Q factor is driven by geometry and the material. It was also noted that, in general parts with a lower pre process Q factor showed better post process Q factor.

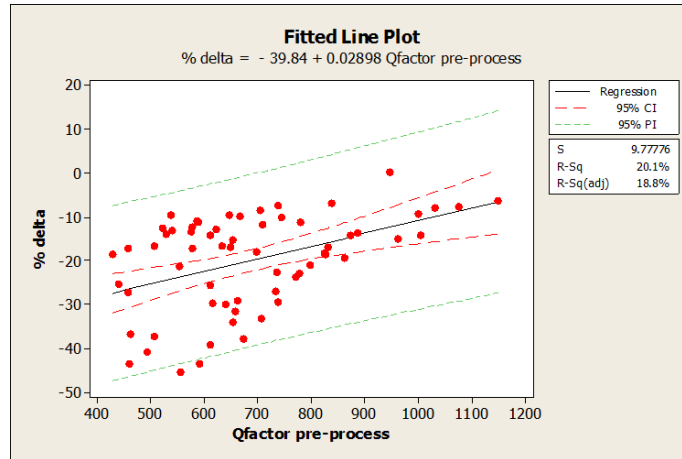


Figure 3.16. Fitted line plot of the % change in Q factor after processing vs pre process Q factor

A very linear relationship is seen between the Pre process vs Post process Q factor as shown in Figure 3.17.

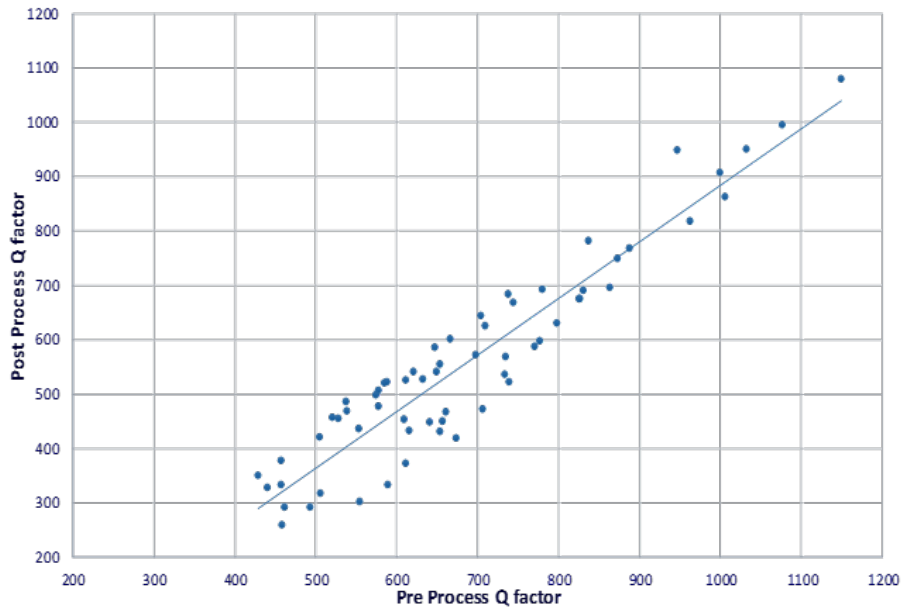


Figure 3.17. Pre process vs post process Q factor results

Since the geometry was very similar, barring minor differences due to casting tolerances, the main difference had to be the material. The material batch data measured for each

foundry batch pour for the different rotors was analyzed and the data correlated with the Q factor improvements.

- Brinell hardness was measured using a 5mm ball at 750 Kg load at 3 locations 120 degrees apart, at the center diameter of the plate.
- Tensile strength test was accomplished using the wedge penetration test method per Rassini specification EI 080.001.

Results show that parts with the lower hardness and tensile strength, showed the most damping improvements from the processing. But there are a lot of overlaps and inconsistencies seen from the contour plot shown in the Figure 3.18.

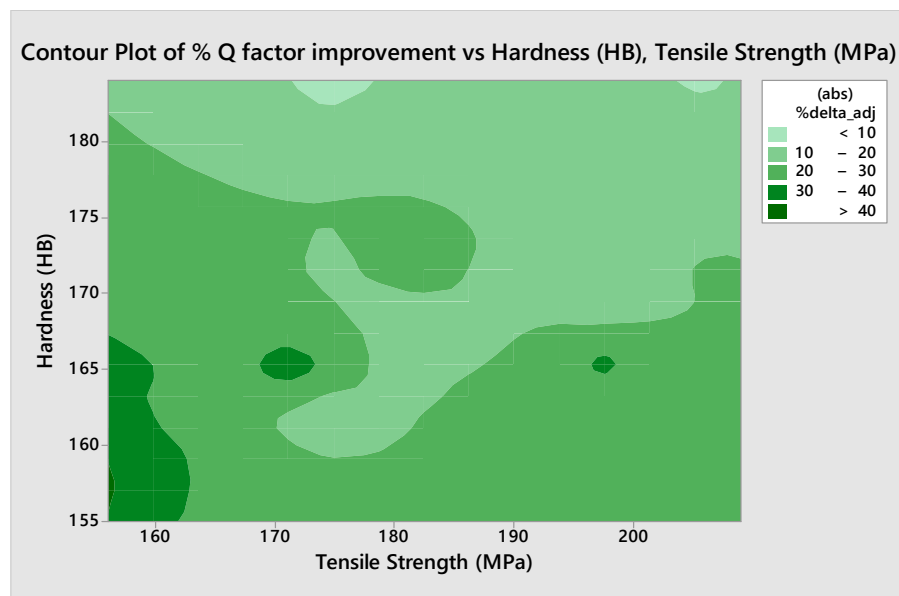
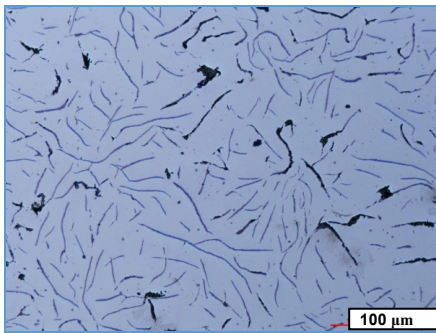


Figure 3.18. Contour plot of % Q factor vs Brinell hardness, tensile strength (MPa)

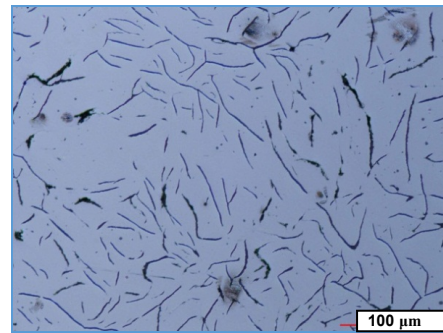
Some of the rotors, that had different ranges of damping and different grades of improvement post processing, were selected to analyze the microstructure:

1. 3 Parts with low pre process Q factor that showed large damping improvements,
2. 3 Parts with low pre process Q factor that did not show a large damping improvement
3. 3 Parts with high pre process Q factor that did not show any damping improvements

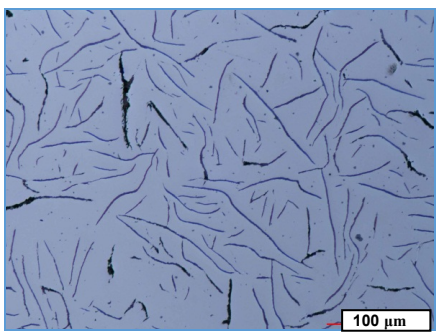
Results are shown below in Figure 3.19. As seen here, the microstructure shows that all 3 rotors have predominantly Type A flake graphite as shown in ASTM A247 charts. The parts with the lowest pre process Q factor (462) Sample # 3 shows predominantly very large flake A graphite size in the range of 2 to 4, with some C Type graphite.



Sample #1 - Q – 521 to 456 - 12%



Sample #2 - Q – 1032 to 951 - 8%



Sample #3 - Q – 462 to 292 - 37%

Figure 3.19. Micrographs (100X) showing the graphite flake distribution in 3 samples of varying Q factor improvements from processing

A very clear aspect in terms of the damping improvements is seen, post processing. The parts that showed the largest improvements have very large graphite flakes in the size range of 2 to 4. The Sample #1 also has large graphite flakes in the 3 to 5 range and a low pre process Q factor but it is not clear why the damping improvements are not as significant. Sample # 2 has finer flakes in the 3 to 6 range, a very high Q factor pre process, and almost no improvements from the processing.

3.6. Noise Validation

Based on the literature review, the main effect of the processing was to reduce the noise occurrences. So, noise testing was conducted on a Link Dynamometer per the SAE J2521 specification with the cold noise section included.

Testing was run first on a baseline rotor with no processing, from one of the EDM projects discussed earlier.

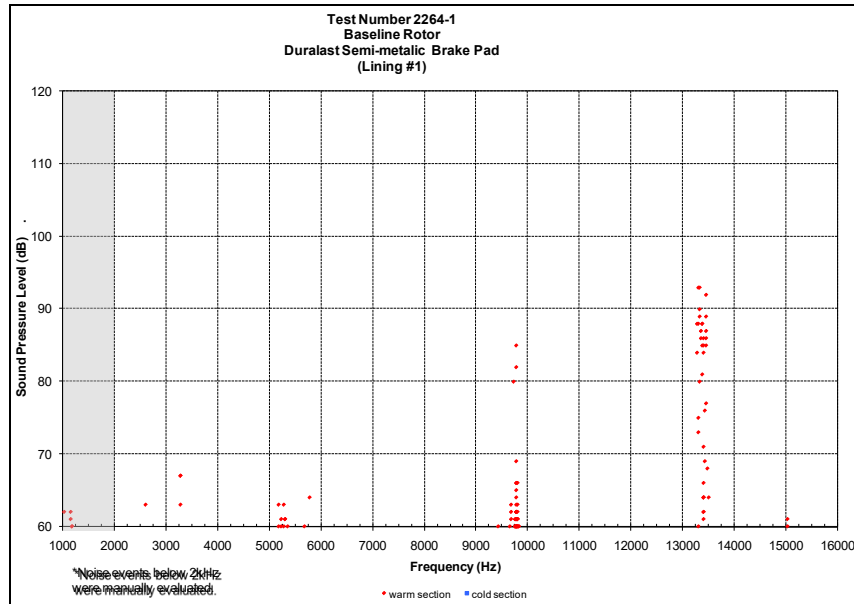


Figure 3.20. Noise Tests results of a baseline rotor

The Q factor on that part was ~ 350. The Baseline test shows a lot of noise occurrences at 10 KHz and 13.5 KHz and a few hits at lower frequencies as seen in Figure 3.20.

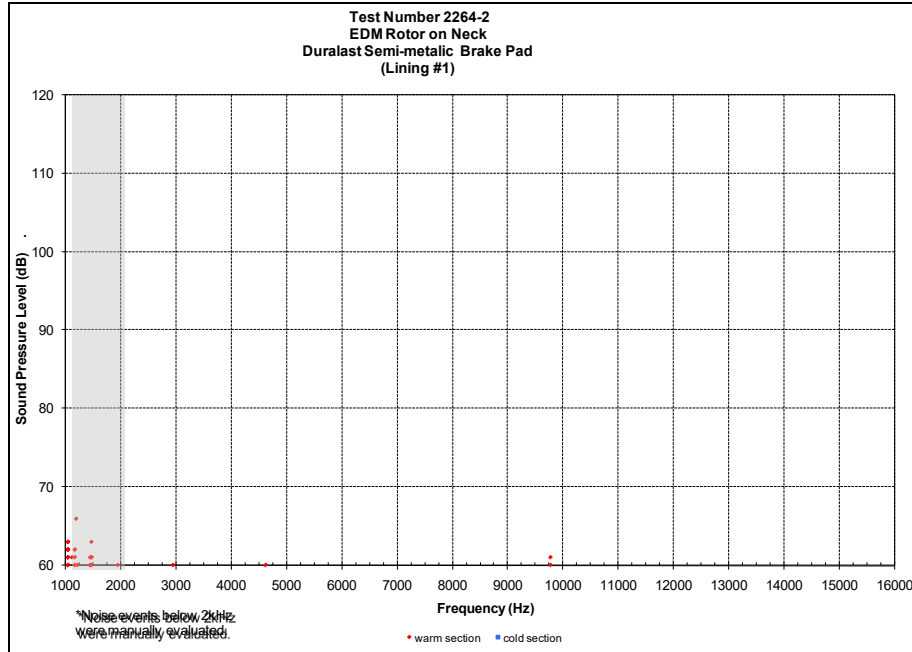


Figure 3.21. Noise test results of EDM processed rotor

A rotor from the same batch was processed using EDM and the processed rotor was tested using the same SAE J2521 test with a new set of brake pads. The processed part had a Q factor of ~ 260, and as seen from the Figure 3.21, the noise occurrences were completely eliminated at 13.5 KHz and 10 KHz. The lower frequency hits are also removed. This is a very positive result since the entire premise of the project is that the additional processing will be able to generate damping improvements that can reduce noise occurrences.

Another confirmation test was run on a different brake system. Baseline parts and test show a lot of noise in the 14 KHz range as well as low frequency noise as shown in Figure 3.22. Baseline Q factor was in the range of ~ 500. Parts were processed using EDM and the

results show a large reduction in the noise hits at the high frequencies and lesser noise occurrences at low frequencies also. In general ~ 80 % reduction in noise hits was seen, as shown in Figure 3.22.

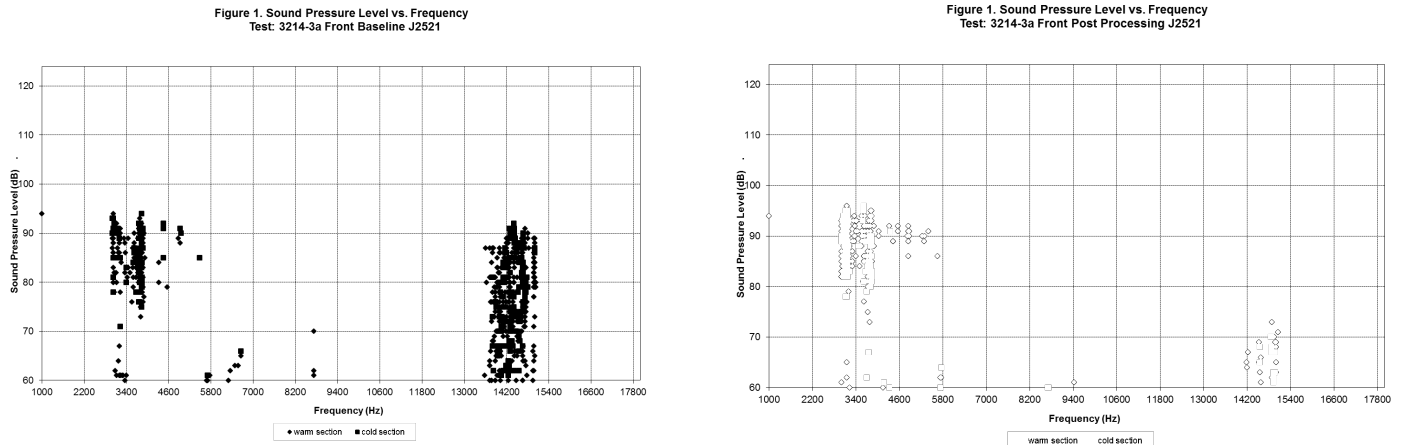


Figure 3.22. Noise testing on baseline and EDM processed rotors

Other noise tests conducted on parts processed by IESV and Magnetic Coil showed similar results (~ 50 % reduction in noise hits) though the magnitude of noise reductions was not as drastic as the EDM process. Parts with no improvements post processing, showed no significant change in the noise performance.

3.7. Summary of Exploratory research

Based on the initial research studies, the following are the major findings and observations

3.7.1. Processing

All magnetic or electrical processing techniques generated improvements in the rotor damping. This discovery is crucial since the rotor geometry is not directly affected and

hence does not affect rotor form or fit. It was also discovered that the rotor does not need to be directly EDM machined to derive the benefits in damping. Initial DOE on all processes showed negligible effects of process variables (time, current and frequency) on damping improvements. A joint patent was filed between Rassini and University of Windsor for **MAGNETIC AND ELECTRICAL PROCESSING OF METALS, METAL ALLOYS, METAL MATRIX COMPOSITE PARTS AND COMPONENTS**

Patent # US 9,133,534 B2.

3.7.2. Material

Damping improvement results vary based on the material microstructure and preprocess Q factor. Larger graphite flake sizes in the 2 to 4 range seem to give very high damping on the initial part and also provide the maximum damping improvements post electrical processing. However, a better understanding of the various material properties and any changes in them during and after processing is necessary. Any changes in the material structure may affect other performance aspects of the brake rotors and will need to be benchmarked.

3.7.3. Noise Validation

Noise testing shows 80 to 100 % reduction in noise occurrences at high frequencies (> 3 KHz) on processed parts compared to the baseline rotors. The effects were not very pronounced at lower frequencies, which typically maybe caliper generated noises as compared to rotor and pad generated noises. Noise testing on different systems with different rotors showed similar reductions in noise occurrences.

This testing also showed an important facet, that there was noise on the baseline parts which already had a damped metal with large graphite flakes. The process and the improvements

and the damping benefits obtained from it, improved the noise performance significantly. This correlates with the literature in terms of very high noise reduction capabilities shown in rotors that had EDM machined plates or the coulomb insert rotors.

3.8. Project Justification

The noise reductions and the ease of the processes shown to achieve it, make the project very important and useful. Based on the warranty and development costs typically associated with noise reductions in brake systems, this option presents yet another idea that could be implemented, depending on the specific noise concern.

Based on the results seen from the exploratory research, the project was set up with a basic objective and various sub goals as shown below:

3.9. Project Objectives and Goals:

To produce a brake rotor with consistently high damping ($100 < Q < 300$)

1. To characterize the **material** properties that provide maximum initial damping, as well as maximum damping improvements from additional processing
 - a. To select rotors with metals from the typical production grey iron rotors database, which are hypoeutectic to near eutectic (C.E in the range of 3.9 to 4.1), medium hyper eutectic (C.E - 4.2 to 4.4) and high hyper eutectic (C.E > 4.5).
 - b. To evaluate the foundry parameters, chemistry, microstructure and mechanical properties of the metals selected.
 - c. To evaluate the changes in material properties during and after EDM processing, using non-destructive tests.
 - d. To generate a map of Q factor improvements post processing, and relate the material properties to these improvements.

2. To confirm the material and define the additional electrical process and the process variables required, to attain the damping improvements consistently.
 - a. To manufacture a new rotor geometry with the material characteristics predicted from Objective 1.
 - b. To run a DOE on the EDM process variables to characterize the process
 - c. To evaluate the effects of processing on the regular machined as well as ferritic nitro carburized (FNC) rotors.
3. To validate the effects of the improved damping from electrical processing on noise performance.
4. To validate the effects on all other rotor performance characteristics including thermal, frequency response, brake output, vibration and roughness, wear and cracking. To determine the effects of wear, as well as time and temperature, on the damping improvements from processing.

CHAPTER 4

MATERIAL CHARACTERIZATION FOR DAMPING IMPROVEMENTS

The initial exploratory research showed that the material microstructure has an impact on the initial as well as post process damping. It was also seen that the mechanical properties, which are a result of the microstructure) showed an effect on the damping. Based on this, the first part of the project was geared toward a clear definition of what material properties need to be controlled and the ranges defined, in order to facilitate the maximum damping improvements from the processing.

4.1. Material Selection

To accomplish this objective, different material grades were picked from the grey iron production rotors database that met the following constraints;

1. High hypereutectic iron with a C.E. ≥ 4.5
2. Near eutectic iron with a C.E. in the range of 4.2 to 4.4
3. Hypoeutectic iron with a C.E. in the range of 3.9 to 4.1

As discussed in the literature review, the C.E. and the Eutectic Carbon were calculated based on the following formulae:

$$\text{C.E.} = \text{C} + 0.03*\text{Si} + 0.033*\text{P} - 0.015*\text{Mn} + 0.26 * \text{S} \quad (1)$$

$$\text{E.C.} = 4.34 + \text{C} - \text{C.E.} \quad (2)$$

The basic idea of picking these grades was based on the observations during the initial research, that the parts with high C.E. and large graphite flakes showed very good improvements from the additional processing and also accomplished noise reductions, while parts with a low C.E and finer flake sizes showed no improvements from the processing.

The rotor ID corresponding to each of the above grades of iron based on the C.E. and E.C. is shown in Table 4.1. The inoculants used for each of the rotor is also listed. As discussed in the literature review, Barium is typically used for its high graphitizing potential and helps in formation of large Type A Graphite flakes.

ROTOR ID	C.E	E.C	INOCULANT
S01	4.58	3.62	Barium
D11	4.30	3.78	Strontium
F11	3.90	3.78	Calcium Bearing 75 % FeSi
F13 (Inoculated)	4.08	3.71	Strontium
F13 (Un Inoculated)	4.08	3.71	None

Table 4.1. Rotor ID picked for the study and the C.E., E.C. and the inoculants used

Pre process Q factor was measured on the rotors as shown in Figure 4.1. The Q factor was correlated with the C.E. of the rotors. As seen in the Figure 4.1 below, there is not a very good linear correlation between the C.E. and the Q factor of the parts. However, in general it can be seen that the Q factor is low on the high C.E. parts and very high on the low C.E. parts, as shown in the contour plot in Figure 4.2.

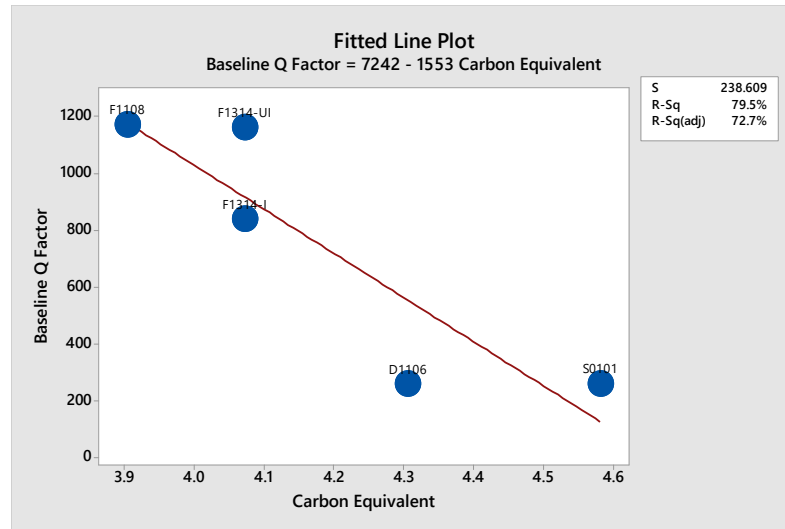


Figure 4.1. Relation between the baseline Q factor vs C.E. of the 5 grades of rotors

It should also be noted that the Q factor on D11 is very low – Good Damping properties even though the C.E. is only 4.3 [Not a very high hyper eutectic rotor].

A deeper analysis of the contour plot of the baseline Q factor vs Carbon Equivalent and Eutectic Carbon as seen in Figure 4.2, shows some overlap areas where good Q factor can be created even with a lower C.E (in the range of 4.2 to 4.3) with a higher Eutectic Carbon, as well as with a High C.E and low Eutectic Carbon. An analysis of the microstructure will be needed to understand these discrepancies a little better.

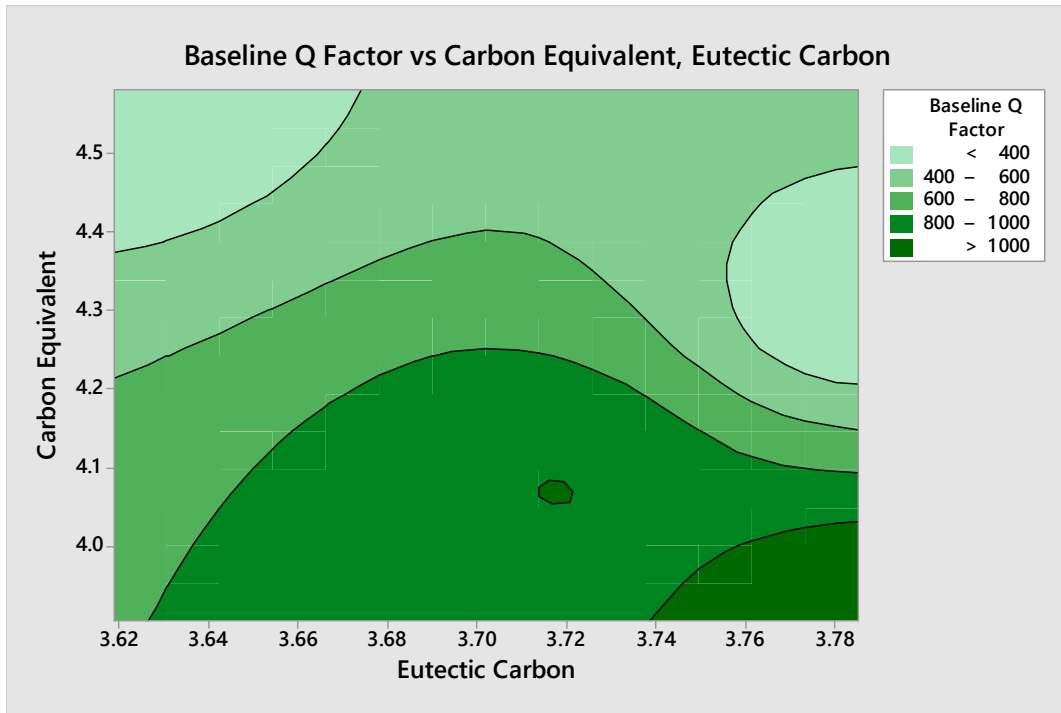


Figure 4.2. Contour Plot of Baseline Q factor vs Carbon Equivalent and Eutectic Carbon

The chemical analysis for all the rotors was conducted at Rassini using a Leco Spectrometer and the chemistry results for all the rotor IDs are shown in Table 4.2. As seen in the table, all the metals have a different chemistry with varying levels of carbon, silicon and other alloys. A much higher carbon and silicon content is noted on the high C.E. S01 rotors, while the D11 part shows a high carbon but a lower silicon which might result in finer flakes and thus higher strength. The F11 rotors have a high Cr and high Cu which are typical additions for higher strength metals.

S01

CARBON	%	3.82
MANGANESE	%	0.63
SILICON	%	2.47
SULFUR	%	0.02
PHOSPHOROUS	%	0.03
CHROMIUM	%	0.10
COPPER		0.12
NICKEL		0.07
MOLYBDENUM		0.01
TIN		0.06

D11

CARBON	%	3.75
MANGANESE	%	0.68
SILICON	%	1.85
SULFUR	%	0.04
PHOSPHORUS	%	0.02
CHROMIUM	%	0.17
COPPER	%	0.20
NICKEL	%	0.14
MOLYBDENUM	%	0.01
TIN	%	0.03
TITANIUM	%	0.01
VANADIUM	%	0.01
CHROME + MOLYBDENUM	%	0.18

F11

CARBON	%	3.35
MANGANESE	%	0.62
SILICON	%	1.80
SULFUR	%	0.09
PHOSPHOROUS	%	0.02
CHROMIUM	%	0.23
COPPER	%	0.53
NICKEL	%	0.12
TIN	%	0.04
TITANIUM	%	0.01
SCANDINAVIUM	%	0.91

F13

CARBON	%	3.46
MANGANESE	%	0.52
SILICON	%	1.98
SULFUR	%	0.11
PHOSPHOROUS	%	0.02
CHROMIUM	%	0.22
COPPER	%	0.17
NICKEL	%	0.05
TIN	%	0.03
TITANIUM	%	0.01
VANADIUM	%	0.01

Table 4.2. Chemistry for the batch of S01, D11, F11 and F13 Rotors

The mechanical properties including Brinell hardness and tensile strength were measured at Rassini, when the batch of these production rotors were poured. The Brinell hardness was measured using an EMCO (M4U-075) hardness tester with a 10 mm ball and 3000 Kg

loads for the low C.E. rotors and a 5 mm ball with a 750 Kg load on the high C.E. metals, to get accurate hardness measurements. Tensile Strength was measured using the wedge penetration test on a Kogel Machine and the wedge strength is correlated to the tensile strength.

The results as shown in Figure 4.3 and Table 4.2 (showing the Q factor and the hardness and tensile strength for all 5 metals) show that the material selected for the study span a wide range of hardness and tensile strength. The relationship of the Q factor and the mechanical properties and C.E. are shown in the Figure 4.3. The plots clearly show that the parts with high hardness and low C.E. have very high Q factor (low damping) and vice versa, which means a very linear relationship exists. High damped low Q metals have high C.E. and lower hardness.

Rotor ID	Hardness (Brinell Hardness)	Tensile Strength (MPa)	Baseline Q Factor
S01	155	162	261
D11	174	178	259
F11	210	278	1172
F13 - I	196	256	841
F13 - UI	213	265	1161

Table 4.3. Rotor mechanical properties (hardness and tensile strength) and Q Factor

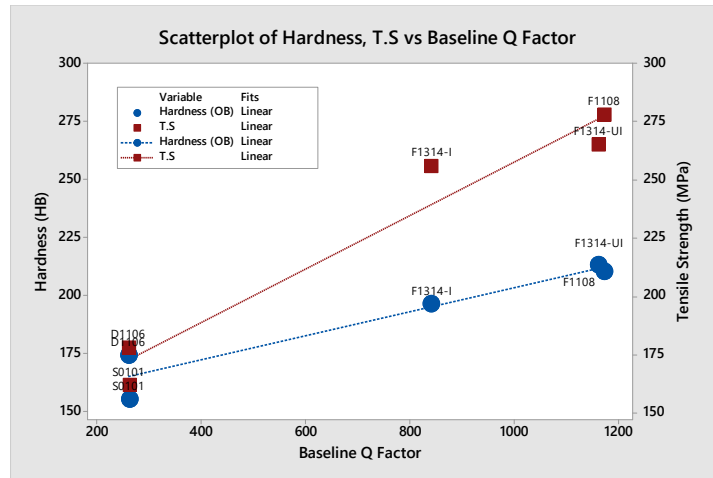


Figure 4.3. Scatterplot of Baseline Q factor vs Hardness and Tensile Strength

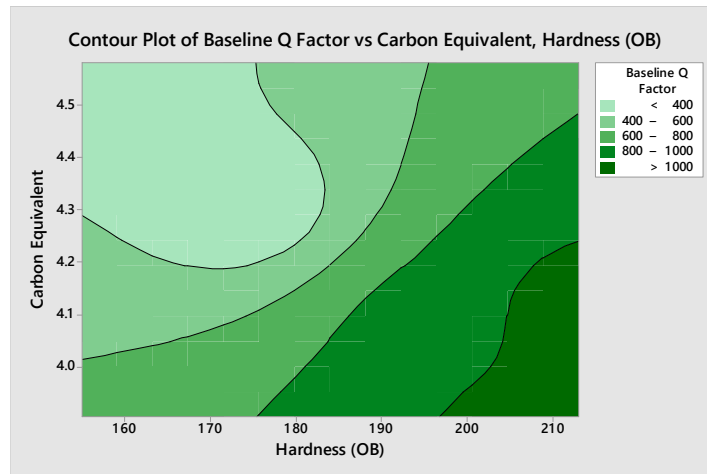
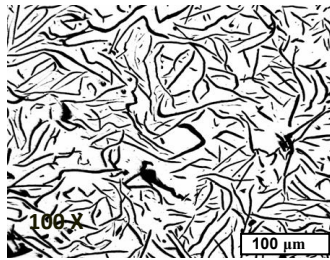


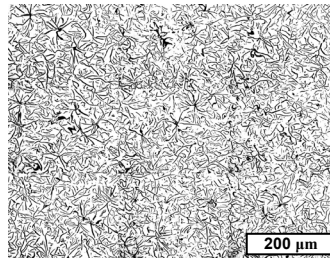
Figure 4.4. Contour Plot of Baseline Q factor vs Hardness and C.E.

As seen from the contour plot in Figure 4.4, the combination of C.E. and hardness has a very linear relationship with the damping properties of the rotors. Low Q at lower hardness and high C.E. and vice versa. The most important fact is that these metals span the entire typical range of properties used in brake rotors and the information shown above validates the successful selection of metals to perform this study.

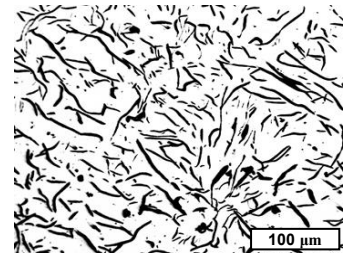
The material structures of the samples were analyzed first on every batch of cast parts and they were again reanalyzed on the parts specifically used in the study, post processing. The microstructures showing the graphite flakes for each of the rotor IDs are shown below:



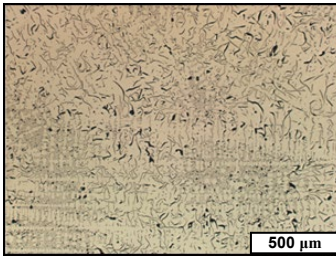
100 X - S01 - A 3-4-5 97% + C 3 %



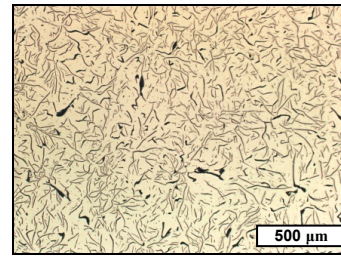
50 X - D11 - A (3) 4-6 95% + B + C



100 X - F11 - A (3) 4-5 98 % + E <2 %



50 X - F13 – UN INOCULATED
A (3) 4-6 85% + B 15 %



50 X - F13 – INOCULATED - A (3) 4-5 90% + B 10 %

Figure 4.5. Microstructure of S01, D11, F11 and F13 inoculated and un-inoculated rotors on an Olympus GX71 Optical Microscope

As we can observe from the microstructures, it may be clear that the larger flake graphite in the S01 is associated with the lower hardness as well as the Low Q factor, as compared to the finer flake graphite seen in the other rotor types. It should be noted that the Part D11 shows a very low Q factor also, but has a higher hardness and tensile strength compared to the S01 rotor. F11 and F13 rotors show a very fine flake microstructure and hence a low damping and higher strength. More analysis on the LOM on the graphite morphology as well as the Pearlite matrix needs to be done on the individual parts.

4.2. Non Destructive Testing

One of the main drawbacks of the previous studies as well as most studies done in the literature, was the inability to check the changes in the part during and after processing. Since microstructure is very difficult to accomplish as a non destructive tests, other properties like the Hardness, Elastic Modulus, Q factor, and Magnetic field were measured before and after processing as part of the study. The non-destructive tests are listed in the Table 4.3 below.

MEASUREMENT VARIABLE (before and after processing on the same part)	METHOD
Q Factor - 2ND on all rotors and Q factor at all modal frequencies and 1 and 2nd tangential on one rotor	LMS equipment with auto hammer and microphone - Measured using the FRF plot and the 3 dB drop at specific modal frequency peaks.
Elastic Modulus	Ultrasound method using the wave speed and time of flight of the longitudinal wave through the part
Brinell Hardness	10 mm ball at 3000 Kg load or 5 mm ball at 750 Kg load depending on the material type
Magnetic Field in and around the rotor	Hall sensors (Honeywell Part # SS49E), Gauss meter

Table 4.3. Non destructive Testing on Rotors before, during and after processing

6 parts of each Rotor ID were used for the study. 5 of the 6 rotors were processed and 1 rotor left unused as baseline. Parts were processed using the Ingersoll EDM machine with the same concept used during the exploratory research. 2 minutes of processing time with 20 amps current and sacrificial steel placed on the Inboard brake plate at 3 locations 120 degrees apart and used for the EDM machining.

4.2.1. Effects of processing on Q Factor

Q factor results from baseline rotors before processing were shown in Table 4.2. The processed parts were re-measured on the same set up and the same LMS equipment at the same temperatures. The master rotor was measured before the project parts were measured. The Q factor improvements from the processing are shown in the Figure 4.6 below.

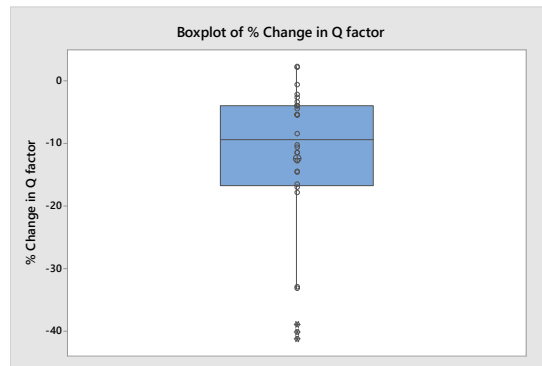


Figure 4.6. Boxplot of % Change in Q factor for the study parts

The results range from 0 % to almost 45 % improvements. This is dependant on the material used, and follows some of the data trends seen in the the exploratory research.

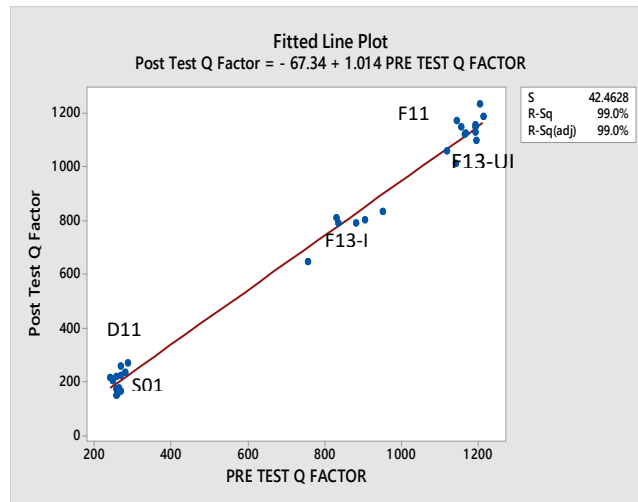


Figure 4.7 Fitted Line plot of pre vs post test Q Factor

As seen from the Figure 4.7, there is a linear relationship between the pre process Q factor and the post process Q Factor. This trend follows the same pattern seen in the exploratory research, that rotors with low baseline Q factor tend to perform better with processing and have better improvements in damping. However the % improvements in damping after processing do not show any relationship with the pre process Q factor, as seen in Figure 4.8. It can be seen that the largest improvements between 35 to 45 % are seen on the S01 rotors. The F11 and F13 (Uninoculated) both have negligible improvements (0 to 10 %). D11 and F13 (inoculated) show improvements in the range of 5 to 20 %. The discrepancy in improvements seen between the S01 and D11 explains the non linearity seen between the pre and post process Q factor.

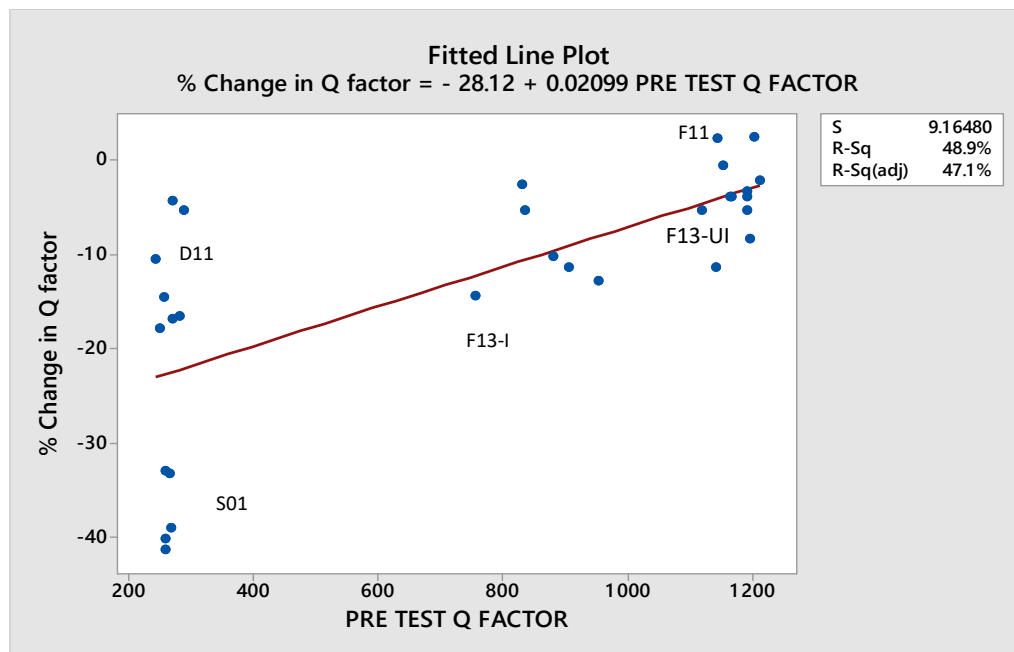


Figure 4.8. Fitted line plot of % change in Q factor vs pre test Q factor

The Q factor was also measured at all modal frequencies on a rotor of each ID, including the nodal and tangential modes.

The intent of the study is to ensure that the damping improvements that have been observed at the 2 ND mode are not limited to only that frequency, but also translate to all other modal frequencies. Q factor results pre and post processing, for the S01 rotor are shown below in Figure 4.9.

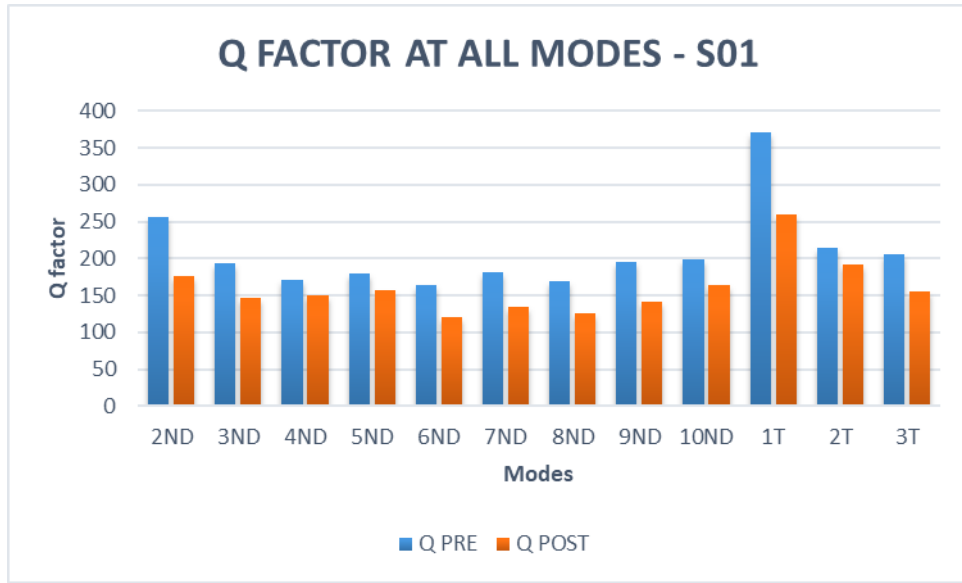


Figure 4.9. Q factor pre and post processing at all bending and tangential modes

It can be observed that the absolute Q factor is fairly consistent across all frequencies and a damping improvement is also seen at all modal frequencies. The improvements at each mode is shown in Figure 4.10. It can be observed that the damping improvements are seen at all modal frequencies. Even though the % change is not extremely consistent (which may be due to the noise at the modal peaks usually seen at some frequencies), it is noted that the damping is improved and should have a favorable effect over the entire frequency range.

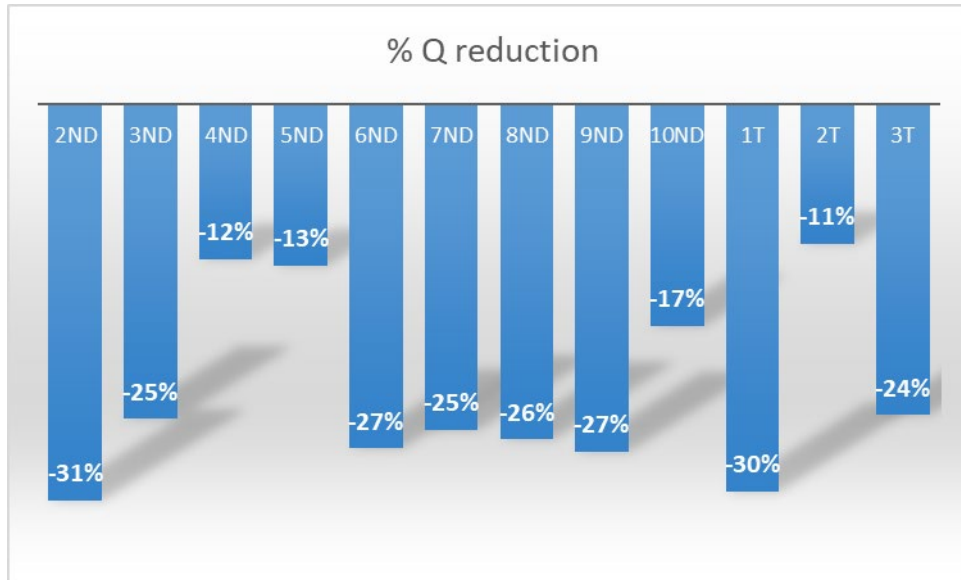


Figure 4.10. % Q factor reduction at each mode on S01 rotor

4.2.2. Effects on Elastic Modulus

The elastic modulus was measured on the parts, before and after processing. Since the test needs to be non destructive, the ultrasonic method was used to measure the static Young's modulus in the radial and the axial (through the thickness) directions, as shown in the Figure 4.11. For the radial direction measurements, only the inboard plate (not connected to the hat) is used. Through the thickness measurements go through both the plates and the fin supports.

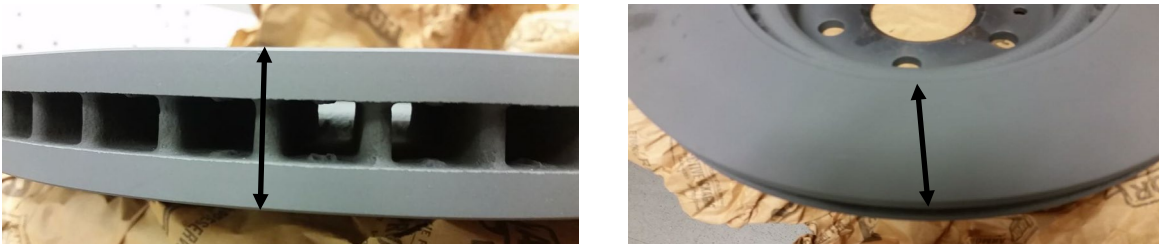


Figure 4.11. Through the thickness and radial directions for Modulus Measurements

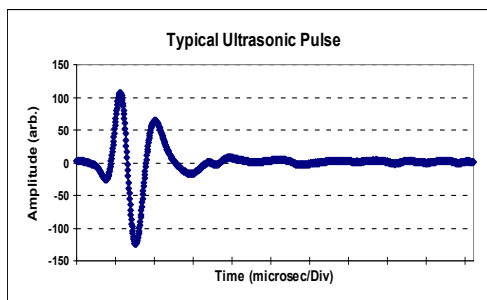
The tests were conducted at IMS (Industrial Measurement Systems Inc.) using the ETEK equipment shown below in Figure 4.12.



Figure 4.12. ETEK Ultrasound equipment

Changes in the wave speed and its attenuation before and after process will give an indication of any changes in the modulus of the rotor due to the process.

Typical ultrasonic pulse and the parameters are shown in Figure 4.13 below.



Frequency = 1 Mhz
Wavelength = 1500 Microns (.060 Inch)
Wave Speed = 1.5 Km/sec (4925 Ft/sec)
Peak Intensity = 100 Watts/cm²
Peak Pressure = 3.11 Mpa (450 Psi)
Particle Velocity = 6.6 Cm/sec (2.6 Inch/sec)
Peak Displacement = 10⁻⁶ Cm (2.54 x 10⁻⁶ Inch)
Particle Acceleration = 40000 G's

Figure 4.13. Typical Ultrasonic pulse and its parameters

Time of flight and the velocity of the longitudinal and shear waves in both the directions are measured. From longitudinal velocity, V_L , and the shear velocity, V_s , along the propagation

path the Young's modulus, shear modulus and the Poisson's ratio can be determined from the following equations.

Young' modulus

$$E = \rho V_S^2 (3V_L^2 - 4V_S^2) / (V_L^2 - V_S^2) \dots\dots\dots (1)$$

Shear modulus

$$G = \rho V_S^2 \dots\dots\dots (2)$$

Poisson's Ratio

$$\nu = [1 - 2(V_S/V_L)^2] / [2 - 2(V_S/V_L)^2] \dots\dots\dots (3)$$

Specific points on rotor were picked (based on gate and riser/vent locations) for measurements, before and after processing. There are 4 points, 90 degrees apart starting at the gate location, and the rest equally interspersed between these points.

In order to establish repeatability of measurements, pre measurements were completed on 1 rotor of each material in the locations shown in the example in Figure 4.14.



Figure 4.14. Example of locations for non-destructive test measurements – S01

Repeatability study shows a variation of less than 1 % in measurements in either direction as shown in Figure 4.15.

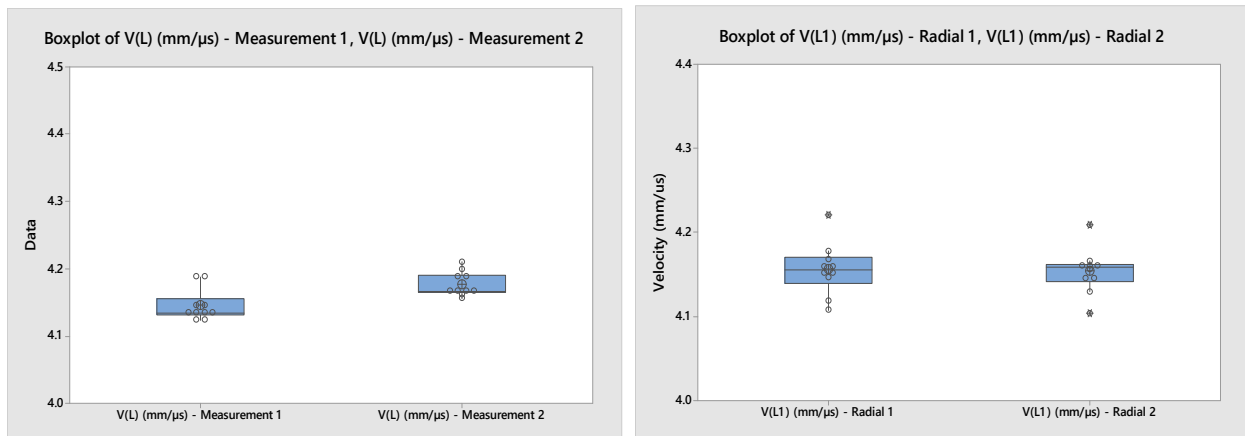


Figure 4.15. Boxplot of the velocity measurement in axial and radial directions

All the parts were premeasured and the results are shown in Figure 4.16, for the through thickness and radial directions. Parts were processed and then re-measured at the same locations on the rotors.

The results are shown in Figure 4.16 for the through the thickness modulus measurements. Results show no change in the modulus on D11, F13-UI and F11. A small drop of ~ 1 % in the Modulus was seen on the F13-I. However, S01 showed an increase in Modulus after processing of ~ 5 %. S01 also showed the highest improvements in damping. Typically lower modulus is associated with better damping, so this was an interesting discovery and further research may need to be done to understand this discrepancy. Even though this change is not very significant in terms of the percent change, it is still interesting, since the better damping properties of S01 would indicate a possible reduction in modulus and not an increase. Similar data was seen in the radial directions also, with negligible changes on the parts.

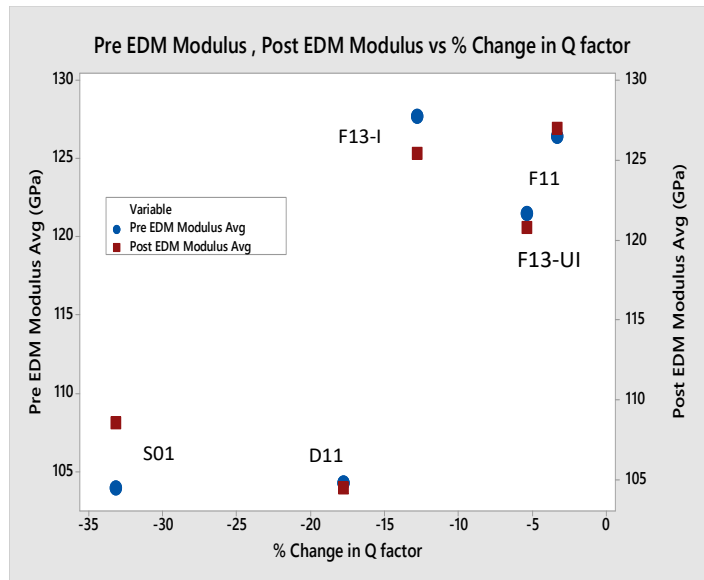


Figure 4.16. Average Modulus Changes in the through the thickness direction on the rotors

4.2.3. Brinell Hardness measurements

Hardness was measured on all the 6 rotors and re-measured in a close location on the same part post processing, as shown on the S01 rotor below in Figure 4.17. The locations for the measurements were based on the gate and riser/vent locations for each of the rotors as seen in Figure 4.17.

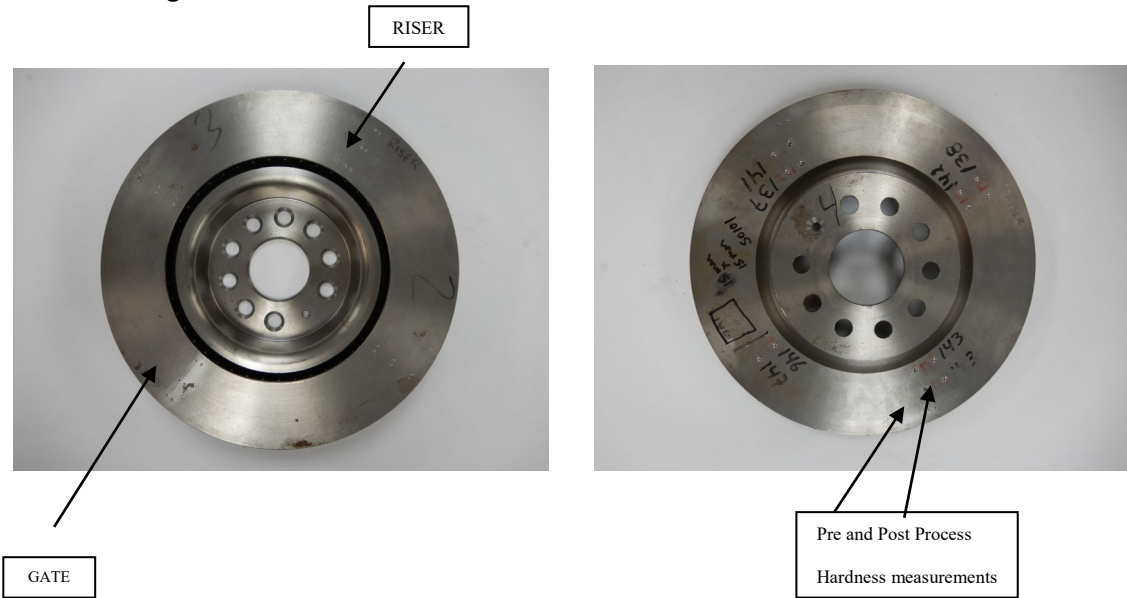


Figure 4.17. Rotors showing the different locations for hardness measurements

Parts were measured at 4 locations - 2 locations, one at the gate and one at the riser/vent and the other 2 locations 90 degrees between the other two. They were also measured at the Outer diameter, center of the plate and at the Inner Diameter and on both the OB and IB Brake Plate as can be seen from the pictures above. This provides 12 measurements on each plate and 24 total measurements on each rotor.

The hardness measurements were compared at the OD on the outer plate, for the study. It can be seen from the Figure 4.18., that there are negligible differences in the hardness on the OB or the IB plate at the same outer diameter (OD) locations.

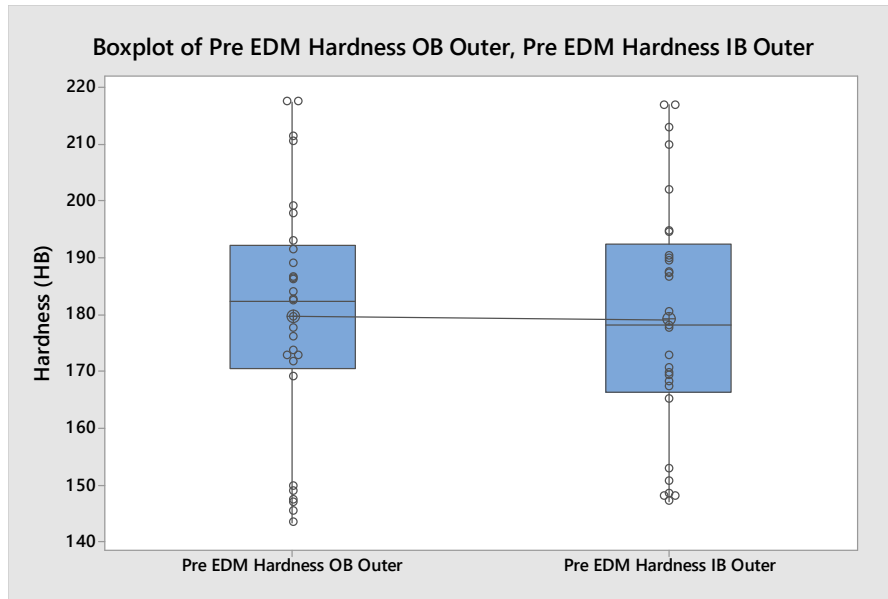


Figure 4.18. Hardness on outer diameter OB and IB plate on all rotors

After electrical processing, the parts were re-measured at points less than 3 degrees from the prior pre processing measurement point. Data for all the points on a D11 rotor, pre and post process, are shown in Appendix 3.

Data comparison for the S01 rotors pre and post processing hardness measurements, at the OD of the OB and IB plates, show the following trends as seen in Figure 4.19. There is no change in the hardness of the unprocessed baseline part and there is negligible change on the processed parts. The largest change is seen on Part 5 of about 5 points on BHN (~ 3 %). All others show less than 1 % change in hardness.

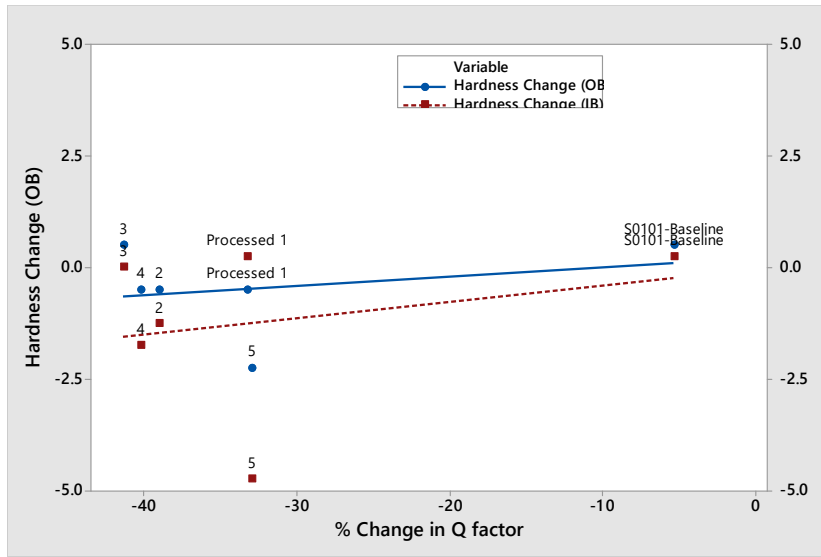


Figure 4.19. Hardness change at OD on OB plate for S01 Rotors

Very similar results are seen for all the other part numbers also as seen from the Figure 4.20 below, with very little changes in hardness post processing.

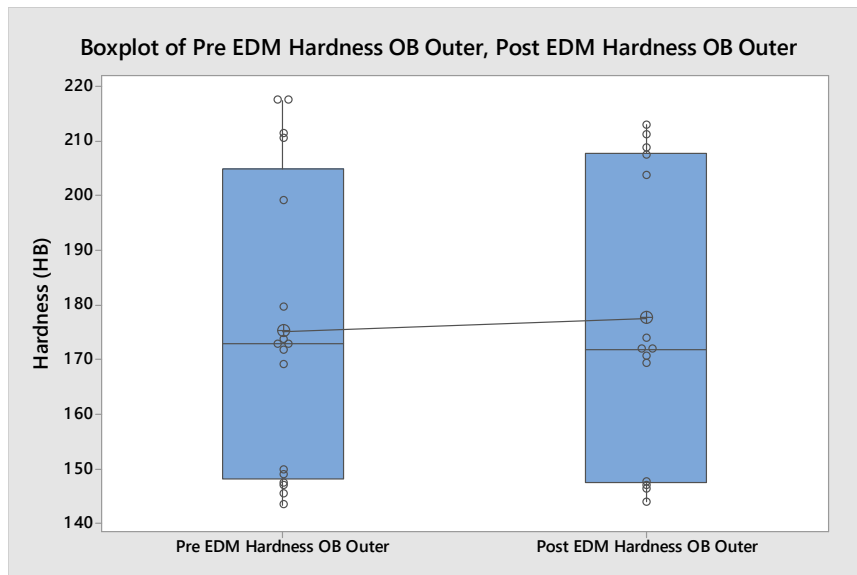


Figure 4.20. Pre and post processing hardness on rotors - OB Outer

The pre vs post processing hardness comparison on the OB and IB plate for all rotor IDs are plotted and shown below in Figure 4.21. It shows a very negligible changes in hardness due to the processing of the parts.

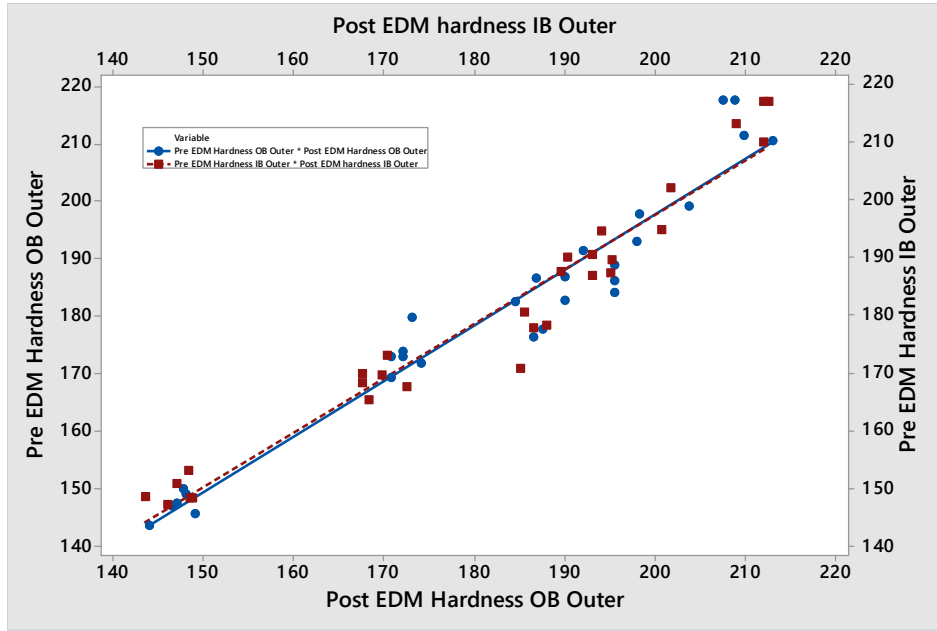


Figure 4.21. Pre vs Post processing hardness on OB and IB outer – all rotors

In summary, negligible changes in hardness are seen after processing. We have observed a significant change in damping, no changes in hardness and no significant changes in the Elastic modulus of these rotors, post processing.

4.2.4. Magnetic Field measurements

The idea of running this non destructive test, was to look for magnetic field changes in the part before, during and after electrical processing. As was noted in the exploratory research, the improvements from the electrical processes are thought to be of a magnetic / electric in nature.

Magnetic field was measured using hall sensors, shown in Figure 4.22. (Honeywell SS49E), glued to the rotor at the desired locations (at gate, vent/riser location and two other locations 90 degrees between the gate and vent). Hall Effect sensors are devices which are energized by an external magnetic field. The output signal produced from the hall effect sensor is the function of magnetic field density surrounding the device. An output voltage known as the Hall Voltage is generated when the magnetic flux density surrounding the sensors crosses a certain pre-set threshold, and is detected by the sensors. These sensors can measure the linear as well as angular fields. For linear sensors, output of voltage linearly depends on magnetic flux density. The sensors were glued to the flat portions of the rotor plates using adhesive tape. Sensors were connected to an oscilloscope and the voltage outputs were measured.



Figure 4.22. Hall sensor. [68]

1V = ~ 1.5 Gauss. Data is recorded for all the parts before, during and after EDM processing. All the parts were measured before processing, during the process and post processing and data collected and analyzed. The magnetic fieldd measured on the rotors did not show major differences based on the location of the meaurements or processing on the EDM. All sensors at 4 different locations (processing at the gate location), showed similar results. An example is shown in Figure 4.23 for the D11 Rotors.

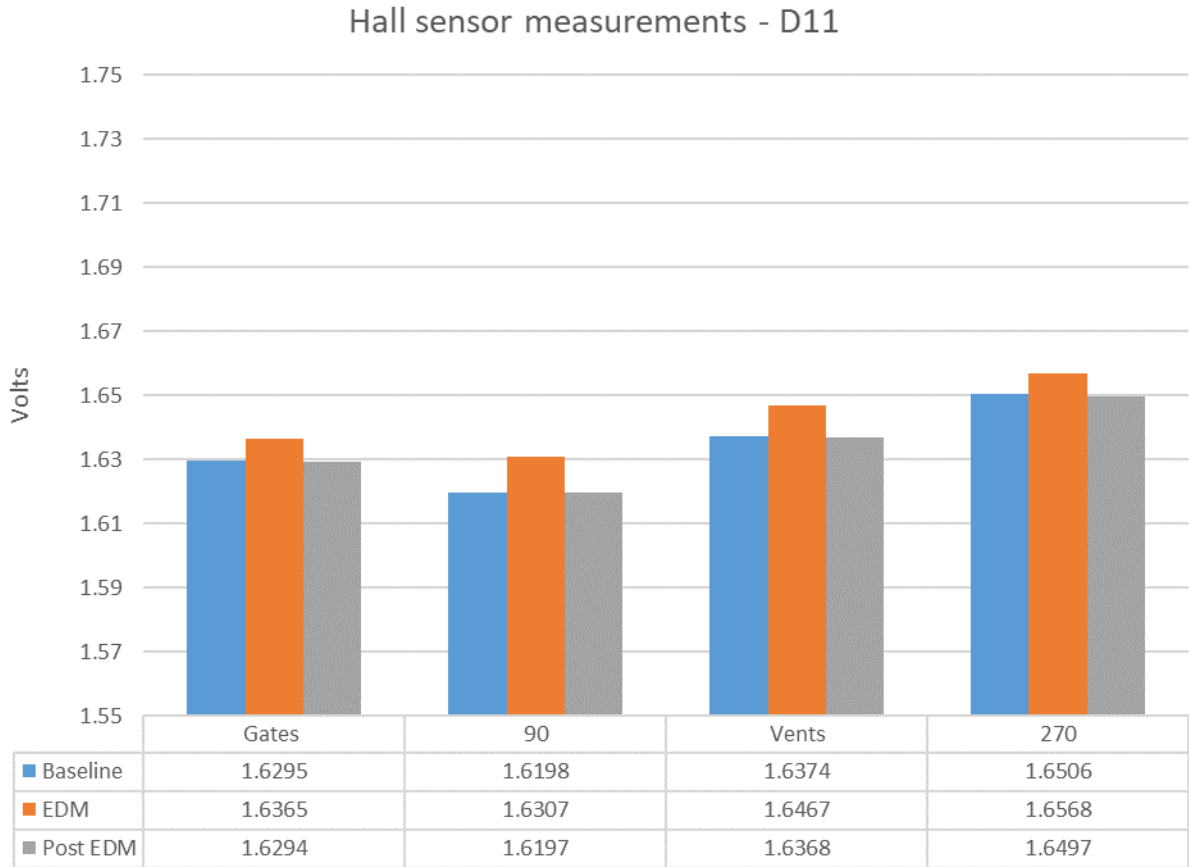


Figure 4.23. Hall sensor Voltage measurements on D1106 rotors before during and after processing at 4 different locations on the brake rotors

As seen above, very small magnetic fields are noted on the rotor plates under all the conditions. A very small increase in the measurement is noticed, during the processing. However, post process fields are the same as pre process. These fields are very negligible and are all less than ~ 5 Gauss. This might indicate that the domain orientations are in a magnetic structure such that the magnetic field is not able to be detected outside the part.

Data for all the F11 rotors is shown in Figure 4.24. As noted, the fields are extremely consistent and not dependent on the part. The same pattern and the same gauss levels pre

and post processing (with a slight increase in the magnetic field during processing), is observed on all rotor ids.

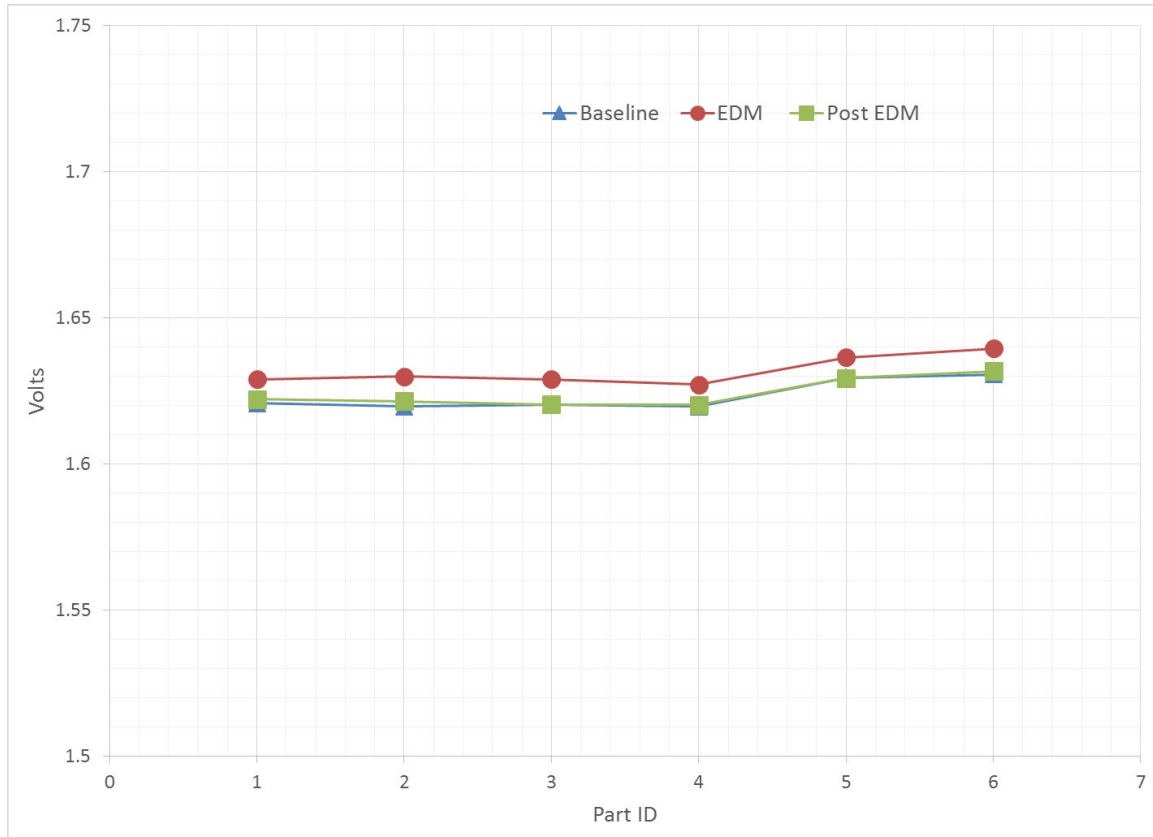


Figure 4.24. Hall sensor magnetic field measurements – F11 – Multiple rotors

As seen in Figure 4.25 data for all the rotors, it shows that the S01 parts have a particularly lower field compared to all the other rotors. The differences pre, during and post process for all the rotor ids are all negligible. However, S01 shows a stark difference in terms of the magnitude of the field.

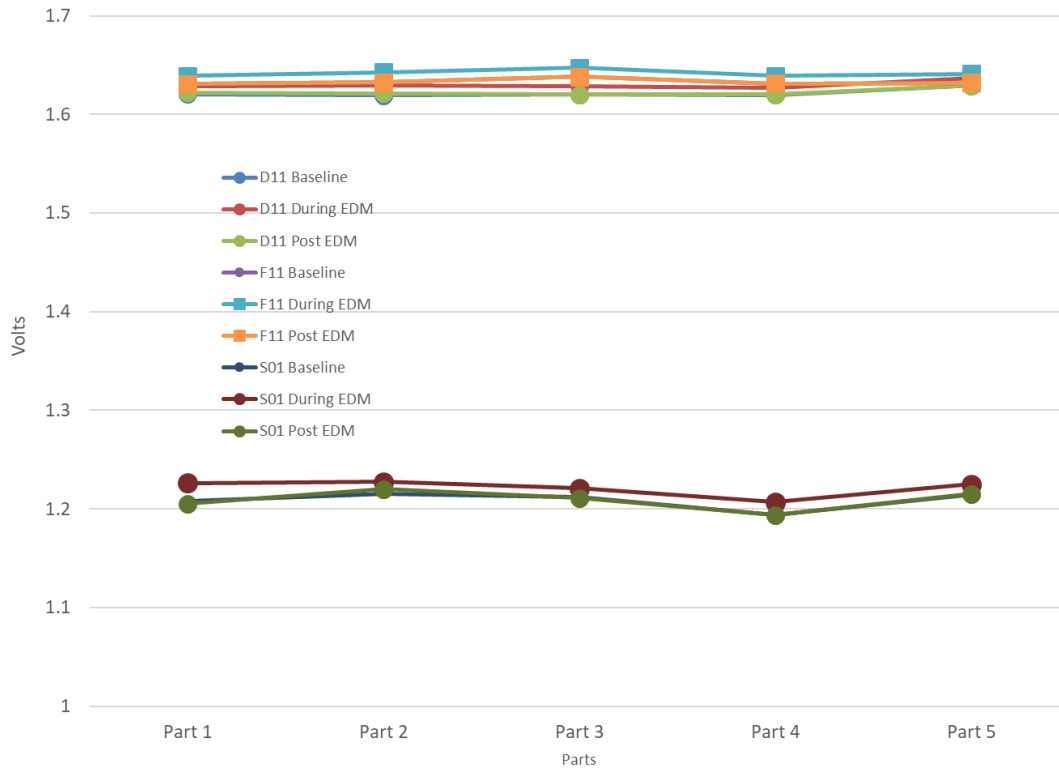


Figure 4.25. Hall sensor field Voltage measurements on all part numbers before, during and after processing

This may be because

1. Larger flake graphite present in the rotors, making it less magnetic.
2. Presence of more 90 degree domains, thus containing the field within the rotor and not have a high measurable field outside the part.

These items will need to be investigated further and can be part of further studies.

4.3. Effect of C.E.

From the non-destructive tests, it was noted that the hardness and modulus showed negligible changes post processing.

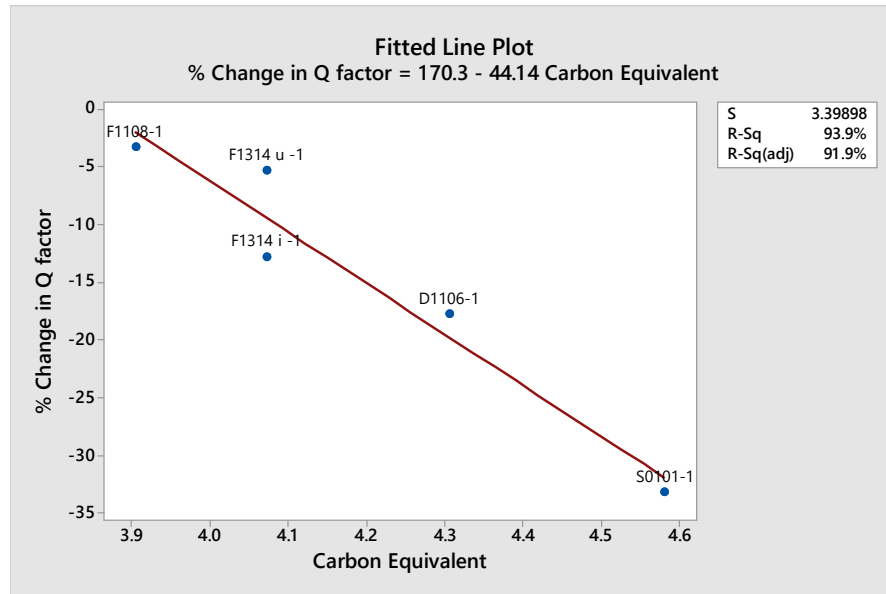


Figure 4.26. % Q factor change vs C.E.

The % Q factor change after electrical processing was related to the C.E., and the results show a very linear relationship between the C.E. of the rotor and the % damping improvements, as shown in Figure 4.26.

A contour plot of the % Q factor change and the C.E. and Eutectic Carbon seen in Figure 4.27, shows a similar trend. However some overlaps exist in the 4.2 to 4.4 C.E. range, where there is variability in the results seen. In general, it can be seen that High C.E. with Low E.C. provides the largest improvements in damping.

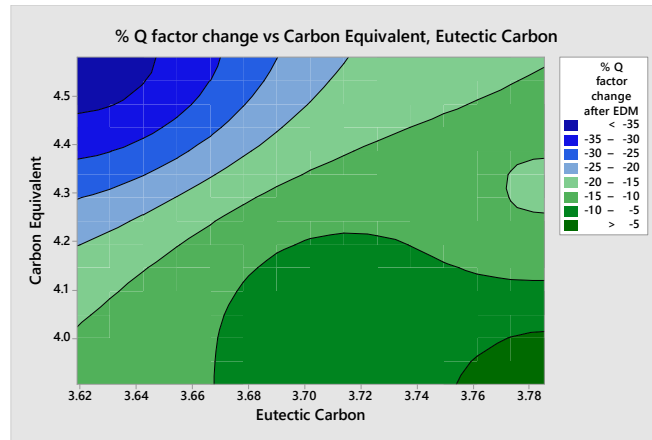


Figure 4.27. Contour plot of the % Q factor change vs C.E. and E.C.

Comparisons of the % Q factor changes in these rotors, to the C.E. and the hardness of the rotors, are shown in the contour plots in Figure 4.28. Result show a very clear relationship between the % damping improvements from processing and the hardness and C.E. Parts with the highest C.E. and lower hardness showed the most improvements, while the parts with lowest C.E. and higher hardness showed negligible improvements from the processing. This information is very critical, since it helps to control and optimise the microstructure of the parts and maximise the benefits from the electrical processing.

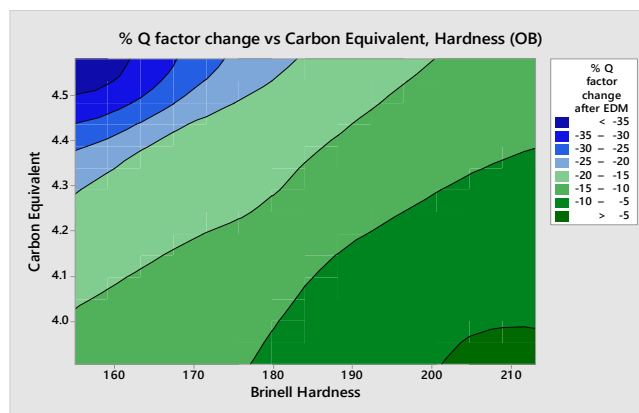


Figure 4.27. Contour plot of the % Q factor change vs C.E. and Hardness

4.4. Microstructure Characterization

Microstructure of the rotors were analyzed to compare the graphite flakes, as well as the Pearlite matrix structure to evaluate the effects on C.E., hardness, modulus, damping and the damping improvements from the processing. Microstructure was analyzed at the University of Windsor under a Light Optical Microscope. Parts were grinded and polished.

S01 – Microstructure Analysis on Processed Parts

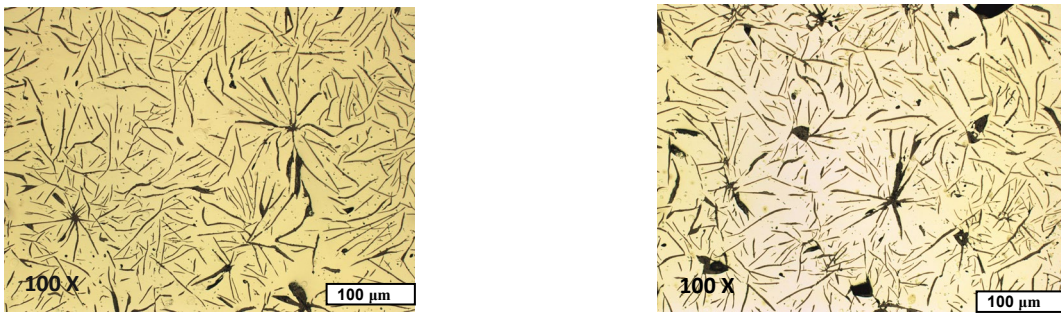


Figure 4.28. 100 X LOM micrographs of S01 rotors on OB and IB Plates

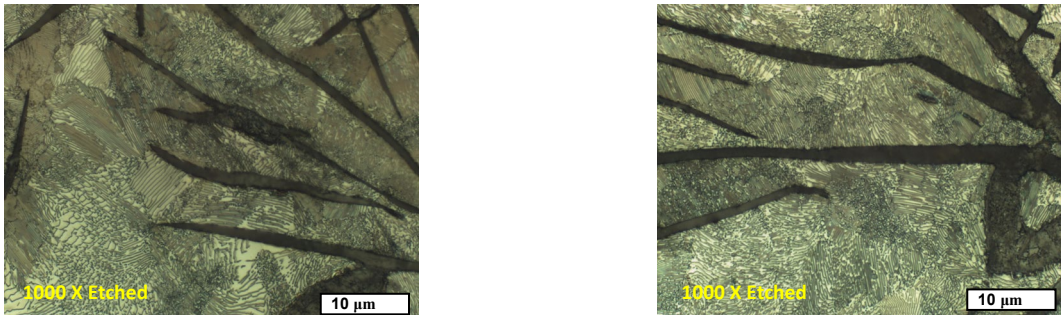


Figure 4.29. 1000 X As Polished and etched LOM micrographs S01 – OB and IB Plate

Graphite flakes were analyzed per ASTM A 247 and micrographs show a large population (98%) of large Type A graphite flakes in the size range of 2, 3 and 4 with < 5 % of Type C graphite. The Pearlite colonies look very coarse. The images were taken on both the plates

and can be seen as OB and IB Plate. The structure has direct relation to the properties of the rotors which are listed below:

C.E. – 4.58 % Tensile Strength - 155 MPa Elastic Modulus – 108 GPa Q - 270

Hardness on S01 OB plate OD gate area - ~ 146 HB

The larger graphite flakes and higher carbon and Si content (High C.E.) result in a lower modulus, lower hardness low strength metal with a very high damping (Low Q).

D11 – Microstructure Analysis

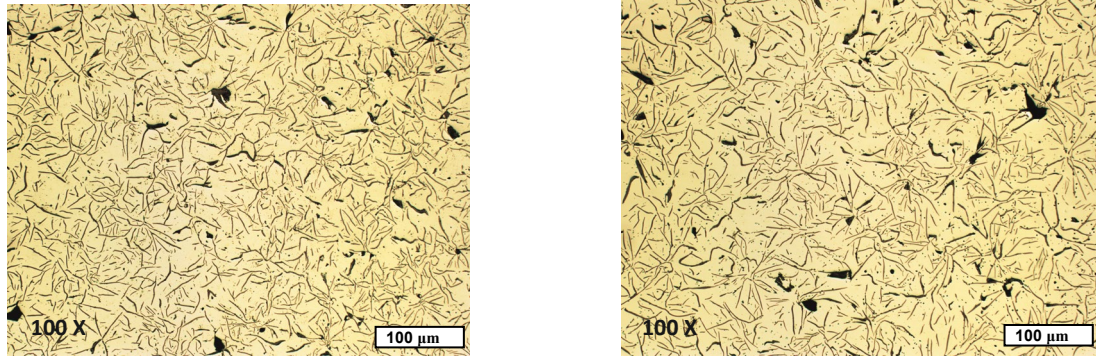


Figure 4.30. 100 X LOM Micrographs of D11 rotors on OB and IB Plates

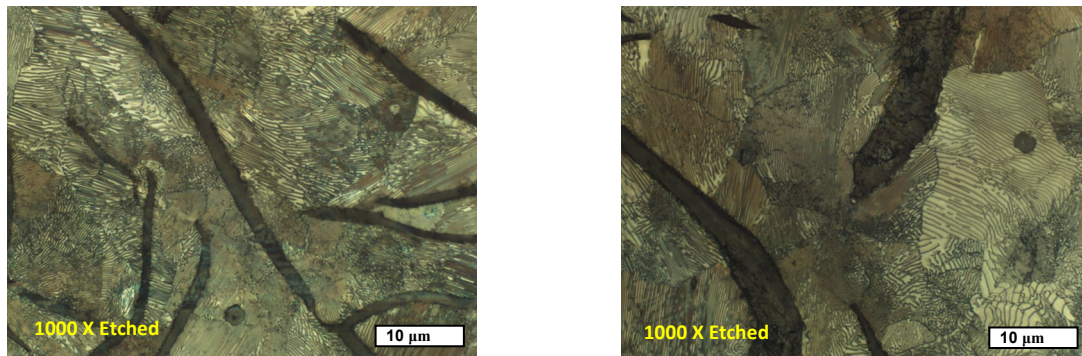


Figure 4.31. 1000 X As Polished and etched LOM Micrographs D11 – OB and IB Plate

Graphite flakes were analyzed per ASTM A 247 and micrographs show a large population (95%) of large Type A Graphite Flakes in the size range of 3, 4 and 5 and the rest is B and C Type Graphite Flakes. The pearlite colonies look coarse. The images were taken on both the plates and can be seen as OB and IB Plate. The structure has direct relation to the properties of the rotors which are listed below:

C.E. – 4.3 % Tensile Strength - 178 MPa Elastic Modulus – 103 GPa Q - 260

Hardness on D11 OB plate OD gate area - ~ 170 HB

It should be noted that the flake size is a bit finer than S01 rotors, but the Q factor is similar on baseline parts. It can also be seen based on the mechanical properties, that this material has higher strength. However the damping improvements seen from the processing are not as high.

F11 – Microstructure Analysis

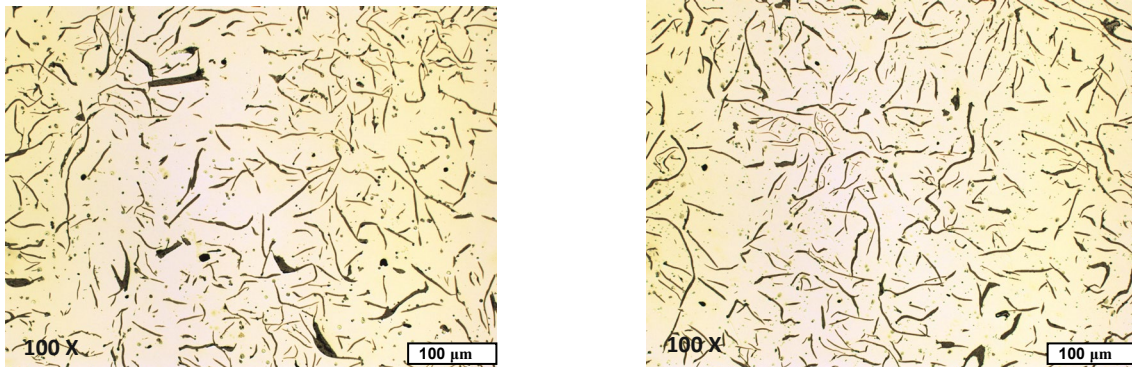


Figure 4.32. 100 X LOM Micrographs of F11 rotors on OB and IB Plates

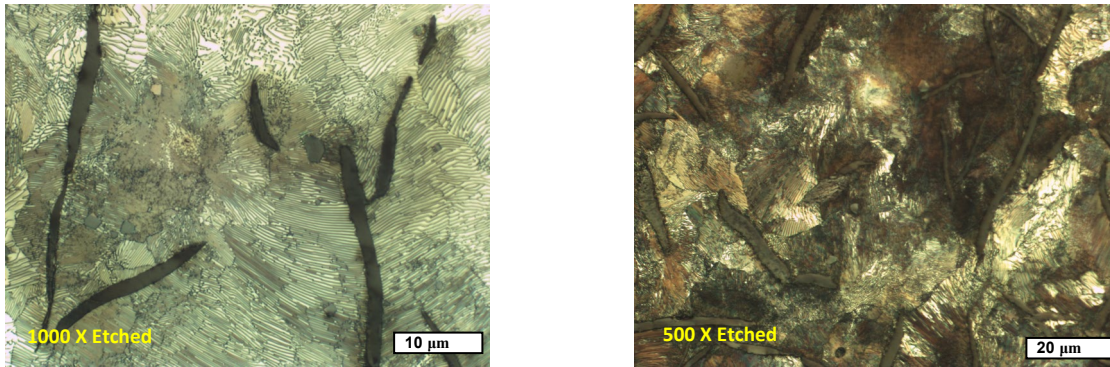


Figure 4.33. 1000 X As Polished and etched LOM micrographs F11 – OB and IB Plate

Graphite flakes were analyzed per ASTM A 247, and micrographs show a large population of large Type A Graphite Flakes in the size range of 4 and 5 and a lot of B type (10 %) and some D and E Type graphite flakes are also seen. The pearlite colonies look finer compared to the S01 and D11 rotors. The images were taken on both the plates and can be seen as OB and IB Plate. The structure has direct relation to the properties of the rotors which are listed below:

C.E. – 3.90 % Tensile Strength - 278 MPa Elastic Modulus – 127 GPa Q - 1172

Hardness on F11 OB plate OD gate area - ~ 210 HB

This is a high strength metal with Cu and Cr added to increase the strength. Microstructure shows finer and smaller graphite flakes, a finer Pearlite matrix (typically a good indicator of strength of the metal) and correspondingly a very low damping (High Q), a very high Elastic modulus, T.S and hardness compared to the other rotors.

F1314 – Microstructure Analysis – Un inoculated Rotor

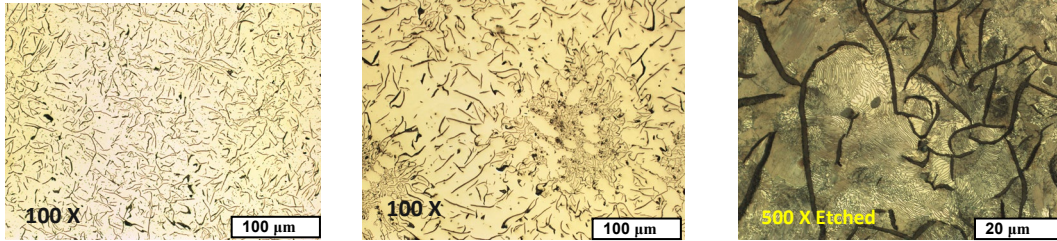


Figure 4.34. 100 X LOM micrographs of F13 rotors on OB and IB Plates and

Figure 4.35. 500 X As Polished and etched LOM micrographs F13 – OB and IB

F1314 – Microstructure Analysis – Inoculated Rotor

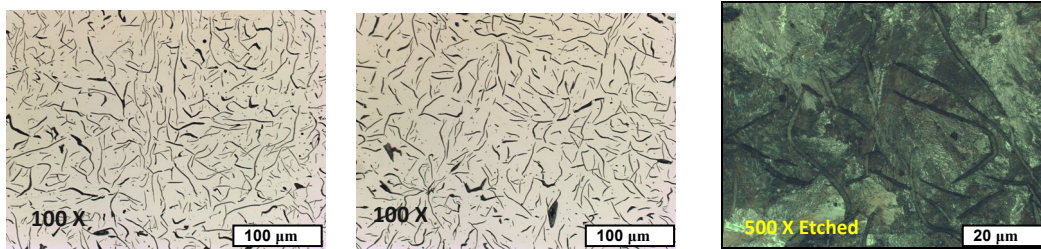


Figure 4.36. 100 X LOM Micrographs of F13 rotors on OB and IB Plates and

Figure 4.37. 500 X As Polished and etched LOM Micrographs F13 – OB and IB

Effects of inoculation can clearly be seen in the differences between the microstructure. Disintegrating graphite structures are seen in the uninoculated rotors as well as open dendrites and lot of E type graphite. Inoculated rotors show a much better distribution of mostly A type graphite.

Only the inoculated rotors will be reported below, since this exercise was mostly to understand the difference in material microstructure when inoculation is skipped.

Graphite Flakes were analyzed per ASTM A 247 and micrographs show a large population of large Type A graphite flakes in the size range of 4 to 6 and a lot of B type (~10 %) graphite flakes are also seen. The pearlite colonies look finer and similar to the F11 rotor. This would indicate a higher strength metal. The images were taken on both the plates and can be seen as OB and IB Plate. The structure has direct relation to the properties of the rotors which are listed below:

C.E. – 4.08 % Tensile Strength - 256 MPa Elastic Modulus – 126 GPa Q - 841

Hardness on F13 OB Plate OD Gate area - ~ 190 HB

4.5. Summary of material characterization

Result show a clear relationship of the type of graphite flakes, their structure and size, on the hardness, tensile strength and the damping properties.

Damping Improvements of over 30 % are consistently achievable post electrical processing, on rotors made with the following characteristics:

- High hyper eutectic material with C.E. > 4.5
- Elastic modulus in the range of 100 to 110 GPa
- Brinell hardness in the range of < 170 BHN
- Large Type A graphite flakes with flake size 2-3-4 with presence of C flakes < 10 %
- Coarse pearlite matrix
- Very low measurable magnetic field on rotor < 1.5 Gauss

CHAPTER 5

MATERIAL AND PROCESS CONFIRMATION STUDY

The main objective of this part of the study, is to use the characterized material structure that showed the best damping improvements, manufacture a new batch of rotors with a different geometry using this material, process the parts, and determine the damping benefits. The study also aims to understand the effects of critical process parameters on the damping improvements.

5.1. Material selection and prototypes:

The study was setup by making prototypes of a new geometry with the material structure suggested by the material characterization Study - High hyper eutectic iron with C.E. > 4.5, large Type A graphite flakes + C graphite using a Barium inoculant. A 345 OD x 30 mm thick MC1 rotor was used for this study. This rotor size has not been used in the previous studies. The main reason to pick this is to ensure that the geometry does not affect the damping improvements seen. Material Microstructure and the Chemistry for the study rotors are shown below in Figure 5.1, Figure 5.2 and Table 5.1.

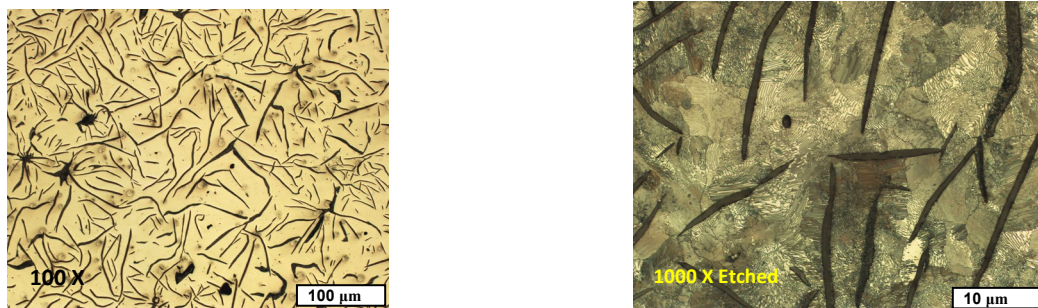


Figure 5.1. Microstructure 100 X LOM micrograph and 1000 X As polished and Etched LOM of the MC1 Rotors (IB Plate)

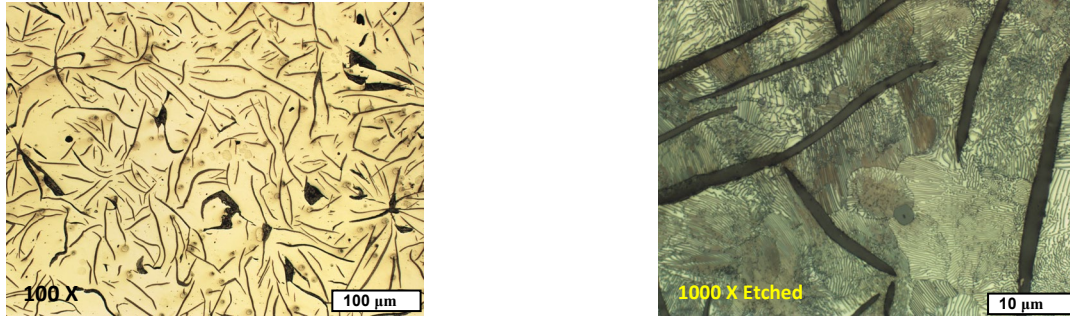


Figure 5.2. Figure 5.1. Microstructure 100 X LOM micrograph and 1000 X As polished and Etched LOM of the MC1 Rotors (OB Plate)

CARBON	%	3.81
MANGANESE	%	0.63
SILICON	%	2.38
SULFUR	%	0.04
PHOSPHOROUS	%	0.02
CHROMIUM	%	0.12
COPPER		0.08
NICKEL		0.04
MOLYBDENUM		0.03
TIN		0.07
C.E		
E.C		3.62

Table 5.1. Chemical analysis for the MC1 rotor batch from production data

As seen from the chemical analysis as well as the microstructure analysis, large Type A Graphite Flakes in the size range of 2 to 3 are predominant. Also Type C graphite is present, similar to the Microstructure of S01. The pattern of multiple long graphite flakes forming from one center is also noticeable in these rotors. Colonies of very coarse Pearlite are noted in the etched 1000 X micrographs on both the OB and IB plates. The C.E. is greater than 4.5 % and the E.C. is low at 3.62 %. The chemical analysis as well as the microstructure show large similarities to the analysis on the S01 rotor.

Since it is already known that the material properties are not changing significantly after processing, non destructive tests were not repeated in this study. This exercise was geared toward producing the characterised metal and ensuring similar improvements from electrical processing as noted before.

The baseline Q factor on the rotors used for this study is shown in Figure 5.3, and matches what was noted on the S01 rotors. All the rotors fall in the 200 to 350 range which is a very good starting point before the processing.

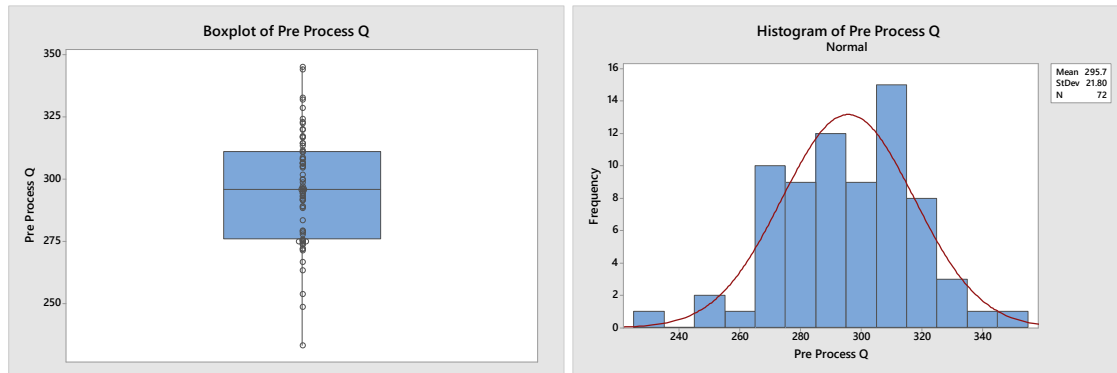


Figure 5.3. Boxplot and Histogram of MC1 Rotors Q factor Pre processing

The next part of the study is to set up the process DOE to understand the effects of process parameters. Based on all the exploratory research on EDM and IESV treatments, only the most critical factors and levels were picked for this study.

The most important factor is the time of processing and the lower the time of processing, the better for high volume production. So, time as a factor is critical. Current is also used as a factor since some of the IESV DOE showed statistical effect of current, even though no significant effects of current were seen in the Magnetic Coil or EDM experiments. The dielectric used in the EDM process can also be a variable since dielectric oil, deionised water or Nitrogen could all be used. Since experiments with deionised water induced extreme corrosion on the rotors, this variable was not considered and discarded. The effects of Nitrogen may be researched at a later time.

Due to the high volume of rotors used in the industry with Ferritic Nitro Carburizing [53, 54], a new variable was introduced into this study. The FNC is a heat treatment process where the rotors are typically heated to a temperature range of 600 C to thermo-chemically diffuse Carbon and Nitrogen beneath the surface to form Ferritic Nitro Carbide White layer as shown in Figure 5.4. This is a patented process for brake rotors. Patent # US 8,287,667.

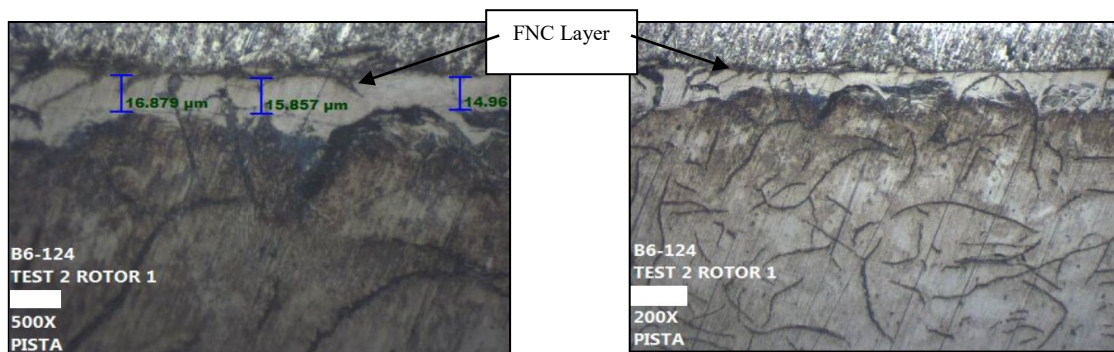


Figure 5.4. FNC white layer as seen in the micrographs of the brake rotor plates

The main function of this white layer, which is hard, smooth and highly wear resistant is to reduce corrosion on the surface, improve the corrosion cleanability of the surfaces in order to avoid oxide layer build up, and prevent corrosion induced vibration [11]. It also improves the wear rate of the rotors and brake pads, and thus increases the life of these components.

So, a portion of the rotors made for the study were FNC treated. The base Q factor of the FNC treated rotors are shown in Figure 5.5

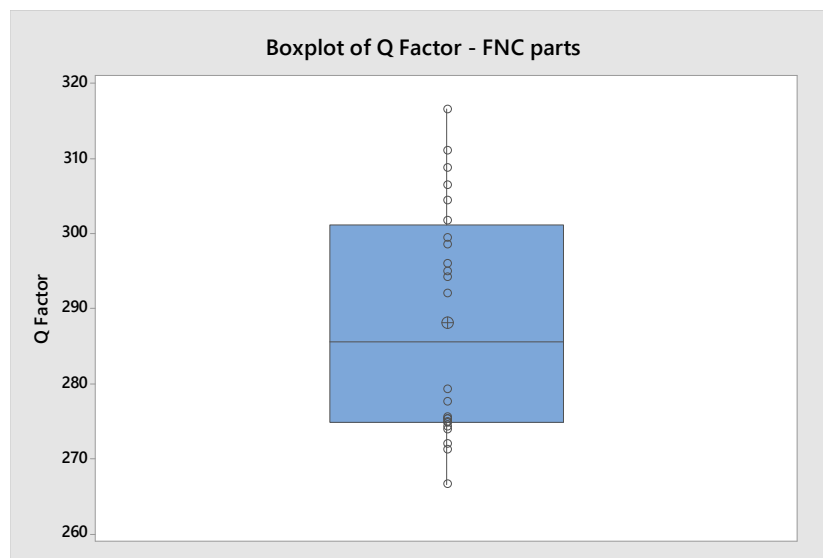


Figure 5.5. Boxplot of Q Factor on FNC rotors

As can be noted, all the parts are within the same range of Q factor as No FNC parts.

5.2. Process DOE

The Process DOE study was set up to run each of the factors briefly discussed above, at multiple levels as shown in Table 5.2.

Factor	Level					
	1	2	3	4	5	6
TIME (secs)	5	10	30	60	90	120
FNC/NFNC	NFNC	FNC	NFNC			
Current (amps)	5	10	20			

Table 5.2. Factors and levels used for the process parameter study

There are 6 levels for time ranging from 5 seconds to 120 seconds, while the current has 3 levels and the range is 5 to 20 amperes. Rotors with and without FNC were also tested. Process used for the study was the same as previously used for all the tests – Ingersoll EDM machine with the sacrificial steel machined at three locations on rotor brake plates 120 degrees apart.

Post process data for the Q factor on all the rotors is shown below in Figure 5.6.

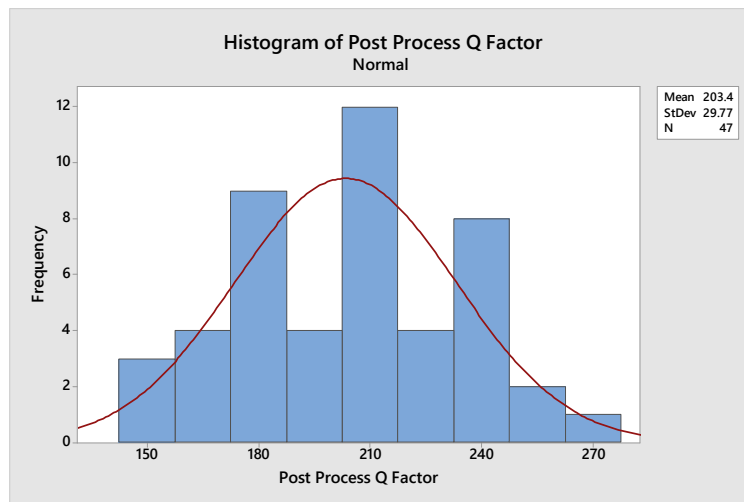


Figure 5.6. Histogram of post process Q factor on all MC1 rotors

In spite of all the varying factors and levels, Q factor on post processed parts are in the range of 150 to 300. Comparison of the pre and post process Q factor is shown in the histograms shown in Figure 5.7. Data shows a clear mean shift in Q factor and damping on the processed parts, irrespective of the variables and factors used in the tests. Boxplots shown in Figure 5.8 shows the mean shift from Q factor of ~ 300 to a Q factor of ~ 200.

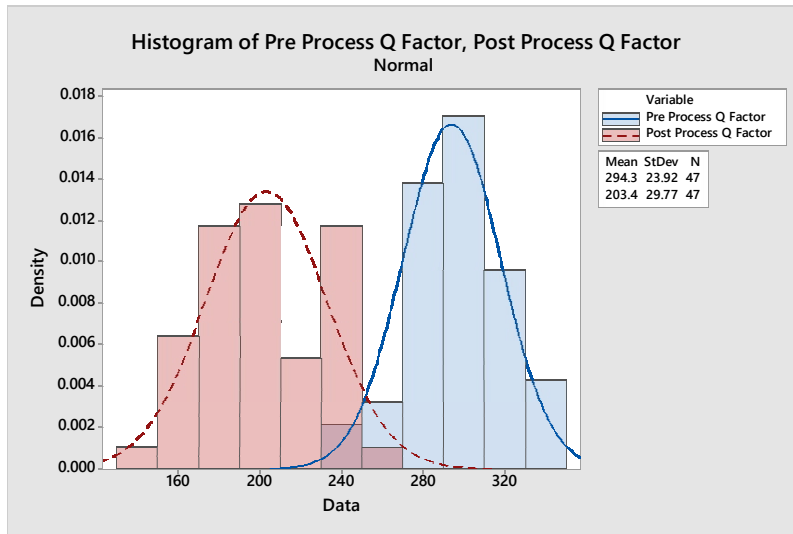


Figure 5.7. Histogram of pre and post process Q factor on MC1 Rotors

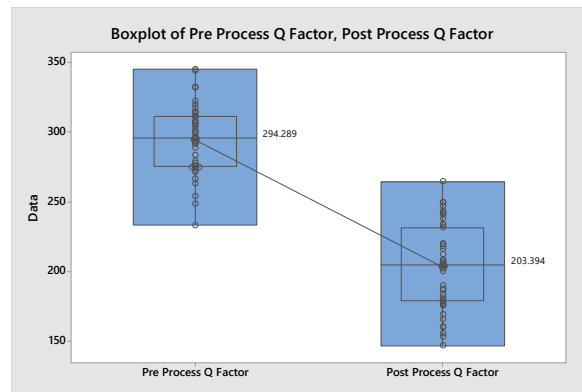


Figure 5.8. Boxplot of pre and post process Q Factor on MC1 rotors

The change in Q factor from the processing is shown in the % Q Factor change as shown in the Figure 5.9. Damping Improvements range from ~ 15 % to 50 % depending on the factors used.

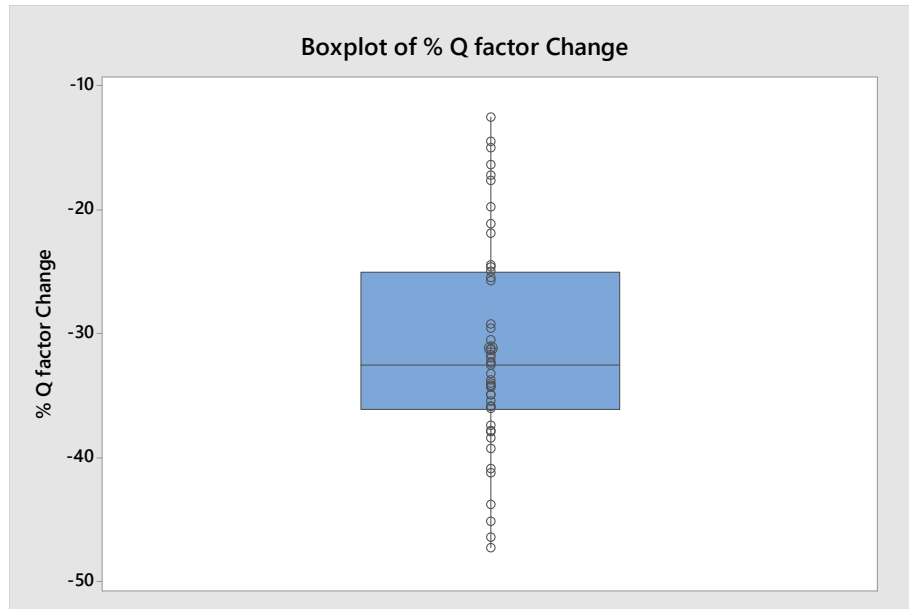


Figure 5.9. Boxplot of % Q factor change due to the electrical processing

The improvements are not all in the 30 to 50 % range as expected, so a more detailed analysis of the data is required. It seems most probable that some of the factors have a larger influence on the % improvements in damping observed.

Mean Effect plots shown in Figure 5.10 show the effects of each of the factors and the levels on the post process Q Factor. As it can be seen, current has NO effect. Time and FNC heat treatment seem to have a statistically significant effect. The effects of all the factors on the % Q Factor improvements are shown in Figure 5.11.

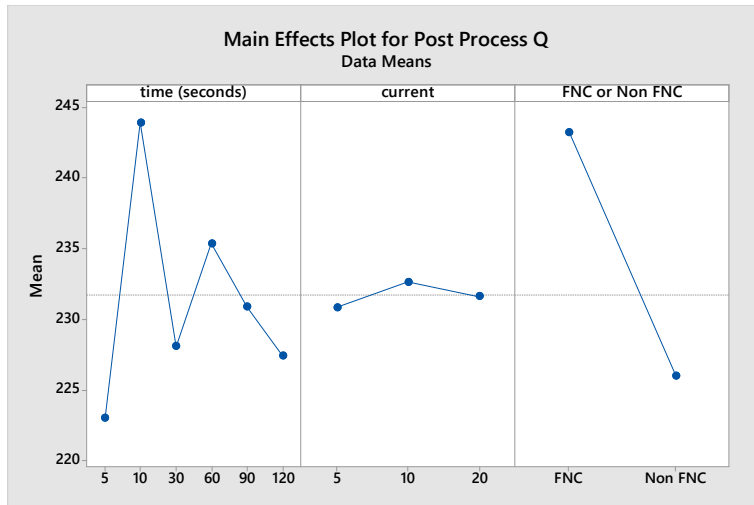


Figure 5.10. Mean Effects plot showing the effects of different factors and levels on post process Q factor

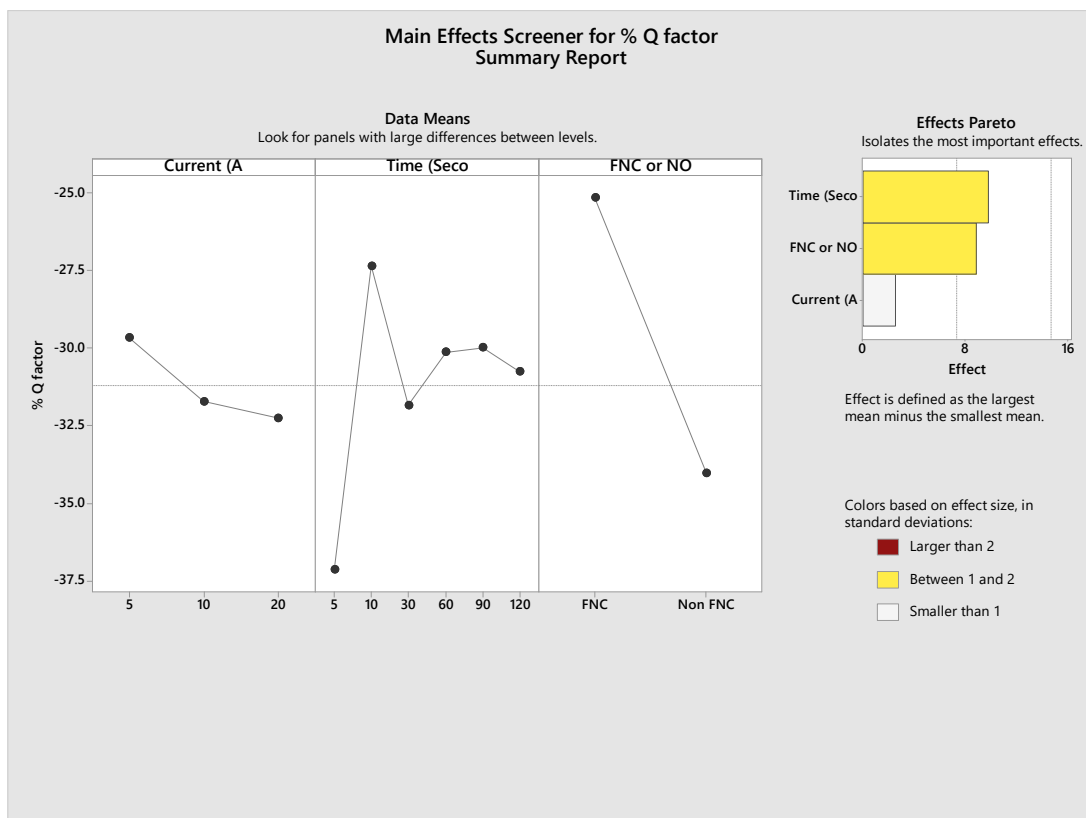


Figure 5.11. Mean Effects Screener plot showing the effects of different factors and levels on % Q factor change

As can be seen from Figure 5.11 the Pareto effects show very clearly the effects of time, FNC and current. It seems fairly clear that current has no effect on the damping improvements. The heat treatment (FNC) seems to have a large effect on the damping improvements. This could be due to the change in the surface and the presence of a nitro carbide layer of 10 to 20 microns beneath the surface and a possible change to the part microstructure due to the temperatures being in the range of stress relief for grey cast irons.

Interaction Plots shown in Figure 5.12 show the interactions between the factors and their effects on damping improvements. There are no interactions between FNC and current but some interactions are noted with time and current as well as time and FNC.

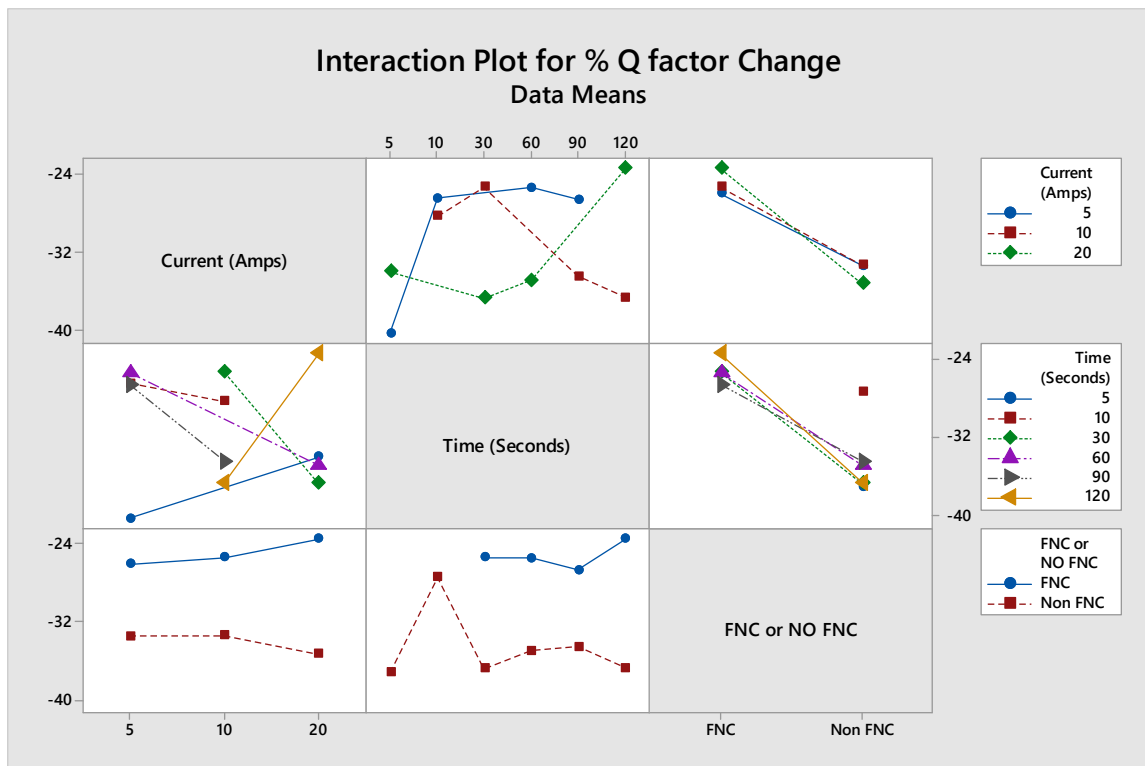


Figure 5.12. Interaction plots for % Q Factor change

5.4. Discussion and Conclusions:

Based on the Mean effects plots it can be seen that parts with No FNC perform better than FNC rotors with electrical processing and all rotors (with and without FNC) show significant damping improvements. There seems to be an interaction between time and current, so an optimised process solution is possible for the best damping improvements from the electrical processing. The best improvements are noted with the least amount of time at 5 seconds. Beyond 10 seconds of processing, there does not seem to be any significant effect of time of processing on the damping improvements as shown in Figure 5.12. This is a very important observation, since it makes the process feasible for high volume production and reduces the costs.

Based on these results another batch of rotors were produced and 20 rotors processed under the process conditions of 5 seconds and 5 amperes. As shown in Figure 5.13, there is a consistent damping improvement on all rotors and a significant mean shift, resulting in a very highly damped rotor with a Q factor in the range of 100 to 300. It should also be noted that improvements in the range of 30 to 50 % are obtained on all the rotors.

These results conclude the two studies to characterise the material and the process to ensure consistent damping improvements from electrical processing, and to produce rotors with a Q factor in the range of 100 to 300. The most important and critical next step is to validate the rotors to determine any improvements in noise performance.

It should also be noted that on some of these rotors, the Q factor was measured across all modal frequencies in order to understand if the damping benefits are not specific to any modal frequency. As can be seen in the Table 5.3., damping improvements are seen across

the full spectrum of frequencies. The % change in damping is variable at different modes but the 2 ND mode is a good indicator of the average damping percent improvements to be expected across the entire FRF spectrum of the rotor,

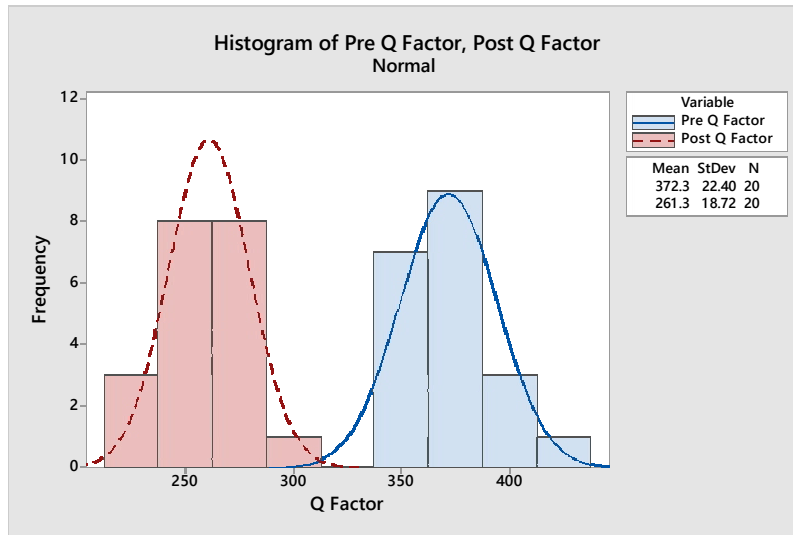


Figure 5.13. Histogram of pre and post process Q factor showing a damping improvement

Mode	Q Factor Pre Processing	Q Factor Post Processing	% Q Change
2 ND	241.82	167.68	-30.66%
3 ND	250.02	179.77	-28.10%
4 ND	323.56	194.55	-39.87%
5 ND	347.86	235.37	-32.34%
6 ND	412.89	274.75	-33.46%
7 ND	507.00	200.38	-60.48%
8 ND	390.30	215.81	-44.71%
9 ND	396.36	230.63	-41.81%
10 ND	427.53	213.72	-50.01%
11 ND	427.12	204.42	-52.14%
1 T	313.20	211.15	-32.58%
2 T	464.56	221.44	-52.33%
3 T	528.35	202.21	-61.73%

Table 5.3. Q factor and % change at all bending and tangential modes

CHAPTER 6

NOISE VALIDATION

The main intent of this entire project is to obtain a reduction in brake squeal noise occurrences. Noise validation forms the most critical part to ensure the study is useful and the damping improvements seen from all the additional processes, help reduce noise.

6.1. Noise tests and test results

The tests were run on the S01 parts. A baseline part and a processed part were tested on a Link Dynamometer per the SAE J2521 specification with the cold noise section added. The test consists of a burnish section, and multiple stop and drag modules to test for noise under different driving conditions. The cold sections are included to simulate noise in colder climates and winter conditions. A Thermatron connected to the dynamometer ensures the environmental control of the dyno to run the colder temperatures needed. The range of temperatures tested typically varies in the range of ~ -10 C to 300 C.

Results of the noise validation are shown below in Figure 6.1. Several noise hits are seen at multiple frequencies, on the baseline part with a Q factor of 405, including cold and warm noise at 9 KHz and 11 KHz. The processed rotor with a Q factor of ~ 300 shows a complete elimination of all high frequency brake squeal noise occurrences. Some noise occurrences at low frequency remain, but all of the 9.1, 11.5 and 14 KHz are completely removed. This test by itself, validates the study and its benefits to brake system development.

Noise hits at 2.5, 9.1, 11.5 and > 14 KHz

No Noise hits at any of the high frequencies

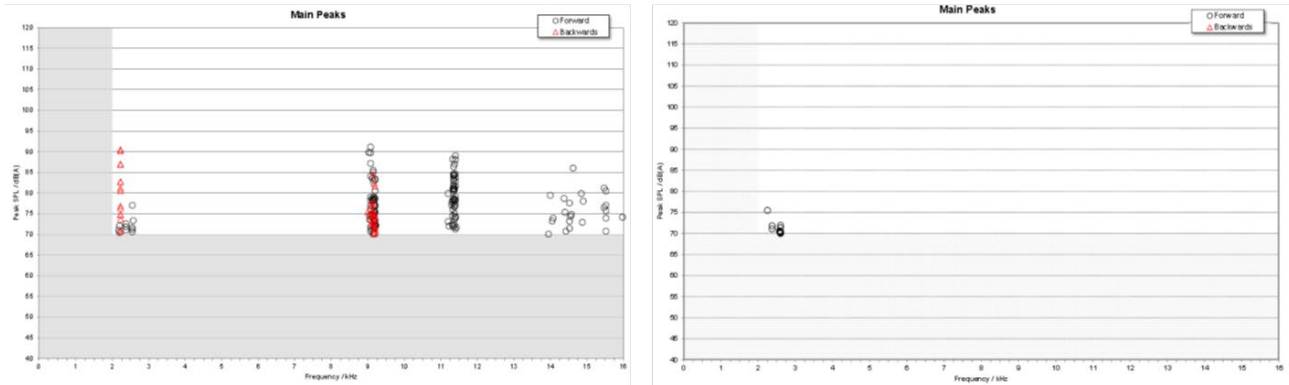


Figure 6.1. Noise testing on baseline and a processed rotor of S01

6.2. Noise Testing and Results on MC1 parts

Noise testing was continued on the parts from the process DOE study. 3 baseline unprocessed rotors and 3 processed rotors were tested.

These parts were tested according to a customer noise test schedule. The results showing the noise occurrences % are shown in the Table 6.1 below. The tabulated form shows the % occurrences at each dB level and frequency levels, and if the parts meet requirements.

Results show a lot of noise on the baseline parts at multiple frequencies of 2.8, 5.5, 12.5, 13.5 and 14.5 KHz (warm noise) and cold noise at 14 KHz, as shown in Figure 6.2 and in the Table 6.1. All 3 baseline parts did not meet the noise requirements.

The noise at ~ 2.8 KHz is a known noise issue with the calipers on this system and hence was not relevant to this study, and damping benefits were expected to have no effects on this noise frequency.

Figure 1. Sound Pressure Level vs. Frequency
Test: 3539-1

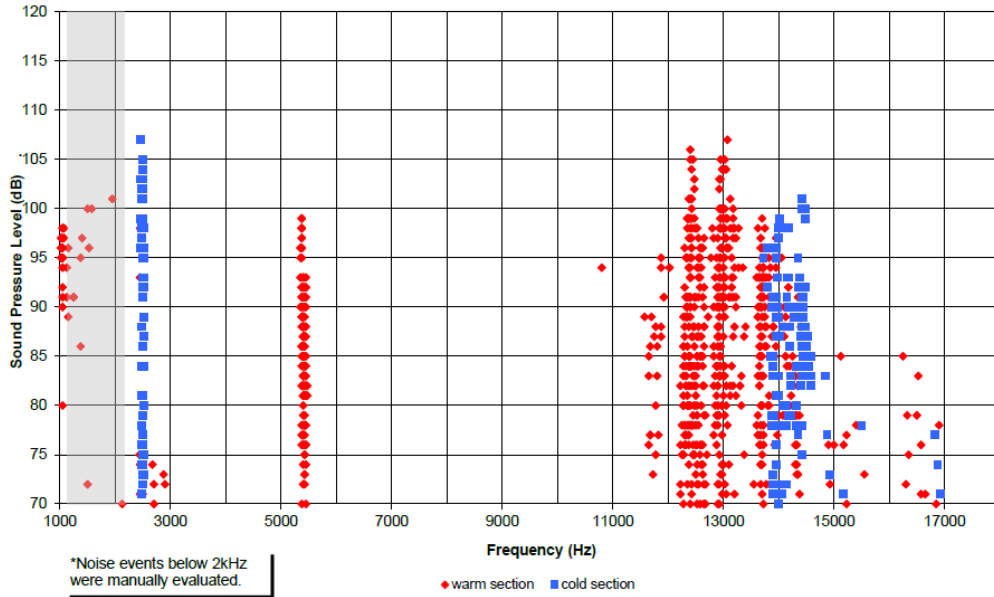


Figure 6.2. Noise test results on a baseline rotor

Test #	Rotor	Caliper	Lining	Dominant Frequencies		>=70 dB	>75 dB	>85 dB	>95 dB	>=70 dB	>75 dB	>85 dB	>95 dB
				Warm [kHz]	Cold [kHz]	< 10	< 3	< 0.8	< 0.2	< 10	< 3	< 0.8	< 0.2
3539-1	345X30 Baseline	4x42mm	HP1000	5.5, 12.5, 13.5, 14.5	14.0	40.17	35.67	21.41	5.67	20.46	17.48	10.73	1.06
3539-2	345X30 Baseline	4x42mm	HP1000	5.5, 14.5		9.91	8.48	4.72	0.48	0.00	0.00	0.00	0.00
3539-3	345X30 Baseline	4x42mm	HP1000	5.5, 14.5		17.86	13.88	5.62	0.32	0.83	0.17	0.00	0.00

Table 6.1. Noise occurrences at different frequencies and dB levels on baseline rotors

Processed rotors show a completely different story as seen below in Figure 6.3. All the noise frequencies are eliminated with a completely green performance on 2 of the rotors. The 3rd rotor has some noise hits at 13.5 KHz which makes it red in some portions, but all the other frequencies are eliminated. Overall, the processed rotors show ~ 85 to 100 % reduction in noise occurrences compared to the baseline rotors.

Figure 1. Sound Pressure Level vs. Frequency
Test: 3485-5

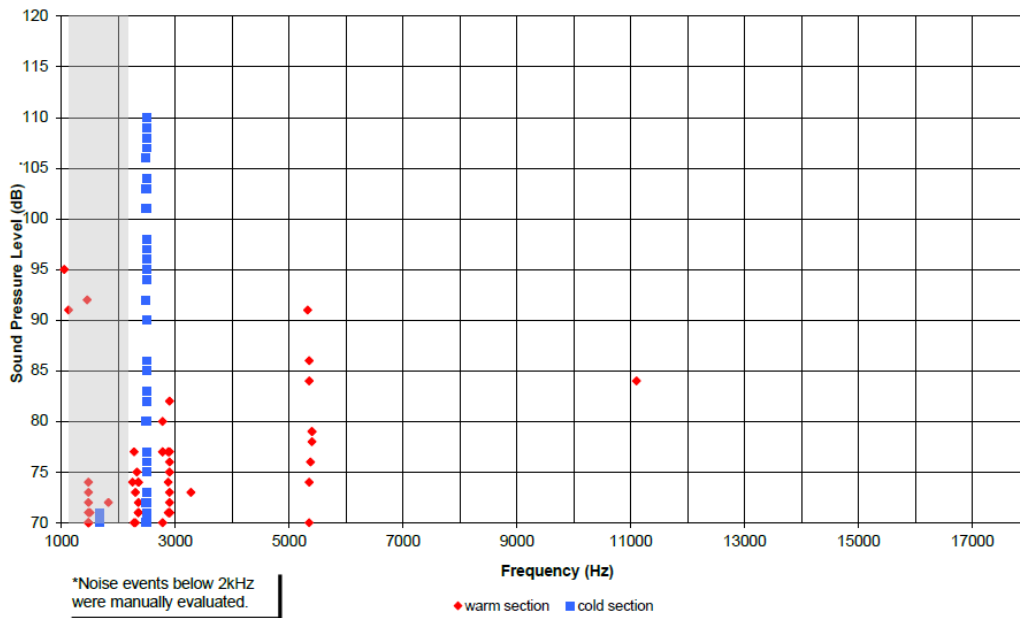


Figure 6.3. Noise Test per customer Noise Test Specification on processed rotors

Pictures in Figure 6.3 and Table 6.2 show the noise occurrences and frequencies and their reduction on processed rotors.

Test #	Rotor	Caliper	Lining	Dominant Frequencies		>=70 dB	>75 dB	>85 dB	>95 dB	>=70 dB	>75 dB	>85 dB	>95 dB
				Warm [kHz]	Cold [kHz]	< 10	< 3	< 0.8	< 0.2	< 10	< 3	< 0.8	< 0.2
3485-1	345X30 Processed	4x42mm	HP1000			0.21	0.21	0.00	0.00	0.17	0.00	0.00	0.00
3485-5	345X30 Processed	4x42mm	HP1000			0.6	0.4	0.1	0.0	0.0	0.0	0.0	0.0
3485-6	345X30 Processed	4x42mm	HP1000	13.5		9.95	8.36	5.40	0.90	2.15	1.49	0.33	0.00

Table 6.2. Noise occurrences at different frequencies and dB levels on processed rotors

6.3. Observations and Conclusions

All the tests show definite noise reduction on the processed rotors compared to unprocessed parts. The material and the process utilized for the research show a Q factor in the range of 100 to 300 and ensure reductions of 80 to 100 % in noise occurrences. Different noise test procedures showed the same results in terms of noise reductions on processed parts, which ensures no effect of small changes in test procedures and test schedules on the observed results.

CHAPTER 7

ROTOR PERFORMANCE VALIDATION

As discussed in the literature review, there is no clear understanding of the effects of electrical or magnetic processing on rotor performance characteristics like thermal cracking, output, wear and corrosion etc. The main objective of this portion of the study was to evaluate the performance of processed rotors.

The following tests were conducted:

1. Thermal Cracking test

To understand the effects on cracking due to thermal abuse of the braking system – tests were run per a typical industry specification. Rotors typically reach a maximum temperature of $\sim 550^{\circ}\text{C}$ during the testing.

2. Thermal Roughness testing

To understand the effects of the rotors on vibration and roughness performance induced by brake torque variation.

3. High temperature Wear testing

To understand the effects of processing on the wear rates of the components, which translates to the life of the rotors and pads.

4. Brake Output tests

To understand the effects of processing on the friction effectiveness and brake output

5. Corrosion tests

To understand if there are any effects on corrosion performance due to the processing. ASTM B117 for 240 hrs was used to evaluate corrosion and red rust.

6. Effects of wear on damping loss

To understand if the damping benefits remain after the rotor is used in service and is machined to its serviceable thickness.

7. Effects of Time and Temperature on the damping benefits

To evaluate the effects of time and temperature in static and dynamic test conditions to understand if the damping improvements from the processing remain after usage, or are diminished.

7.1. Thermal Cracking Tests

Test is run on a LINK dynamometer at Rassini per a typical thermal cracking specification. Test involves thermal cycling of the rotor and running multiple stops until the rotor reaches a temperatures of over 500 °C, use of high speed cooling air to cool the rotor back to an IBT, before the next cycle. This test ensures the rotor can perform well through thermal fatigue as well as thermal shock. The rotor needs to run through several hundred cycles of the above, without cracking through the plates or having a radial crack extending 2/3 of the swept area of the brake plate.

3 processed rotors were tested. Results showed no cracking on the rotors, as shown in the Figure 7.1. All the tests passed the requirements and were similar to baseline rotors.

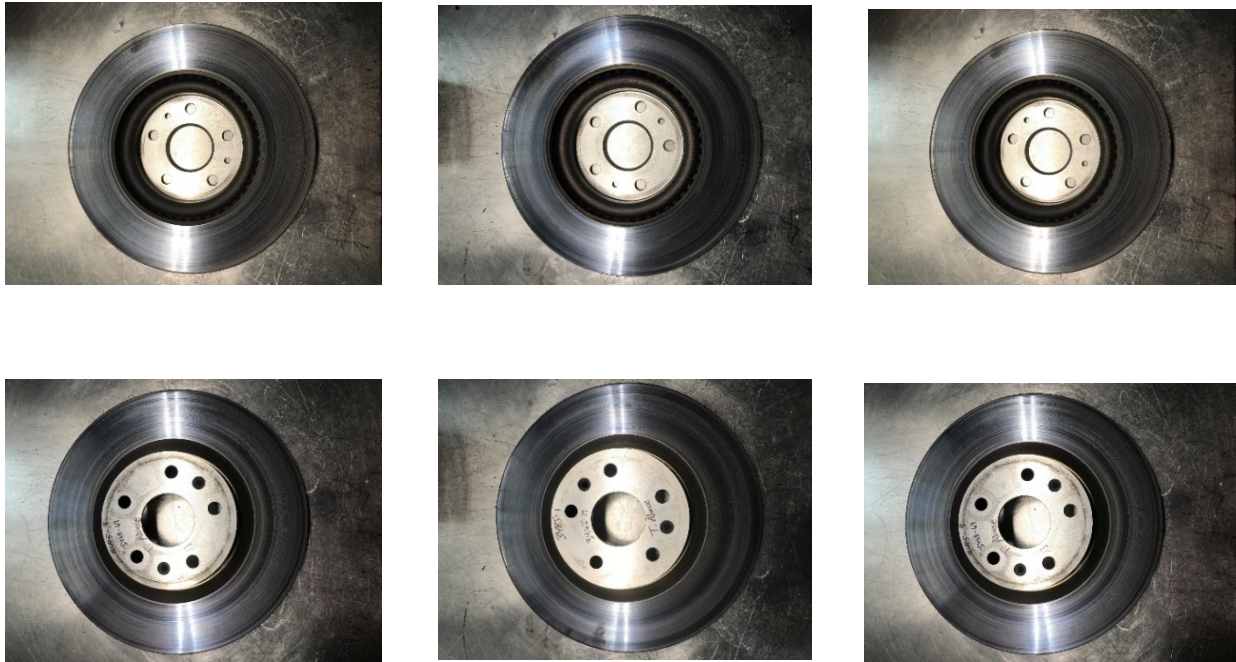


Figure 7.1. Post test parts from Thermal Cracking tests on processed rotors

7.2. Vibration Tests

Test was run per a typical industry specification on a dynamometer. Processed rotors and baseline rotors were tested. Testing comprises of stop schedules, typically comprising of cycles of multiple stop tests at specific speeds and decelerations, and the rotor brake torque variation (BTV) is recorded. Temperatures seen in these sections are in the range of 250 – 300 °C. High BTV results during these tests flag vibration issues on the vehicle and customer dissatisfaction.

Results showed similar results for Brake Torque Variation (BTV) on baseline and processed rotors, as shown in the Figure 7.2 on the test schedules.

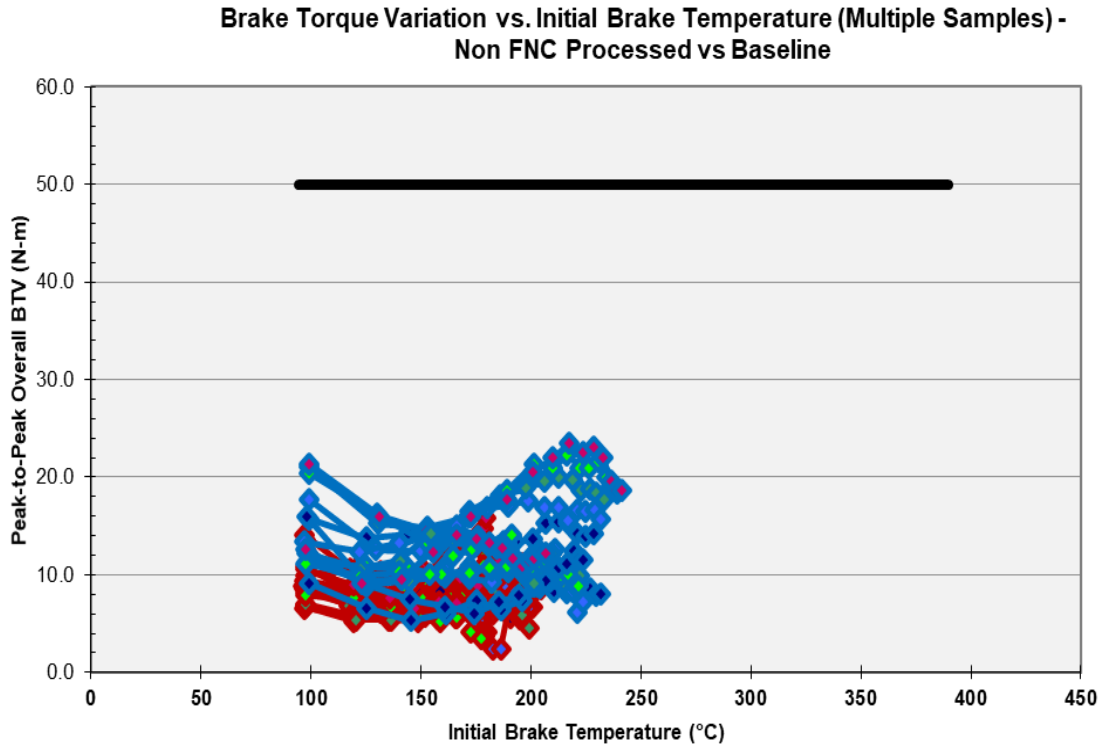


Figure 7.2. BTV Data for Baseline and Processed Rotors for the Base Test Schedule

All the tests passed the requirements and were similar to baseline rotors. The effects on the torque variation are negligible.

7.3. Wear Tests

Testing was conducted on a dynamometer per a standard industry specification. The tests were run on a baseline rotor and a processed rotor as well as with and without FNC. As seen in the Figure 7.3, Results show no differences in the wear rates and life predictions between the baseline and processed rotors for non FNC versions of the rotor. Figure 7.4 shows the test results on the baseline FNC and processed FNC rotors, which also show negligible differences.

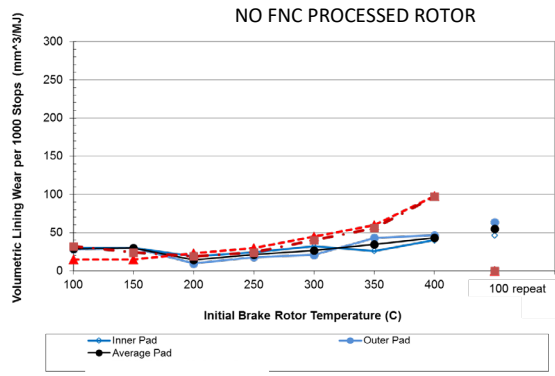
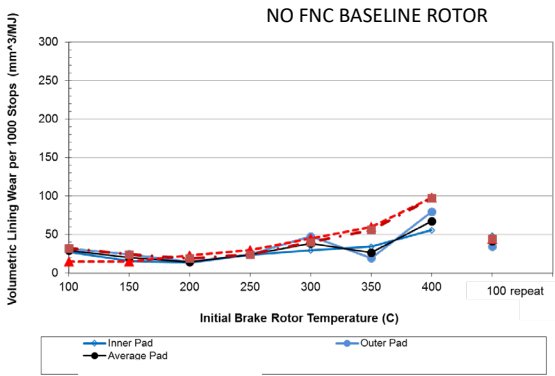


Figure 7.3. Wear Tests on No FNC Baseline and Processed Rotors

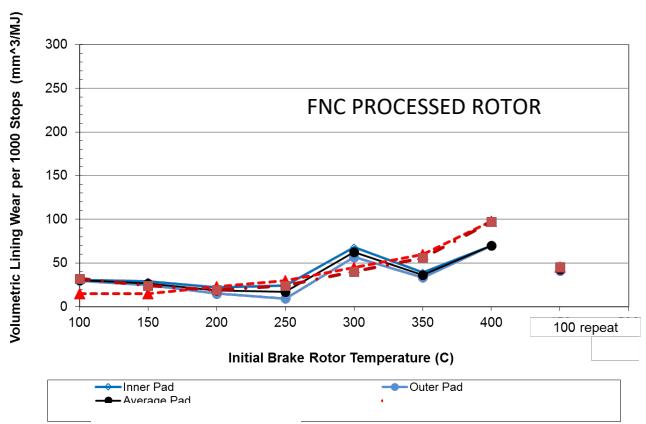
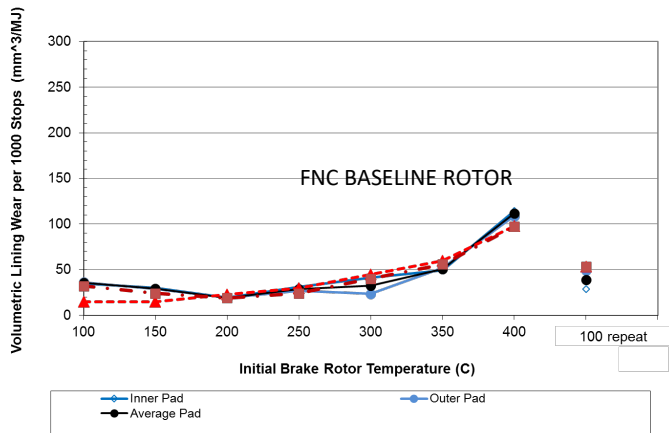


Figure 7.4 Results of wear test on baseline and processed rotors with FNC

7.4. Corrosion Tests

Parts were tested per the ASTM B117 specification - salt spray testing for 240 hrs (10 days) at Rassini in a Cyclic Corrosion Chamber shown in Figure 7.5. The requirements criteria for these tests is less than 10 % red rust in the evaluated areas after the 240 hr test.

Post test pictures are shown in Figure 7.6, 7.7 and 7.8, and shows no rust in the evaluated areas of the hat, brake plates and the outer diameter of the rotors. Some rust is seen in the cast vent areas, as expected.

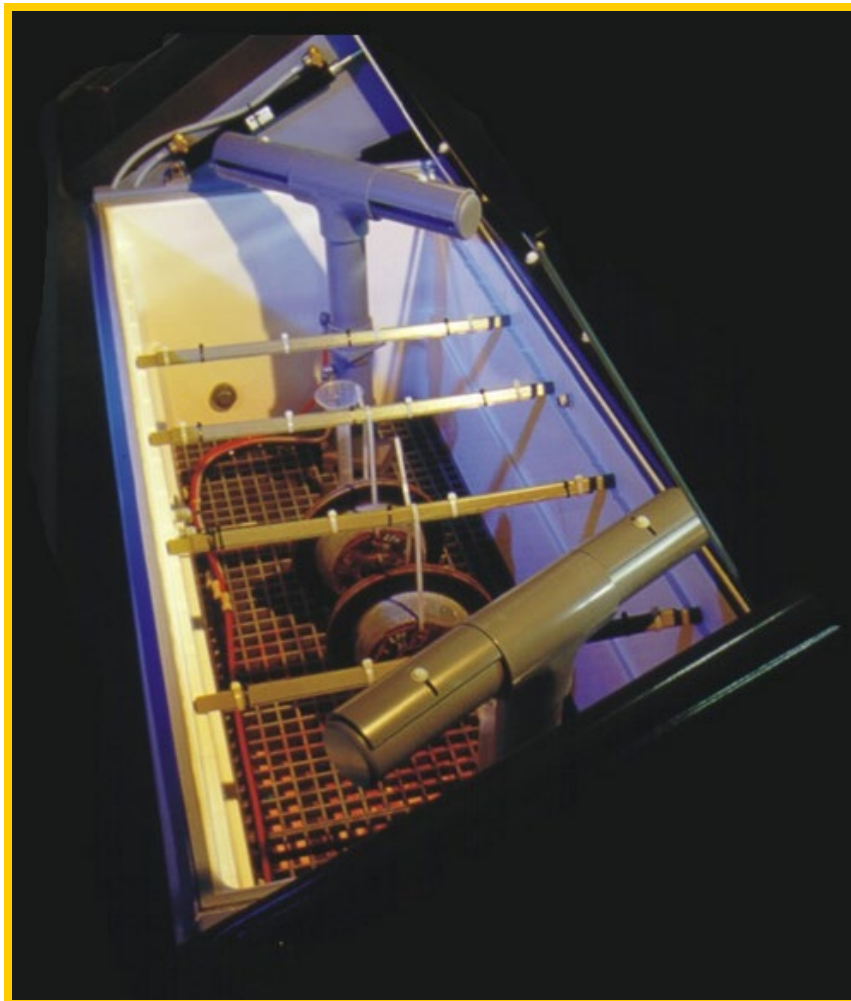


Figure 7.5. Corrosion Test Chamber to run salt spray testing



Figure 7.6. Post ASTM B117 Corrosion test pictures on processed part # 1



Figure 7.7. Post ASTM B117 Corrosion test pictures on processed part # 2



Figure 7.8. Post ASTM B117 Corrosion test pictures on processed part # 3

7.5. Brake Output Testing

Tests were conducted on a dynamometer, per standard industry specification. Baseline rotors and processed rotors were both tested, with and without FNC. Test is designed to understand the friction effectiveness changes through multiple stop schedules, to understand performance in green rotor and pad conditions, through burnish sections, as well as high speed and deceleration stops, and also to determine the fade and recovery performance of the brake linings. The test is a critical performance indicator on stopping distance of the system in green and used conditions.

Results show very similar results on baseline and processed no FNC rotors. As can be seen in Figure 7.9, the friction results for the rotors are very similar and within the normal range of variations typically seen in these tests.

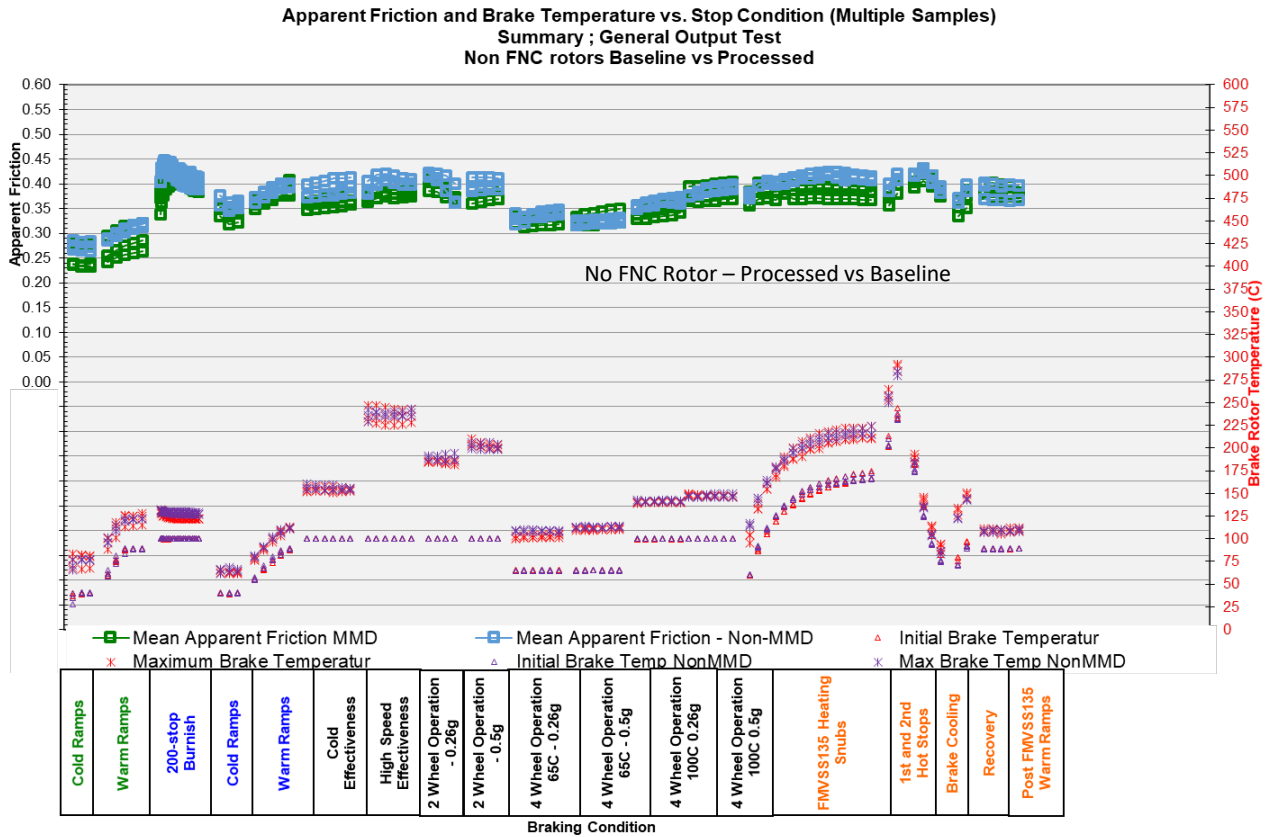


Figure 7.9. Brake Output testing results for baseline and processed rotors with no FNC. However on the FNC rotors as shown in Figure 7.10, a drop in friction is seen in the green sections of the tests during the cold and warm ramp ups schedules, between the processed and baseline rotors. After the burnish section, the effectiveness data is similar, which means the brake output is the same on baseline or processed rotors. However the 10 to 20 % drop in effectiveness in green condition on FNC rotors needs to be analyzed further.

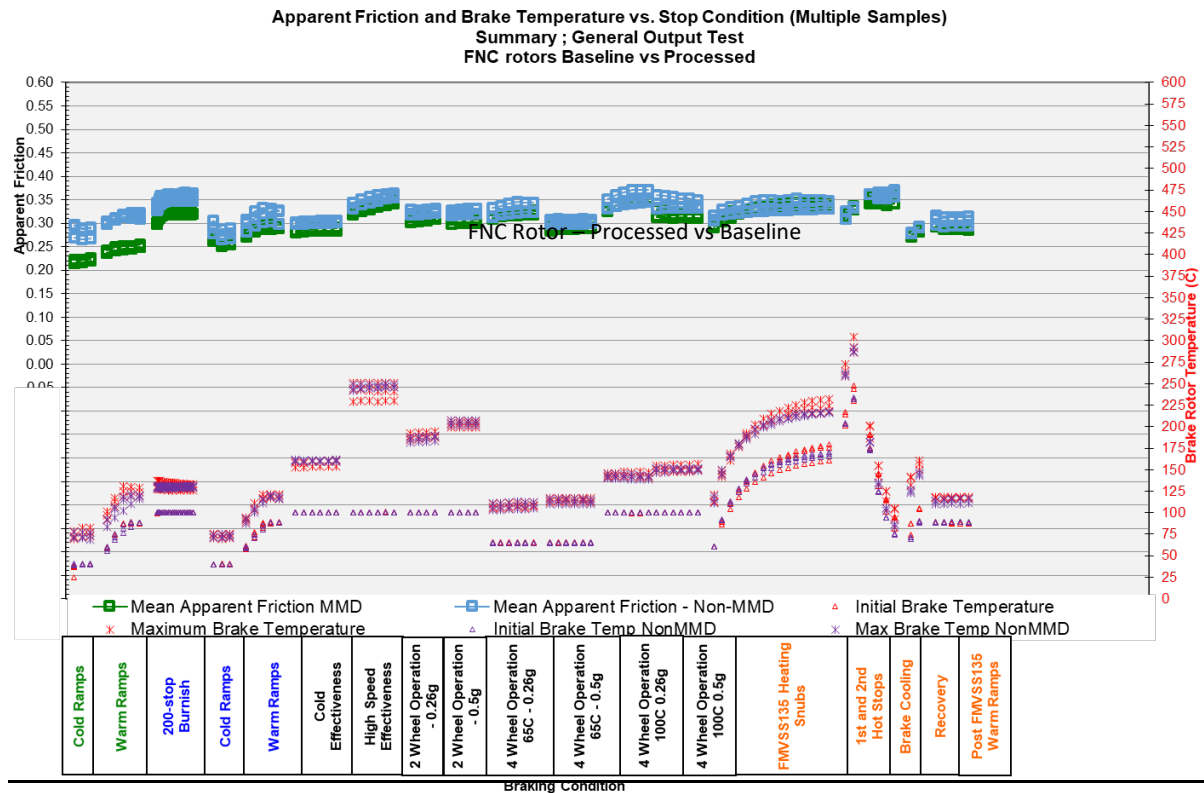


Figure 7.10. Brake Output testing results for baseline and processed rotors with FNC

7.6. Effects of Machining on Rotor Damping Improvements

This test was designed primarily to evaluate the damping benefits after the rotors reach their minimum service thickness. Typically, all brake rotors have a minimum service thickness requirement beyond which the rotor needs to be replaced, since there cannot be any braking output (since the pads cannot contact the rotor surface). In most cases, this is approximately 2 to 3 mm lower than the full thickness of the rotors. For e.g. for a 30 mm thick rotor, the minimum thickness could be between 27 to 28 mm depending on the caliper type.

To study this, 3 baseline and 3 processed rotors – rotors of same geometry and base metal from the same batch (parts from the process DOE study) were measured for Q factor. Then 1.5 mm was machined off of each brake plate, thus removing a total of 3 mm thickness on the 30 mm rotors. The final thickness after machining was 27 mm on all 6 rotors. Q factor was re-measured on all the rotors after machining.

Objective of this test is to determine if the damping benefits obtained from the processing remain, or are lost after wear. Results are shown in the Figure 7.11. As can be observed, the processed parts retain the damping benefits after machining and have a better Q factor than baseline rotors even after 3 mm of wear on the brake plates. There is a drop in Q factor on all 6 rotors (better damping). However, the processed parts which had better damping compared to baseline rotors initially, still retained the better damping.

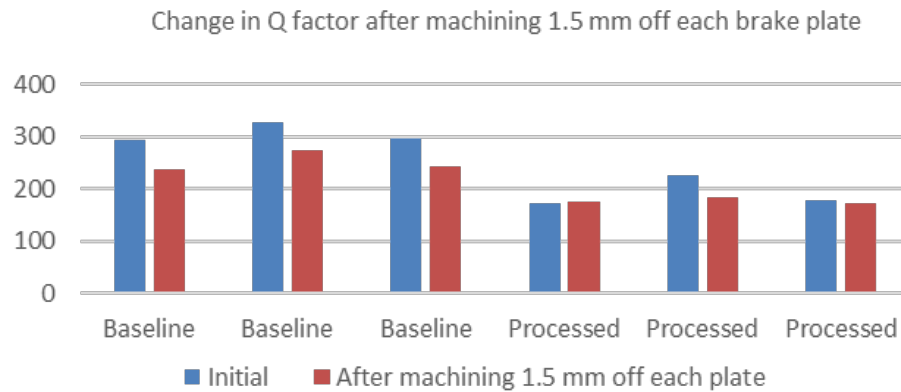


Figure 7.11. Change in Q factor with machining and wear

7.7. Effects of Time and Temperature

Objective of this study is to evaluate the effects of time and temperature on processed parts to ensure the damping benefits are still available after usage.

A static test DOE on the rotors was completed in a gas furnace as shown per the Table 7.1 below. Rotor Q factor were monitored after exposure to different times and temperatures as shown in Table 7.1.

	Time (minutes)	Temperature (C)						
		50C	150C	250C	350C	450C	550C	650C
Q Factor Initial	0	425.67	417.67	407.33	394.67	426.00	442.67	443.67
Q Factor Post Day 1	15	428.67	403.67	425.33	401.67	454.33	525.33	825.33
Q Factor Post Day 2	30	423.00	413.67	426.00	411.33	520.00	770.00	697.33
Q Factor Post Day 3	60	419.00	416.67	443.00	421.00	762.67	869.33	695.00
Q Factor Post Day 4	120	421.67	424.33	467.00	464.33	855.33	659.33	674.00
Q Factor Post Day 5	240	424.00	439.33	471.00	529.00	804.00	663.67	810.00
Q Factor Post Day 6	420	428.00	436.33	473.67	621.33	796.33	712.00	820.00

Table 7.1. Effects of time and temperature on Q factor on processed rotors

Waterfall plots shown in Figure 7.12 clearly discern the effects of time and temperature. It can be observed that the Q factor does not change significantly until ~ 350 °C even with prolonged exposure times of 60 minutes. However, at temperatures of over 450 °C, exposure for much lower times of 15 minutes, results in a loss of damping. Higher exposure time results in significant loss of damping. At even higher temperatures closer to 600 °C, very little exposure times result in significant loss of damping. However, stress relieving effects start playing a role which helps improve the damping (lower Q factor). At some point, the loss of damping benefits due to temperature and time exposure, and damping benefits due to stress relief balance each other out. It must be noted that at typical service

braking temperatures (50 to 300 C) the damping benefits are not diminished and the Q factor changes are minimal. This is very important and critical for the use of this technology.

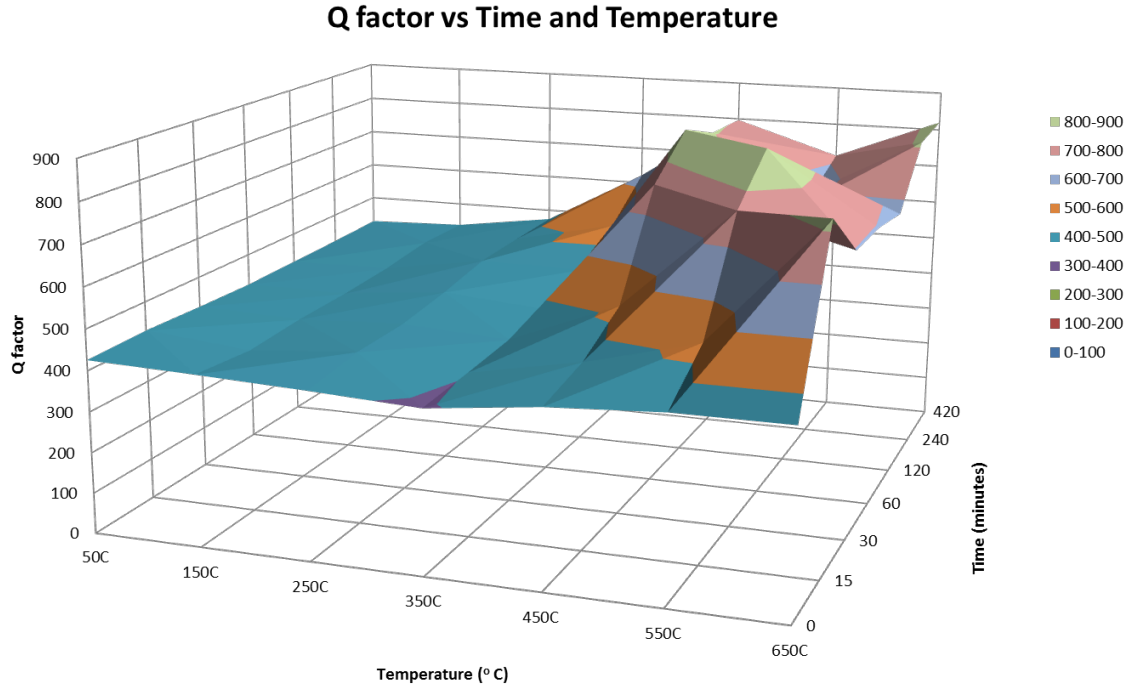


Figure 7.12. Waterfall Plot of Q factor changes with Time and Temperature

Q factor results from post test processed parts from some of the tests are also shown below. It can be seen that the processed and baseline rotors show similar changes, which means the damping benefits still remain intact, after extensive thermal cycling over 500 °C under regular testing conditions, as long as the exposure times are low.

Test Procedure	Pre Test Q Factor	Post Test Q Factor	Max. Temperature
Thermal Shock Test	287	221	620 C
Noise Test	1022	987	250 C

Table 7.2. Test procedures and temperatures before and after testing - baseline rotors

Test Procedure	Pre Test Q Factor	Post Test Q Factor	Max. Temperature
Thermal Shock Test	314	241	610 C
Noise Test	948	931	250 C

Table 7.3. Test procedures and temperatures before and after testing - processed rotors

The Noise tests cover a range of service conditions that are more representative of normal driving conditions and rotor temperatures. The Q factor changes post test as seen from the Table 7.2 and 7.3, are negligible. Similar studies were done on all post test parts from the validation schedules and negligible changes observed.

The Q factor and FRF was also measured at all modal frequencies and monitored before and after testing on some of the tests. Results from the output tests are shown in Table 7.4.

Rotor	NFNC Processed - Pre Test		NFNC Processed - Post Test		
	Mode	Frequency (Hz)	Q Factor	Frequency (Hz)	Q Factor
2 ND		684	161.29	682	172.41
3 ND		1622	166.67	1617	172.41
4 ND		2614	192.31	2603	192.31
5 ND		3638	238.10	3622	277.78
6 ND		4666	238.10	4649	227.27
7 ND		5720	250.00	5691	238.10
8 ND		6799	217.39	6766	238.10
9 ND		7897	217.39	7854	238.10
10 ND		9019	294.12	8968	250.00
11 ND		10169	200.00	10200	208.33
12 ND		11338	185.19	11345	227.27
13 ND		12582	185.19	12528	217.39
1 T		5488	185.19	5466	178.57
2 T		8398	208.33	8365	238.10
3 T		11519	208.33	11621	250.00

Table 7.4. Pre and post output test FRF and Q factor measurements on MC1 rotors

As can be noted from the Table 7.4, there is very little change in the average Q factor or the FRF across all modal frequencies, post testing. The damping is still maintained post testing.

7.8. Validation Summary

Processed rotors perform better than baseline rotors in Noise tests ensuring a reduction of 80 to 100 % in noise occurrences. Processed rotors performed similar to the baseline rotors on all critical validation tests, with no differences seen in the performance characteristics. A loss in green output was noted on processed FNC rotors and needs to be further investigated. No issues were seen in the corrosion performance of processed rotors. The effects of time and temperature on the damping benefits on processed rotors became significant once temperatures are over 400 °C and rotors are exposed to these bulk temperatures for extended periods of time of over 15 minutes.

CHAPTER 8

CONCLUSIONS AND FUTURE WORK

This chapter summarises the conclusions from the research, and opportunities for future work, are discussed.

8.1. Conclusions

Based on the project objectives, the conclusions are divided into individual sections and summarized below:

1. Material for best damping improvements

- Highly damped brake rotors with a Q factor in the range of 100 to 300 and adequate strength can be achieved in production, through proper selection of material properties. Medium to High hyper eutectic metals, with low hardness and elastic modulus, combined with optimized electrical processing through EDM or a power generator like an IESV, can generate highly damped rotors.
- Damping improvements of over 30 % are consistently achievable post electrical processing, on rotors made with the following characteristics:
 - Hyper eutectic material with Carbon Equivalent > 4.5
 - Elastic Modulus in the range of 100 to 110 GPa
 - Brinell Hardness in the range of < 170 BHN
 - Predominantly large Type A graphite flakes with flake size 2-3-4
 - Coarse pearlite matrix
 - Low magnetic field on rotor < 1.5 Gauss

- A linear relationship exists between the Carbon Equivalent and the % damping improvements achieved through electrical processing. Parts with low carbon equivalent (near eutectic or hypoeutectic) showed no damping improvements.

2. Material Confirmation and Process Characterization

- All electrical and magnetic processing techniques like EDM, magnetic coils, IESV showed significant improvements in rotor damping. Highest damping improvements were achieved on parts made with the material structure characterized in Objective 1, of this study.
- Process DOE showed that the processing current has no effect on damping improvements. However, processing time showed a significant effect. It is found that a minimal processing time of 5 seconds is sufficient, to realize high damping improvements.
- Parts with no FNC showed a higher improvement in damping post processing, compared to FNC rotors.
- Study also showed that the rotor geometry has no effect on the damping improvements from electrical processing.

3. Noise Validation

- Rotors, produced with the characterized material structure from this study, combined with the optimized processing techniques discussed in Conclusion 2, show a noise occurrence reduction of 80 to 100 % in the brake systems.
- Noise reductions are predominantly observed in the frequency ranges of 3 KHz – 20 KHz. Lower frequency noises of < 3 KHz are typically caliper driven, and the processed rotors show no effect on noise at these frequencies.

4. Performance Tests Validation

- No significant effects are seen on rotor performance attributes, like thermal cracking, wear, torque variation, corrosion and output, on the rotors processed electrically.
- Benefits of the damping improvements from the processing are not diminished in regular rotor service conditions. However, extended exposure to high temperatures above 400 °C results in a loss of damping.
- Damping improvements are not lost due to rotor wear.
- There is a reduction in the green output (friction effectiveness) on the processed FNC rotors compared to an un-processed FNC rotor. However, the non FNC rotors did not show a reduction.

8.2. Future Studies

This research objective was primarily geared toward creating a high damped metal that could reduce or eliminate brake noise occurrences through material and cost effective additional processing. More research can be conducted in the following areas:

1. Better understanding of the process and its effects on the rotors
 - a. No effects on bulk material properties or structure of the rotor have been noticed due to the processing. Since the changes are assumed to be electromagnetic in nature, more work can be accomplished through magnetic imaging, to determine any changes in the magnetic domain structure of the iron.
 - b. Easier processing methods through use of the IESV should be researched, to determine if similar damping benefits can be obtained.

- c. Determine methods to realise the damping benefits on near eutectic and hypoeutectic rotor materials.
 - d. Investigate the effects of various heat treatment processes and surface treatment conditions like Grinding, Roller burnishing etc., on the damping benefits.
2. Investigate the use of this technology in other applications
- a. Determine if the damping benefits can translate into processing of other metals including steel, aluminum etc. Initial data shows an improvement on both metals and could be investigated.
 - b. Determine usage in other industries, with components made of ferromagnetic and paramagnetic materials.
3. Shaker tests to quantify the damping across all modal frequencies, and to evaluate the effects of temperature on the Q factor.

REFERENCES

- [1] This information is property of Rassini and is confidential. It may not be copied, disclosed to others, or used without the written consent of Rassini.
- [2] Limpert, R., (1999) Brake Design and Safety, SAE Inc.
- [3] Gillespie, T.D., Fundamentals of Vehicle Dynamics_(1992), Society of Automotive Engineers Inc.
- [4] Macnaughtan M.P., Krosnar, J. G., “Cast Iron-A Brake Disc Material for the Future?” (1998) International Seminar on Automotive Braking-Recent Developments and Future Trends. pp. 3–10.
- [5] Cueva, G., Sinatora, A., Guesser, W.L., Tschiptschin, A.P. (2003). Wear resistance of cast irons used in brake disk rotors. *Wear*, 255, 1256-1260.
- [6] Rhee, S.K, DuCharme, R.T. (1973). The friction surface of gray cast iron brake rotors, *Wear*, 23, 271–273.
- [7] Riahi, A.R., Alpas, A.T. (2003). Wear map for grey cast iron, *Wear*, 255, 401-409.
- [8] Chen, F., Tan, A.C., Quaglia, R.L., (2006), Disc Brake Squeal – Mechanism, Analysis, Evaluation and Reduction / Prevention, SAE International.
- [9] Cho, M.K., Kim, S.J., Basch, R.H., Fash, J.W., Jang, H. (2003). Tribological study of grey cast iron with automotive brake linings: The effect of rotor microstructure. *Tribology International*, 36, 537-545.

- [10] Yamabe, J., Takagi, M., Matsui, T., T. Kimura, T., Sasaki, M. (2002) “Development of Disc Brake Rotors for Trucks with High Thermal Fatigue Strength,” *JSAE Rev.*, vol. 23, no. 1, pp. 105–112.
- [11] Shin, M.W., Cho, K. H., Kim, S. J., and Jang, H. (2010). “Friction Instability Induced by Corrosion of Gray Iron Brake Discs,” *Tribol. Lett.* vol. 37, no. 2, pp. 149–157.
- [12] Liu, X., Takamori, S., Osawa, Y. (2004). “The Effect of Aluminum Addition on the Damping Capacity of Cast Iron,” (2004) *J. Mater. Sci.*, vol. 39, no. 19, pp. 6097–6099.
- [13] Miller, E.J., (1969). Damping Capacity of Gray Iron and Its Influence on Disc Brake Squeal Suppression. SAE 690221.
- [14] Metals Handbook. (1995). Vol.1 – Properties and Selection: Ferrous Metals, 2nd ed. *CASTI Publishing*.
- [15] M. I. Ripley and O. Kirstein, “Residual Stresses in a Cast Iron Automotive Brake Disc Rotor,” (2006) *Phys. B Condens. Matter*, vol. 385-386 I, pp. 604–606.
- [16] IN-EN-ISO-945, (2009) *Microstructure of Cast Irons*, p. 26.
- [17] ASTM-A247-16a, (2016). *Standard Test Method for Evaluating the Microstructure of Graphite in Iron Castings*, p. 13.
- [18] DIN-EN-ISO-6506, *Metallic Materials Brinell Hardness Test*. 2016, p. 24.
- [19] Triches, M., Gerges, S.N.Y., Jordan, R. (2004). Reduction of Squeal Noise from Disc Brake Systems using Constrained Layer Damping. *Journal of the Brazilian Society of Mechanical Sciences*, Vol. XXVI, 3.

- [20] Oberst, S., Lai, CS, J. (2008), A Critical review of Brake Squeal and its Treatment in Practice, 37th International Congress and Exposition on Noise Control Engineering, Shanghai.
- [21] Akay, A., (2002) “Acoustics of friction,” *Journal of the Acoustical Society of America*, 111(4), 1525–1548.
- [22] Abendroth, H., Wernitz, B. (2000). “The integrated test concept: Dyno-vehicle, performance-noise,” SAE Technical Paper Series, 2000-01-2774.
- [23] Dunlap, K.B., Riehle, A.M., Longhouse, E. R. (1999). “An investigative overview of Automotive Disc Brake Noise”, SAE Technical Paper Series, 1999-01-0142.
- [24] Cao, Q., Friswell, M. I., Ouyang, H., Mottershead, J. E., & James, S. (2003). “Car Disc Brake Squeal: Theoretical and Experimental Study”. *Materials Science Forum*, 440-441, 269–277.
- [25] Nouby, M., Abdo, J., Mativanan, D., Srinivasan, K. (2011). “Evaluation of Disc Brake Materials or Squeal Reduction”. *Tribology Transactions*, 54: 644 – 656.
- [26] Murakami, T., Inoue, T., Shimura, H., Nakano M., Sasaki, S. (2006). “Damping and tribological properties of Fe-Si-C cast iron prepared using various heat treatments”. *Material Science and Engineering A* 432, 113-119.
- [27] Golovin, S.A. (2011). “On the Damping Capacity of Cast Irons”. *The Physics of Metals and Metallography*, Vol. 113, No.7, pp. 716-720.
- [28] Malosh, B.J. (1998). “Disc Brake Noise Reduction through metallurgical control of rotor resonances”. SAE Technical Paper Series, SAE 982236.

- [29] Bagwan, S.S., Shelge, S.V. (2018). "Study and Analysis of Disc Brake to Reduce Disc Brake Squeal". International Journal for Research in Applied Science & Engineering Technology, Volume 6 Issue IV.
- [30] Belhocine, A., Ghazaly, M.N. (2016). "Effects of Young's Modulus on Disc Brake Squeal using Finite Element Analysis". International Journal of Acoustics and Vibration, Vol. 21, No. 3.
- [31] Papinniemi, A. (2007). "Vibro-acoustic Studies of Brake Squeal Noise". Thesis submitted for the Degree of Doctor of Philosophy.
- [32] Glisovic, J., Miloradovic, D. (2010). "Eliminating Brake Noise Problem". Mobility and Vehicle Mechanics, Volume 36, Number 3.
- [33] Ghazaly, M.N., Sharkawy, M., Ahmed, I. (2013). "A Review of Automotive Brake Squeal Mechanisms". Journal of Mechanical Design and Vibration, Vol.1, No.1, 5-9.
- [34] Graesser, R., & Relationship, T. (2009). The Relationship of Traditional Damping Measures for Materials with High Damping Capacity : A Review, 316–343.
- [35] Park, J., Han, J., Lee, S., Yi, K., Kwon, C., Lee, Y. (2016). "Inhomogeneity of Microstructure and damping Capacity of a FC25 Disc-Brake Rotor and their interrelationship". The Minerals, Metals & Materials Society and ASM International.
- [36] Vadiraj, A., Tiwari, S. (2014). "Mechanical and Wear Properties of High Carbon Grey Cast Iron for Automotive Brake Application". Transactions Indian Institute of Metals, 68 (3): 491-494.

- [37] Adams, R.D. (1972). “The damping characteristics of certain steels, cast irons and other metals”. *Journal of Sound and Vibration*, 23(2), 199-216.
- [38] Zhao, B., Ueno, S., Abe, T., Nakae, H. (2004). “Influence of Graphite Morphology and Matrix on Damping capacity of Hypereutectic cast iron”. *Research Article, J. JFS*, Vol.76, No.4, pp. 303-308.
- [39] Daudi, A., Dickerson, W., (2000). Ultra Q Process, SAE 2000-01-2760.
- [40] Skvortsov, a. I. (2004). Effect of Structure on the Damping Capacity and Mechanical Properties of Iron Alloys with Magneto mechanical Damping. *Metal Science and Heat Treatment*, 46(5/6), 196–202.
- [41] De Batist, R. (1983). High Damping Materials : Mechanisms and Applications. *Le Journal de Physique Colloques*, 44(C9), C9–39–C9–50.
- [42] Birss, R. R., Faunce, C. a, & Isaac, E. D. (1971). Magnetomechanical effects in iron and iron-carbon alloys. *Journal of Physics D: Applied Physics*, 4(7), 1040–1048.
- [43] Udovenko, V. A., Chudakov, I. B., Alexandrova, N. M., Kakabadze, R. V, & Perevalov, N. N. (2008). On the Formation of High Damping State and Optimization of Structure of Industrial Damping Steels, *137*, 119–128.
- [44] Uhlig, P.R. (2000). “Method and apparatus for measuring vibration damping”. US Patent # US6314813B1.
- [45] Hanna, D.M., Schroth, J.G. (2008). “Coulomb Damped Disc Brake Rotor and Method of Manufacturing”. United States Patent Application Publication, US Patent # US 2008/009289 A1.

[46] Dessouki, O.S., Lowe, B.D, Riefe, M.T. etc. (2006). “Coulomb Friction Damped Disc Brake Rotors”. United States Patent Application Publication, US Patent # US 2006/00976200 A1.

[47] Hanna, D.M., Schroth, J.G. etc. (2011). “Bi-metal disc brake rotors and method of manufacturing”. United States Patent Application Publication, US Patent # US 20110198169A1.

[48] Karpenko, Y., Allen, D., etc. (2018). “Coulomb Friction Damped Components and method for manufacturing same”. United States Patent Application Publication, US Patent # US 20180298964A1.

[49] Daudi, A.R., Dickerson, W.E. Milosavlevski, C., Walkowiak, R. (2003). “Damped Disc Brake Rotor”. United States Patent Application Publication, US Patent # 6505716B1.

[50] Dickerson, W.E. Jakovljevic, P. (2003). “Brake Rotor with Non-directional braking surface”. United States Patent Application Publication, US Patent # 6279697B1.

[51] Daudi, A.R., Dickerson, W.E. (2001). “Method of increasing the length and thickness of Graphite Flakes in a gray iron brake rotor”. United States Patent Application Publication, US 20010040075 A1.

[52] ASM International, *ASM Specialty Handbook Cast Irons*, Edit. 1996. United States of America: ASM International.

[53] Holly M.L., DeVoe L., and Webster J., (2011). “Ferritic Nitro carburized Brake Rotors”, SAE Technical Paper 2011-01-0567, SAE International.

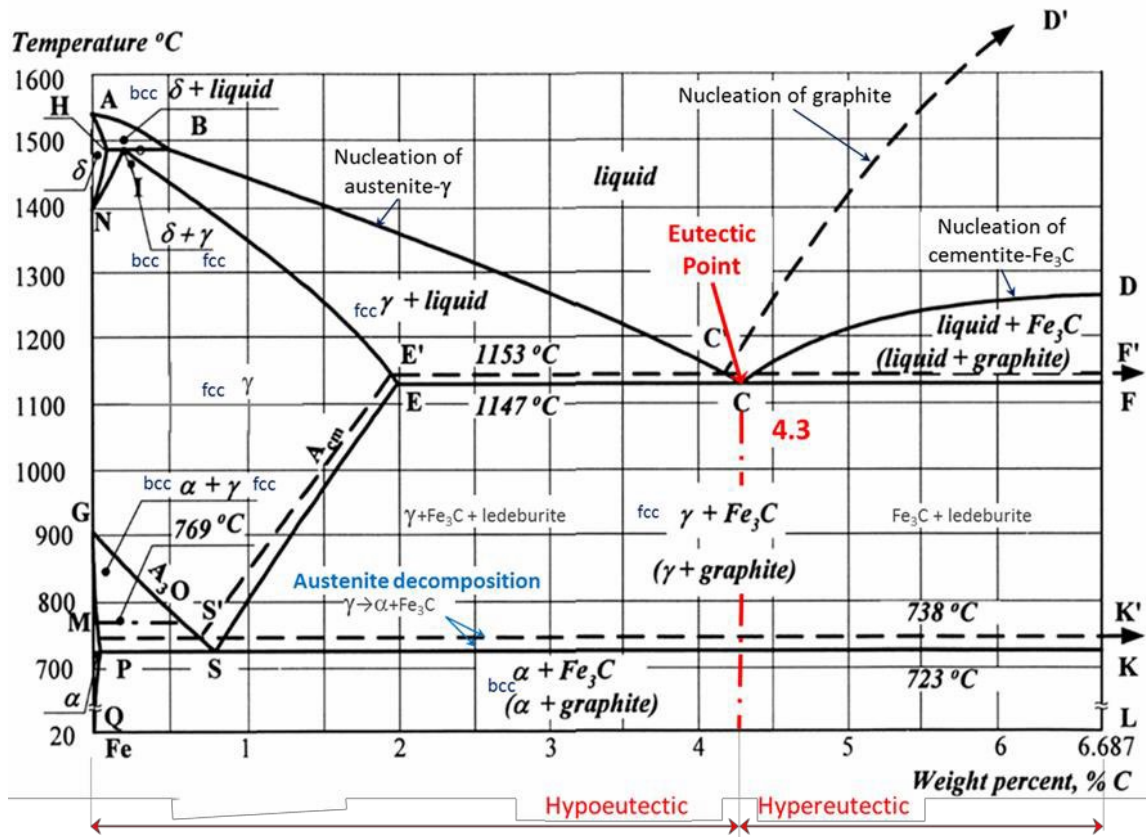
- [54] Pye D., (2001). “Practical Nitriding and Ferritic Nitrocarburizing, Materials Park, ASM International.
- [55] Yamabe, J., Takagi, M., Matsui, T., Kimura, T., Sasaki, M. (2002) “Development of Disc Brake Rotors for Trucks with High Thermal Fatigue Strength,” JSAE Rev., vol. 23, no. 1, pp. 105–112.
- [56] Heine, R.W., Loper, C.R., Rosenthal, P.C. (1955) “Principles of Metal Casting”, Second Edi. New York: McGraw-Hill Book Company, Inc.
- [56] Tisza, M. (2002). “Physical Metallurgy for Engineers”, Second Edi. Ohio: ASM International.
- [57] Maluf, O., Angeloni, M., Milan, M.T., Spinelli, D., Wladimir, W., Filho, B. (2003). “Development of Materials for Materials for Automotive Disc Brakes,” *Pesqui. e Tecnol. Minerva*, vol. 4, no. 2, pp. 149–158.
- [58] Ankamma, K. (2014) “Effect of Trace Elements on The Properties Of Grey Cast Iron,” *J.Inst.Eng.India Ser.*, vol. 95, no. 1, pp. 19–26.
- [59] Jiyang, Z. (2009). “Preface,” in *Colour Metallography of Cast Iron China Foundry*, pp. 57– 69.
- [60] Muhmond, H.M. (2014). “On the Inoculation and Graphite Morphologies of Cast Iron,” Doctoral Thesis, The Royal Institute of Technology.
- [61] Sillén, R. (2008). “Finding the True Eutectic Point – An Essential Task for Efficient Process Control of Ductile Iron,” *Ductile Iron News*, no. 2, pp. 100–104.

- [62] Sil'man, G.I. (2002). "Carbon Equivalents of Elements in Cast Iron," *Met. Sci. Heat Treat*, vol. 44, no. 1–2, pp. 28–31.
- [63] Riposan, I., Chisamera, M., Stan, S., White, D. (2007). "Chilling properties of Ba/Ca/Sr inoculated grey cast irons," *Int. J. Cast Met. Res.*, vol. 20, no. 2, pp. 90–97.
- [64] Bazhenov, V.E., Pikunov, M.V. (2011). "Determining the Carbon Equivalent of Cast Iron by the Thermo-calc Program," *Steel Transl.*, vol. 41, no. 11, pp. 896–899.
- [65] Shobolov, E.V., Kozlov, L.Y., Romanov, L.M., Rozhkova, E.V., Romanov, O.M., Yurasov, S.A. (1984) "Predicting the Properties of Chromium Cast Irons on the Basis of the Carbon Equivalent," *Met. Sci. Heat Treat*, vol. 26, no. 7, pp. 497–499.
- [66] Song, Y., Hua, L. (2011). "Mechanism of Residual Stress reduction in low alloy steel by a low frequency alternating magnetic treatment". *J. Mater. Sci. Technol.* 28(9), 803-808.
- [67] Klamecki, B. (2003). "Residual Stress reduction by pulsed magnetic treatment". *Journal of Materials Processing Technology* 141, 385-394.
- [68] Honeywell. "Hall Effect Sensing and Application". MICRO SWITCH Sensing and Control.
- [69] Honeywell. "Datasheet SS39ET/SS49E/SS59ET Series". Linear Hall-effect Sensor ICs
- [70] Holly, M.L., Riefe, M.T., Kaatz, R.A., Learman, Antanaitis, D.B., Devoe, L.G. (2017). "Brake corner output with fnc brake rotors". United States Patent Application Publication, US 20170058982 A1.

[71] Holly, M.L., Reed, D.N. (2017). “Brake rotor”. United States Patent Application Publication, US 9651105 B2.

[72] Garcia, A.D., (2019). “HT-UMSA Physical Simulations of brake rotor metallurgical processes” Doctoral Thesis, University of Windsor.

APPENDIX 1



Equilibrium Iron (Fe) – Carbon (C) Phase Diagram [57]

APPENDIX 2

Carbon Equivalent (C.E.) Formulae			
Conventional [1]	$C.E. = C + (Si/3)$	Formula use on the majority of industrial processes.	(1)
Conventional ASM Handbook [52]	$C.E. = C + 0.33 Si + 0.33P$	Formula commonly use for industrial processes.	(2)
Sillen [61]	$C.E. = C + (Si/4) + (P/2)$	Formula proposed by Sillen	(3)
Silman [62]	$C.E. = C + G_i B_i$ Where G_i depend on the carbon content. B_i are the true contents of the i th alloying element in the cast iron respectively, considering Si, Al, Cu, Ni, Co, Mn, Mo, Cr and V	<i>With increase in the C content in hypoeutectic cast iron, the numerical values of the equivalents increase for elements stimulating graphitization and decrease for elements suppressing it.</i> [62]	(4)
Bazhenov [64]	$C.E. = C + 0.3 Si + 0.33P - 0.015Mn + 0.26S$		(5)
Shobolov [65]	$C.E. = C + 0.3Si - 0.03Mn + 0.07Ni + 0.05Cr$	<i>The formula was developed base on the wear resistance, which can be improved by varying the content of three elements: Cr, C and Mn.</i>	(6)

Carbon Equivalent Formulae [72]

APPENDIX 3

Hardness measurements on D11 rotors – Pre-process hardness measurements

D1106					PIECE 1				
Superficial Hardness HBW 5/750 (On Machined Brake Plate)	OBP				IBP				POSITION
	12 H	3 H	6 H	9 H	12 H	3 H	6 H	9 H	
	171	169	181	171	160	161	165	168	Outer
	169	164	171	167	160	164	161	161	Middle
	158	158	169	156	159	163	171	167	Inner
D1106					PIECE 2				
Superficial Hardness HBW 5/750 (On Machined Brake Plate)	OBP				IBP				POSITION
	12 H	3 H	6 H	9 H	12 H	3 H	6 H	9 H	
	171	173	179	169	162	167	177	165	Outer
	168	167	172	174	168	165	169	173	Middle
	160	160	159	157	171	168	162	164	Inner
D1106					PIECE 3				
Superficial Hardness HBW 5/750 (On Machined Brake Plate)	OBP				IBP				POSITION
	12 H	3 H	6 H	9 H	12 H	3 H	6 H	9 H	
	162	169	177	169	163	163	174	173	Outer
	163	173	171	169	162	161	164	165	Middle
	156	152	163	163	161	165	171	168	Inner
D1106					PIECE 4				
Superficial Hardness HBW 5/750 (On Machined Brake Plate)	OBP				IBP				POSITION
	12 H	3 H	6 H	9 H	12 H	3 H	6 H	9 H	
	172	168	176	171	163	173	175	168	Outer
	165	170	171	169	164	173	170	165	Middle
	152	163	162	162	162	167	169	163	Inner
D1106					PIECE 5				
Superficial Hardness HBW 5/750 (On Machined Brake Plate)	OBP				IBP				POSITION
	12 H	3 H	6 H	9 H	12 H	3 H	6 H	9 H	
	174	174	173	174	162	163	172	164	Outer
	172	170	172	170	162	169	162	163	Middle
	160	162	163	161	163	168	175	168	Inner

Post process hardness measurements on the same rotor

D1106					PIECE 1				
Superficial Hardness HBW 5/750 (On Machined Brake Plate)	OBP				IBP				POSITION
	12 H	3 H	6 H	9 H	12 H	3 H	6 H	9 H	
	164	164	174	176	167	168	181	163	Outer
	167	165	178	171	169	162	165	160	Middle
	150	161	156	150	161	174	173	159	Inner
D1106					PIECE 2				
Superficial Hardness HBW 5/750 (On Machined Brake Plate)	OBP				IBP				POSITION
	12 H	3 H	6 H	9 H	12 H	3 H	6 H	9 H	
	168	173	179	168	172	172	176	169	Outer
	166	169	178	169	168	165	174	167	Middle
	151	156	154	159	162	170	178	165	Inner
D1106					PIECE 3				
Superficial Hardness HBW 5/750 (On Machined Brake Plate)	OBP				IBP				POSITION
	12 H	3 H	6 H	9 H	12 H	3 H	6 H	9 H	
	165	168	179	171	159	165	173	173	Outer
	168	171	172	165	163	163	170	158	Middle
	152	151	150	150	160	164	168	164	Inner
D1106					PIECE 4				
Superficial Hardness HBW 5/750 (On Machined Brake Plate)	OBP				IBP				POSITION
	12 H	3 H	6 H	9 H	12 H	3 H	6 H	9 H	
	171	175	176	174	161	167	172	170	Outer
	165	170	178	169	165	167	176	17	Middle
	152	153	158	164	162	16	163	162	Inner
D1106					PIECE 5				
Superficial Hardness HBW 5/750 (On Machined Brake Plate)	OBP				IBP				POSITION
	12 H	3 H	6 H	9 H	12 H	3 H	6 H	9 H	
	169	169	175	175	167	164	173	169	Outer
	167	165	173	172	165	169	170	168	Middle
	149	152	151	151	162	163	168	164	Inner

VITA AUCTORIS

NAME: Raju Karthik

PLACE OF BIRTH: Nagpur, India

YEAR OF BIRTH: 1973

EDUCATION: Osmania University, Hyderabad, India
Bachelor of Science, 1990 - 1994

West Virginia University, WV, USA
Masters of Science, 1994 - 1997